Master Thesis, Department of Geosciences

Snow melt

Evaluation of an energy balance model

Anne Kristina Tvedalen

UNIVERSITY OF OSLO

FACULTY OF MATHEMATICS AND NATURAL SCIENCES

Snow melt

Evaluation of an energy balance model

Anne Kristina Tvedalen

Master Thesis in Geosciences

Discipline: Hydrology

Department of Geosciences

Faculty of Mathematics and Natural Sciences

University of Oslo

June 1st 2015

Cover image: Bjørstad, H. H.

Abstract

The Norwegian Water Resources and Energy Directorate (NVE) has an ambition of introducing energy balance snow melt modelling in their hydrological models, preferably on a finer resolution than daily in order to account for diurnal variations. In that context the physically based point energy balance model seNorge_eb, with precipitation and temperature as input data, was evaluated on 3 and 24 hour resolution in terms of its precision in predicting snow melt rates. Simulated snow melt rates during the main ablation season in April/May were evaluated against observed values from NVEs snow research station at Filefjell. Simulated radiation components and variables were compared with observed radiation and meteorological data. Parametrizations and variables in seNorge_eb were, one at the time, replaced with observed data, with the aim of deciding the minimum input data requirement.

In terms of the overall model performance, both the 3 and 24 hour resolution versions performed well in predicting snow melt rates, with the best results on 24 hour resolution. From the analysis of the individual components, deviations between simulated and observed data were identified. The cloud cover fraction was found to be a main source of error and the component most urgent to correct as it is embedded both in the incoming solar radiation and atmospheric long-wave radiation, the most important energy sources for snow melt. The clear-sky atmospheric emissivity was found as another source of error in the simulated atmospheric long-wave radiation. Local calibration of the clear-sky atmospheric emissivity may be worth testing. Regarding the minimum input data requirement, relative humidity is recommended as additional input data for both resolutions, in addition to wind and snow surface temperature on 3 hour resolution.

seNorge_eb, as it is set up today, should not be implemented in a hydrological model. For that to happen, the model's problem areas have to be improved, in particular the cloud cover fraction and the parametrization of the atmospheric long-wave radiation.

Forord

At jeg skulle bli hydrolog var det nok ingen som hadde forestilt seg. Jeg visste nemlig ikke selv hva hydrologi var da jeg begynte på Blindern høsten 2007. Rett før søknadsfristen til Samordna opptak gikk ut, endret jeg studiested fra Trondheim til Oslo og geofag. Plutselig skulle jeg flytte til hovedstaden, som jeg hadde inntrykk av som grå og stor, og en by å være ensom i. Alt ble innfridd. I løpet av studietida har Oslo heldigvis vokst på meg. Byen fremstår nå som penere, mindre og hyggeligere. Oslo har også satt sine merker i meg. Spesielt Blindern, hvor jeg har vandret mellom realfag og humaniora, før jeg til slutt bestemte meg for å bli hydrolog, motivert av at sammfunnet alltid vil ha behov for kunnskap om vann. Yrkesvalget er også påvirket, om mer i underbevisstheten, av vestledningen som jeg ble kjent med første dag på Universitetet og som presenterte seg som en kommende hydrolog. Derfor, en stor takk skylder jeg Astrid.

Når det gjelder masteroppgaven min, vil jeg takke Thomas og Thomas. Thomas Skaugen (NVE) og Thomas Vikhamar Schuler (UiO) har begge gitt meg god veileding i arbeidet med oppgaven. Thomas Skaugen hadde idéen til oppgaven og har gjennom hele prosessen vært en engasjert veileder som har bistått med god og jevnlig oppfølging, samt opplæring i feltarbeid. Takk for samarbeidet, Thomas og Thomas!

Takk også til medstudent Ingunn Hultgreen Weltzien for en fin felttur på Filefjell i snøsmeltesesongen våren 2014. 17. mai kommer vi begge sent til å glemme, med snømåling klokka åtte om morgenen, kaker og taler i Øvre Årdal, samt ny snømåling klokka åtte om kvelden.

NVE har vært en flott institusjon å skrive masteroppgave for, og det på grunn av personene som jobber der. Takk til Sverre Husebye og HV for kontorplass og et hyggelig arbeidsmiljø. Takk til Heidi Bache Stranden og Knut Møen for innspill om måledata. Og takk til øvrige NVE'ere som har vært svært behjelpelige med diverse spørsmål.

Takk til Dag, Armin og Rafael som tilbød seg å lese korrektur en lørdag kveld. En spesiell takk til Peder som har holdt ut med meg også i nedturene som følger med arbeidet med en masteroppgave. Takk også til min familie.

Anne Kristina Tvedalen Oslo, 1. juni 2015

Contents

1 Introduction and study area

1.1 Introduction

Snow melt is an important process in the hydrological cycle in cold regions. Modelling snow melt is essential in predicting inflow to the hydro-power industry's reservoirs as well as in flood forecasting. Modelling snow melt still remains a complicated aspect of many hydrological models (Walter et al. 2005).

Basic temperature-index models are the most common snow melt models (Dingman 2002). Omhura (2001) is among the advocates of the temperature-index model due to the importance of air temperature to melt and that the method gives sufficiently accurate results for most situations. Anderson's (1976) study of snow melt in the USA is known to be the most thorough comparison of temperature-index and energy balance modelling at point scale (Dingman 2002). Anderson (1976) concluded that the energy balance model gave improved results over the temperature-index model. Moreover, Anderson found that the energy balance model gave good results for snow melt under all meteorological conditions, whereas the approximations from the temperature-index model were not satisfactory in cases where the relationship between air temperature and additional meteorological variables deviated significantly from normal. Besides that the energy balance method has proved to be superior to the temperature-index method, its advantage over the latter is that sources of error can more readily be identified and corrected (Walter et al. 2005).

Physical based models, such as energy balance models, are regarded as better suited to study future climate changes (Hock 2005). These models are better in quantifying the response in melt and discharge because calibrated parameters in simpler models may not be valid under a changed climate.

The Norwegian Water Resources and Energy Directorate (NVE) is the Norwegian state institution responsible for the national flood forecast service and has for a long time had the ambition of introducing energy balance into its hydrological models (Skaugen and Saloranta 2015). There are two main motivations for doing so. Firstly, it will strengthen the competence of NVEs snow modellers. Secondly, several studies have concluded that on a sub-daily resolution energy balance models are preferred over temperature-index models (Skaugen and Saloranta 2015). Also, higher temporal resolution models are necessary for more precise forecasts, particularly in terms of the timing of the peak flow due to diurnal snow melt fluctuations (Hock 2005). Moreover, an energy balance approach has the benefit that calibrated parameters can be avoided (Skaugen and Saloranta 2015).

This thesis is carried out in cooperation with NVE. The point energy balance model seNorge_eb (Skaugen and Saloranta 2015) is evaluated in terms of its precision in predicting snow melt rates using data from NVEs snow research station at Filefjell, where all the radiation components of the energy balance and various meteorological parameters are measured. The model as a whole and its different components are evaluated on a daily and sub-daily (i.e. 3 hour) basis. The ideal outcome of this study is an energy balance model that requires as few input data as possible, preferably only precipitation and temperature since they are available at a national scale, and hence seNorge_eb will be applicable for the whole of Norway.

The main objective of the thesis is to assess seNorge_eb's minimum requirement for input data in order for the model's precision in predicting snow melt rates to be as good as possible compared with observed values. seNorge_eb is originally set up with the input data precipitation and temperature, whereas other components are parametrized. Additional observed data are included successively by replacing parametrizations or variables. Secondly, deviations between simulated values and observations of the individual energy fluxes and variables are to be identified and possible improvements suggested. It is also an aim to identify for which resolution, 3 or 24 hour, seNorge_eb has the best precision in terms of predicting snow melt rates.

1.2 Structure of the thesis

The first part of the thesis consists of a theory chapter and a presentation of the particular energy balance model that is being used (ch.2 and 3). Chapter 4 first describes the field campaign, whereas the second part relates to the model simulations. The evaluation and input data and the method of how the latter are included in seNorge_eb, as well as the model evaluation criteria that lays the foundation for the results and analysis, are outlined. The results are divided between outcomes from field campaign and simulations (ch. 5 and 6). The simulation results are further split between sub-daily (i.e. 3 hour) and daily resolution. First, seNorge_eb as it was first set up is evaluated in terms of its ability to predict snow melt rates with precipitation and temperature as the only input data, and how the parametrizations of the radiation fluxes and individual variables perform compared to observations. Secondly, additional observational data are, one at the time, included as input data by replacing their corresponding parametrization or variable. The results are analysed in the discussion (ch. 7).

1.3 Study area

The study area is located at Kyrkjestølene at Filefjell in Vang municipality in Oppland county (Fig. 1). Filefjell is a high mountain area (915-1815 masl) where snow constitutes a major part of the hydrological cycle since a large part of the annual precipitation falls as snow, 45 % in the period 1967-73 (Furmyr and Tollan 1975). The large altitude difference within the area results in an unevenly distribution of the snow cover and its duration. The winter season usually covers the period from end of October to mid May.

Figure 1: *Map view, location of the study area, Filefjell, indicated in red (Norge i bilder 2015).*

During the period of the International Hydrological Decade (IHD), 1965-74, Filefjell was one out of three representative Norwegian areas that were established with the aim of conducting a hydrological measuring program (Furmyr and Tollan 1975). A result of the IHD-period were several publications, among others reports by Furmyr (1975) and Furmyr and Tollan (1975) concerning results from surveys of precipitation and snow respectively. Moreover, the first snow pillow in Norway was installed at Filefjell during the IHD-period. Thus the study area of this thesis has a long tradition of snow investigations in Norway.

Today there are two measuring stations of recent date in the study area, owned and driven by NVE and Meteorological Institute (MET) and located at a distance 8 m apart (Stranden and Grønsten 2011). Data from these stations are used as input and/or evaluation in this thesis. The stations are located 160 m South of E16 (red line in Fig. 1) in a valley directed East-West and around 955 masl. The area around the stations are characterised by low shrub vegetation, heather and swamp, and it is drained towards West by a tributary of the catchment Sula. The stations are located in a flat valley plateau, however on both sides of the valley the distance to the mountains at 1300-1500 masl. is rather short. The average snow maxium at the stations in snow water equivalent (SWE) is 320 mm, measured with a snow pillow at NVEs station (Stranden and Grønsten 2011).

Since 2009 NVEs station at Filefjell (73.11 Kyrkjestølane) has been upgraded to become a snow research station where several snow parameters (snow depth, snow temperature, SWE) as well as radiation elements and meteorological variables are being automatically recorded . METs station is an ordinary weather station dating from Autumn 2010

(Stranden and Grønsten 2011). An overview of NVEs station is seen in Fig. 2.

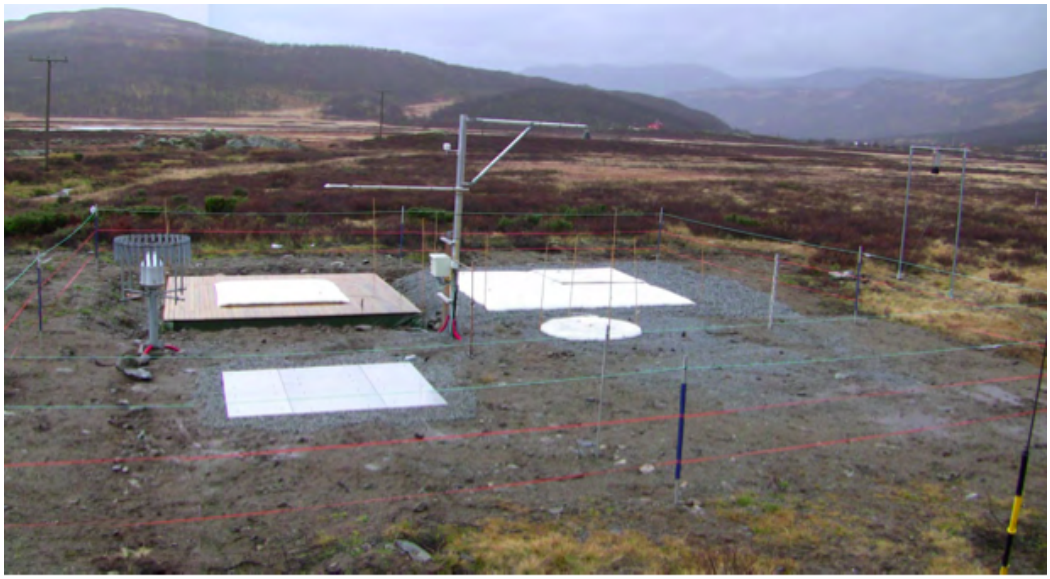

Figure 2: *Overwiew of NVEs research station for snow. Rain gauge, radiation and gamma sencors attached to the mast and snow pillows and snow weight in white on the ground. Data from the snow weight (wooden plateau) is used as reference upon evaluating the simulated snow melt rates in this thesis. (Stranden and Grønsten 2011).s*

2 Theoretical background

In this chapter general theory about snow melt, snow melt models and the energy balance of snow is outlined. The latter constitutes the basis for the snow model used in this thesis.

2.1 Snow melt

Prior to the melt period the snow pack goes through an accumulation period in which the snow water equivalent increases and the snow pack temperature decreases, and the net energy inputs are as a rule negative (Dingman 2002). When the snow pack's net energy input becomes more or less continually positive the melt period starts. According to Dingman (2002) the melt period can be separated into three phases: the warming, ripening and output phase.

In the warming phase the snow pack temperature increases steadily until the snow pack is isothermal at 0 ℃. The ripening phase is a period in which the snow has started to melt, however the melt water is retained in the snow pack. When the snow pack cannot maintain any more melt water, additional inputs of energy will cause outflow.

The three phases are only a rough description, however convenient tools for understanding the snow melt process (Dingman 2002). Melt may occur on the surface of the snow pack and percolate into the snow pack, refreeze and release energy that raise the snow pack temperature. Moreover, during a melt period the snow temperature might fall below freezing on cold nights, and as such energy is first used to warm the snow pack before melt can resume.

2.2 Snow melt models

In predicting snow melt rates two basic approaches exist: the temperature-index model and the energy balance model (Harding 1986). The former is a fully empirical model and usually site specific, whereas the energy balance model is physically based. The energy balance model is, however, more complex and requires good meteorological data.

The temperature-index approach estimates snow melt rates, ΔSWE [$mm\ s^{-1}$], that are found from a linear relationship of the average air temperature, T_a [℃]:

$$\Delta SWE = D \cdot (T_a - T_m) \tag{1}$$

where D is the melt coefficient [$mm\ s^{-1}$ ℃$^{-1}$], empirically determined, and T_m is the temperature at which the snow starts to melt [℃]. When $T_a < T_m$, $\Delta SWE = 0$ mm.

Energy balance models are physically based models and are classified as either distributed or point models. In this thesis a point model is used. The parameters of the energy balance model can be written in slightly different ways. The parametrizations used in the model used in this thesis are described in ch. 3.

2.3 Energy balance of snow

The energy balance involves the evaluation of the energy fluxes at the snow surface (Hock 2005). The exchange of energy at a snow surface is recognised as one of the major factors controlling the amount of melt water and is thus important to consider in any snow-covered watershed (Male and Granger 1981). From thoroughly studies of snow cover energy exchange and melt processes in the USA and former Soviet Union, the Corps of Engineers (1956) and Kuzmin (1961) gave an in depth discussion. Male and Granger (1981) give a review of radiation turbulent heat transfer at a snow surface, and a summary of the processes of hydrology and snow melt is presented by Dozier (1987) .

The energy balance for a column of snow (i.e. including the internal energy of the snow pack) with units $[W\ m^{-2}]$ can be expressed as in Eq. 2 (Skaugen and Saloranta 2015; King et al. 2008; Hock 2005, Walter et al. 2005). Assumptions are that there is no lateral energy transfer, no effects of blowing snow or vegetation (King et al. 2008).

$$M = N + SH + LE + G + R + CC \tag{2}$$

where M is the energy flux available for melt, N is the net radiation, SH is the sensible heat flux, LE is the latent heat flux, G is the ground heat flux, R is the sensible heat flux supplied by precipitation and CC is the cold content.

Fig. 3 illustrates the fluxes in the energy balance (i.e. right handside of Eq. 2) of an open snow pack. Net radiation in Eq. 2 comprises incoming, $\downarrow$, and outgoing, $\uparrow$, solar (S) and long-wave (L) radiation (i.e. $N = S + L$).

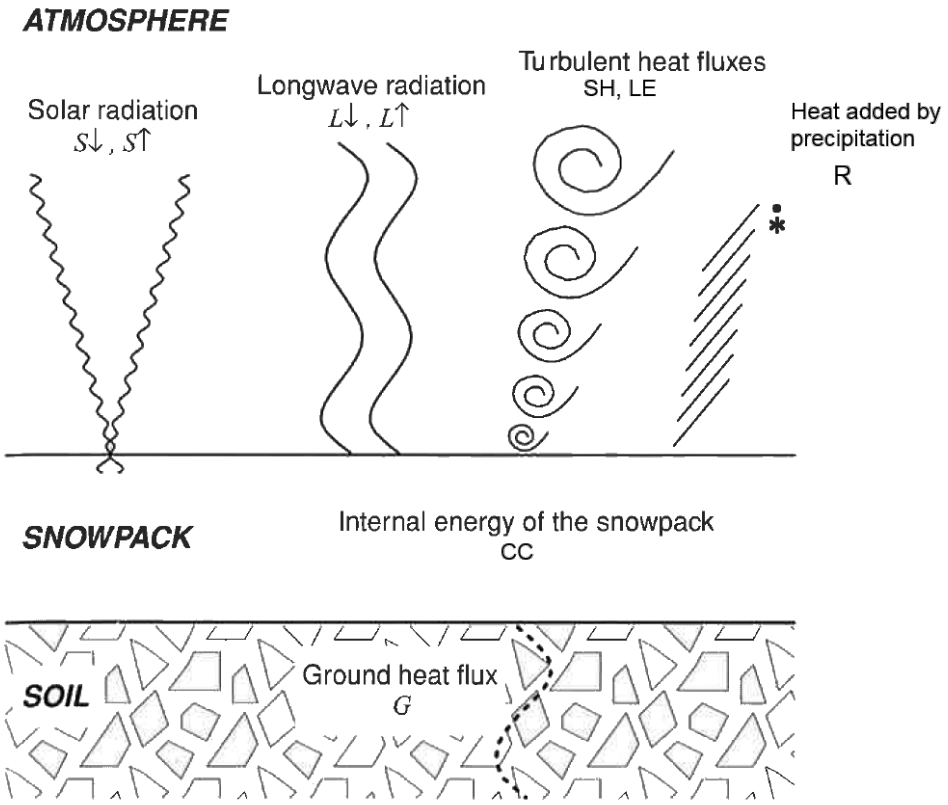

Figure 3: *Energy balance of an open snow pack (modified from King et al. 2008).*

The energy balance assumes that once the snow pack temperature has reached 0 °C any additional energy will contribute directly to melting (Hock 2005). From the available energy, M, snow melt rates, ΔSWE $[mm\ s^{-1}]$, are computed as:

$$\Delta SWE = \frac{M}{\rho_w \lambda_F} \cdot 1000 \tag{3}$$

where ρ_w is the density of water (1000 $kg\ m^{-3}$) and λ_F is the latent heat of fusion (335 $kJ\ kg^{-1}$).

The net radiation is the most important of the fluxes when it comes to producing melt water, and the turbulent fluxes, i.e. the sensible and latent heat fluxes, are the second most important fluxes (Male and Granger 1981). When considering the net radiation over longer periods such as weeks or months the turbulent fluxes constitute a small fraction, however, when the time interval is reduced to hours or days, they can outdo the radiation fluxes (Hock 2005). Rain on snow and ground induced fluxes are of minor importance compared to the other fluxes (Male and Granger 1981). Once a snow pack is formed, the above fluxes and the atmosphere-ground interface are affected. The snow pack is in turn influenced by the underlying terrain (King et al. 2008).
The turbulent fluxes (SH and LE) are generally estimated by empirical formulae as they are not so susceptible to direct measure, whereas the net radiation and heat input from rain can be directly measured. The radiation fluxes can also be estimated from

empirical formulae (Harding 1986).

Net radiation
Net radiation (N) is the net all-wave radiation at the snow surface, consisting of incoming and outgoing short-wave and long-wave radiation (Male and Granger 1981).

$$N = S + L \tag{4}$$

where S is the net incident (short-wave) solar radiation, and L is the long-wave radiation.

Due to the effect of slope, aspect and effective horizon the radiation fluxes vary considerably in space and time in mountainous areas. This is particular so for the short-wave radiation as the clouds reduce incoming radiation and due to emission and reflection by surrounding slopes (Hock 2005). Incoming long-wave radiation exhibit the opposite and is increased with increasing cloud cover, whereas outgoing long-wave radiation remains relatively uninfluenced (Male and Granger 1981). Thus the energy streams of the net radiation are affected in contrasting directions.

Solar radiation
Solar radiation primarily originates directly from the sun and covers a wavelength of 0.15-4 μm (Hock 2005). Crucial for site-specific computation of solar radiation on complex topography are atmospheric conditions and clouds, slope and aspect.

Solar radiation can be measured with a pyranometer, however it is generally estimated (Dingman 2002). The parametrization of net incident solar radiation at the snow surface is given by (King et al. 2008) (a more detailed parametrization is provided in ch. 3):

$$S = S\downarrow (1 - A) \tag{5}$$

where $S\downarrow$ is incoming solar radiation and A is the albedo.

Albedo
Albedo is a measure of reflection, and the amount of short-wave radiation absorbed by the snow pack is a result of the variations in albedo (King 2008) . Typical albedo values are given in Table 1. The albedo depends on the properties of the incoming radiation (zenith angle and wavelength) and the material properties of the surface (Hock 2014). A physically based calculation of albedo involves calculating the metamorphism of the different snow layers as the snow albedo depends strongly on the size and shape of snow grains (Brun 2008).

Table 1: *Common albedo values for different surfaces (Hock 2014)*

Fresh snow	$\sim 0.7 - 0.9$
Firn	$\sim 0.5 - 0.6$
Ice	$\sim 0.3 - 0.4$
Grass	$\sim 0.1 - 0.3$
Forest	$\sim 0.1 - 0.2$

Long wave radiation
Wavelength within the spectrum 4-120 μm is referred to as long-wave radiation mainly of terrestrial and atmospheric origin (Hock 2005). Thus

$$L = L\downarrow - L\uparrow = L_a - L_t \tag{6}$$

where L_a is the atmospheric long-wave radiation and L_t is the terrestrial long-wave radiation.

L_a is emitted mainly by carbon dioxide, water vapour and atmospheric water (Hock 2005). Variations in cloud cover and in water vapour temperature contribute to the main part of the variations in L_a. L_t is emitted by the snow cover itself and the terrestrial objects.

Pyrgeometers can be used to directly measure long-wave radiation, or indirectly by considering the difference between measurements from a radiometer (all-wave radiation) and pyranometer (short-wave radiation) (Dingman 2002). Parametrizations of L_a are commonly based on the Stefan-Boltzmann equation
(König-Langlo and Augstein 1994):

$$L = \varepsilon \sigma T_K^4 \tag{7}$$

where ε is the atmospheric emissivity, σ is the Stefan-Boltzmann's constant and T_K is the temperature of the radiative body [K].

Embedded in ε are various unknowns such as the vertical temperature distribution, water vapour distribution and cloud effects (König-Langlo and Augstein 1994).

Turbulent fluxes
The driving forces behind the sensible (SH) and latent heat flux (LE) (i.e. the turbulent heat fluxes) are the turbulence in the lower atmosphere (mechanism of vertical air exchange) and the moisture and temperature gradients between the surface and the air (Hock 2005). Eddy-correlation techniques can be used to measure the turbulent fluxes directly. However, due to the difficulty of using these techniques in practice the turbulent fluxes are generally parametrized by gradient-flux relation. The equations for the sensible and latent heat fluxes used in this thesis are presented in chapter 3.

Sensible heat flux
The sensible heat flux, SH, is a function of the temperature gradient and wind speed, and is zero if any of these is zero (Hock 2014).

Latent heat flux
The latent heat flux, LE, is related to energy released or consumed during a phase change (i.e. condensation, re-sublimation, evaporation or sublimation), and is a function of the vapour pressure gradient and wind speed (Hock 2014). If either of the the vapour pressure or wind speed is zero, LE will be zero. Evaporation will take place if the vapour-pressure gradient is directed upward (i.e. mass movement from the snow to the air and relative humidity is less than 100 %), and if the gradient is negative condensation will take place (Dingman 2002). Sublimation can take place only for cold snow packs with a snow surface temperature less than 0 ℃.

Ground heat conduction
The heat flux from the ground, G, to the base of the snow pack is, as already mentioned, a minor source for snow melt (DeWalle and Rango 2008). This is because soil is mostly a poor heat conductor and, moreover, that the ground beneath the snow holds a low temperature. G is considered small and often constant in simulation models.

Heat induced by precipitation
A snow pack at its freezing point gains heat from melting when rain falls upon it and is cooled to the snow temperature. The heat input form rain, R, is a small contributor to snow melt (Dingman 2002).

Cold content
The cold content of a snow pack, CC, is the amount of energy needed for the snow pack to reach a temperature of 0 °C (Dingman 2002).

The following chapter gives an overview of the energy balance model used in this thesis.

3 The energy balance model: seNorge_eb

The model used in this thesis is named seNorge_eb and is based on the energy balance concept described in chapter 2. It is a point model that considers the energy balance, including the internal energy, CC, of a snow pack. Slope and aspect are not included in the model. seNorge_eb was set up in R by NVE and is described in Skaugen and Saloranta (2015). The model is set up to work with only precipitation [mm], P, and air temperature [℃], T_a, as input data. The algorithms used in the parametrizations of the energy fluxes are taken from various sources and used directly or in a modified form. In the follow sections (3.2-3.3) the parametrizations of the fluxes are given. Constant values are given in Table 2. The snow pack and snow surface temperatures are computed by the model itself (see section 3.3). Unless otherwise stated, seNorge_eb follows the same procedure for all choices of time step.

Table 2: *Constant variables. The roughness height, z_0, is defined as the heigh above the ground surface where the wind speed, when plotted against ln(height), extrapolates to zero (DeWalle and Rango 2008).*

Variable	**Value**
Threshold temp. snow/rain	0.5 ℃
Max. water content in snow	5 %
Air pressure, P_a	101.1 kPa
Density of air, ρ_a	1.29 $kg\ m^{-3}$
Wind speed, u	1.75 $m\ s^{-1}$
Measuring height of u, z_a	2 m
Roughness height, z_0	0.001 m

3.1 Calculating SWE and snow melt

Before the estimation of melt rates can start the model must run from the beginning of the snow season in order to allow for accumulation of snow water equivalent (SWE). SWE is the sum of the snow pack's snow water and water content. According to a temperature threshold (Table 2) precipitation falls either as rain or snow. When precipitation is recorded as snow, new snow is accumulated to the existing SWE. Likewise, when melt is predicted (Eq. 8) the existing SWE is reduced accordingly. If rain is recorded given snow and predicted melt, the water content is increased by the corresponding amount if it is below its maximum value.

The energy available for melt, M [$W\ m^{-2}$], is given by the energy balance of the snow pack:

$$M = \lambda_F \rho_w \Delta SWE = S + L_a - L_t + SH + LE + G + R + CC \tag{8}$$

And the change in SWE, ΔSWE [$mm\ s^{-1}$], is found from:

$$\Delta SWE = \frac{(S + L_a - L_t + SH + LE + G + R + CC)}{\rho_w \lambda_F} \tag{9}$$

The components in Eq. 8 and 9 are the same as described in chapter 2.

3.2 Calculating energy fluxes and cold content

The energy fluxes have units $[W\ m^{-2}]$.

3.2.1 Solar radiation

The net solar radiation striking a horizontal surface is written as (Skaugen and Saloranta 2015):

$$S = S_0(1 - A)\Upsilon sin(0.5\pi - \varpi) \tag{10}$$

where S_0 is the potential solar radiation on a horizontal surface (estimated as the solar constant: $\frac{1}{86400}117.6 \cdot 10^3\ W\ m^{-2}$), Υ is the net daily average sky transmissivity and ϖ is the average solar zenith angle [radians].

Note that nor slope, aspect or elevation is included in the parametrization in Eq. 10.

Albedo
The albedo algorithm is set up as in the Utah Energy Balance Snow Accumulation and Melt Model (UEB) (Tarboton and Luce 1996). The albedo is estimated as a function of snow and surface age and illumination angle, after Dickinson et al. (1993). The snow albedo, A_s is calculated as the average of two reflectances, α_{vd} and α_{ird} over bands of different wavelengths λ; Visible $\lambda < 0.7\ \mu$, and near infrared $\lambda > 0.7\ \mu$.

$$A_s = \frac{\alpha_{vd} + \alpha_{ird}}{2} \tag{11}$$

$$\alpha_{vd} = (1 - C_v F_{age})\alpha_{v0} \tag{12}$$

$$\alpha_{ird} = (1 - C_{ir} F_{age})\alpha_{ir0} \tag{13}$$

where α_v and α_{ir} are the diffuse reflectances in the visible and near infrared band, C_v and C_{ir} are constants accounting for sensitivity of the band albedo to snow surface ageing (0.2 and 0.5 respectively), F_{age} is a function accounting for the ageing of snow surface (Eq. 14), and α_{v0} and α_{ir0} are fresh snow reflectance in each band (0.95 and 0.65 respectively).

$$F_{age} = \frac{\tau}{1 + \tau} \tag{14}$$

where τ refers to a non dimensional snow surface age. At each time step τ is increased/incremented by a quantity that imitates the effect of surface grain growth:

$$\Delta\tau = \frac{r_1 + r_2 + r_3}{\tau_0}\Delta t \tag{15}$$

where Δt is time step in seconds, r_1 is a parameter dependent on snow surface temperature with the purpose of accounting for the effect of the growth of surface grain sizes (Eq. 16), r_2 accounts for the (additional) effect near and at freezing point due to melt and refreeze (Eq. 17) and r_3 represents the effect of dirt and snow (Eq. 18).

$$r_1 = exp(\frac{1}{273.16} - \frac{1}{T_{ss}}) \tag{16}$$

$$r_2 = r_2 = min(r_1^{10}, 1) \tag{17}$$

$$r_3 = 0.03 \tag{18}$$

The snow surface is restored to new conditions ($\tau = 0$) with 0.01 m of snowfall.

The radiation reflectance with solar zenith angle ϖ is computed as:

$$\alpha_v = \alpha_{vd} + 0.4f(\varpi)(1 - \alpha_{vd}) \tag{19}$$

$$\alpha_{ir} = \alpha_{ird} + 0.4f(\varpi)(1 - \alpha_{ird}) \tag{20}$$

$$\begin{array}{lcll} f(\varpi) & = & \frac{1}{b}[\frac{b+1}{1+2bcos(\varpi)}] & for\ cos(\varpi) < 0.5 \\ f(\varpi) & = & 0 & otherwise \end{array} \tag{21}$$

where the parameter b i set at 2 (Dickinson et al. 1993). For ϖ larger than 60°, $f(\varpi)$ is being increased.

ϖ is defined as the angle between a line from the sun and an observed on the earth and vertical line at observer's position (Dingman 2002). ϖ is averaged over ω at each hours. ω is estimated as (Dingman 2002):

$$\omega = acos(sin\varphi\ sin\delta + cos\varphi\ cos\delta\ cos0.2618\varsigma) \tag{22}$$

where φ is latitude [radians], δ is the solar declination angle [radians] and ς is the number of hours from solar noon.

δ is illustrated in Fig. 4 and estimated as (Liston 1995):

$$\delta = 0.4092(\frac{2\pi}{365})(DN - 173) \tag{23}$$

where DN refers to the Gregorian day number.

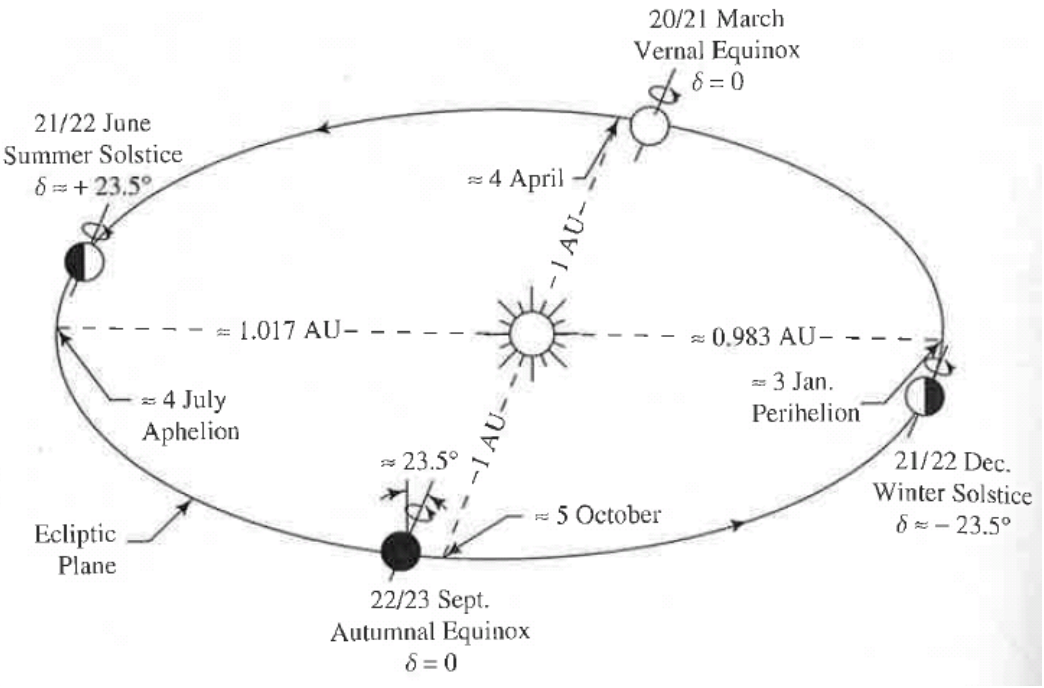

Figure 4: *Illustration of the solar declination angle δ. AU: astronomical unit (Dingman 2002).*

The depth of the snow pack, SD, is taken into consideration when computing the albedo. SD is shallow (i.e. $SD < h = 0.1\ m$) the albedo is calculated as:

$$A = rA_{bg} + (1 - r)A_s, \tag{24}$$

where A_{bg} is the bare ground albedo and

$$r = (1 - \frac{SD}{h})exp(-\frac{SD}{2h}), \tag{25}$$

where the exponential term approximating the exponential decline of the amount of radiation penetrating the snow.

Transmissivity

The transmissivity, Υ, accounts for the scattering, absorption and reflection of solar radiation (Liston 1995). Υ is estimated as (inspired by Liston (1995)):

$$\Upsilon = (0.6 + 0.2sin(0.5\pi - \varpi))(1.0 - 0.5Cl) \tag{26}$$

Cloud cover
The fractional cloud cover (Cl) is estimated as 1 if precipitation and 0.1 if not.

Solar radiation for Δt less than daily
When the model is run on intervals less than 24 hours for each time step it evaluates whether the surface might be exposed to solar radiation. This is done by calculating the hour of the sunrise, S_r, and sunset, S_s:

$$S_r = \frac{(n - \Psi + T_Z)}{60} \tag{27}$$

$$S_s = \frac{(n + \Psi + T_Z)}{60} \tag{28}$$

where

$$n = 720 - 10sin(\frac{4\pi(DN - 80)}{365.25}) + 8sin(\frac{2\pi DN}{365.25})) \tag{29}$$

and

$$\Psi = \xi + 5 \tag{30}$$

where

$$\xi = \frac{1440}{2\pi acos(\frac{R - Zsin\varphi}{Fcos\varphi})} \tag{31}$$

where R is the radius of the earth (6378 km)

and

$$Z = r_s sin((\frac{2\pi}{365.25})(DN - 80)0.4092) \tag{32}$$

where r_s is the distance to the sun (149598000 km)

$$F = \sqrt{(r_s^2 + Z^2)} \tag{33}$$

T_Z is the time zone calculated as:

$$T_Z = -4(|\kappa| \, mod 15)sign(\kappa) \tag{34}$$

where κ refers to the longitude.

3.2.2 Long-wave radiation

The long-wave radiation is computed with the Stefan-Boltzmann equation (Eq. 7). The emissivity, ε, is either atmospheric or terrestrial .

The atmospheric emissivity, ε_a, is estimated as (Swinbank 1963; Monteith and Unsworth 1990):

$$\varepsilon_a = \varepsilon_{cs}(1 - 0.84Cl) + 0.84Cl) = (0.72 + 0.005T_a)(1 - 0.84Cl) + 0.84Cl) \quad (35)$$

where ε_{cs} is the clear sky atmospheric emissivity suggested by Swinbank (1963). Swinbank assumed that the components of ε_{cs} arising from carbon dioxide and water vapour depend on the air temperature, T_a [°C]. Carbon dioxide is here assumed to originate near the surface at a temperature close to T_a, and a shallow surface layer with temperature close to T_a contains enough water vapour to provide sufficiently radiation in the relevant wave band.

If T_{ss} [°C] is the snow surface temperature then the snow emissivity, ε_s, is estimated as a dark body (i.e. $\varepsilon_s = 0.97$). We have:

Atmospheric long-wave radiation

$$L_a = \varepsilon_a \sigma (T_a + 273.2)^4 \quad (36)$$

Terrestrial long-wave radiation from snow

$$L_t = \varepsilon_s \sigma (T_{ss} + 273.2)^4 \quad (37)$$

3.2.3 Turbulent fluxes

The parametrizations of the sensible and latent heat fluxes (SH and LE respectively) are presented in the following.

Sensible heat flux (SH)

The sensible heat flux can be estimated with (Dingman 2002):

$$SH = c_a \rho_a \frac{k^2}{(log(\frac{z_a - z_d}{z_0}))^2} u \cdot (T_a - T_a) \quad (38)$$

where c_a is the eat capacity of air $[kJ(kgK)^{-1}]$, ρ_a is the density of air $[kg\ m^{-3}]$, k^2 is the von Karman's constant (0.41), u is the wind speed, z_a is the height of wind speed and air temperature measurements [m], z_0 is the roughness height [m] and z_d is the zero-displacement height [m].

Latent heat flux (LE)

LE for snow surface temperature less than zero (i.e. $T_{ss} < 0$ ℃) can be calculated with (Dingman 2002):

$$LE = (\lambda_V + \lambda_F) \cdot 0.622(\frac{\rho_a}{P_a})\frac{k^2}{(log(\frac{z_a - z_d}{z_0}))^2} u \cdot (e_a - e_s) \tag{39}$$

where λ_V is the latent heat of vaporization-condensation (2470 $kJ\ kg^{-1}$), λ_F is the latent heat of fusion (335 $kJ\ kg^{-1}$) ($\lambda_F = 0\ kJ\ kg^{-1}$ when $T_{ss} = 0$ ℃), P_a is the air pressure (101.1 kPa), e_a is the vapour pressure in the atmosphere [kPa], e_s is the vapour pressure at the surface [kPa].

In the model the vapour pressure of the air, e_a, and snow, e_s, are set equal to their saturation vapour pressures, e_a^* and e_s^* respectively (eqs. 40 and 41). This assumption implies that the vapour pressure gradient is directed upward (i.e. transportation from the snow to the air) only if the air temperature, T_a, is less than the snow surface temperature, T_{ss}. Then

$$e_a = e_a^* = 0.611 \cdot exp(\frac{17.3 \cdot T_a}{T_a + 273.3}) \tag{40}$$

$$e_s = e_s^* = 0.611 \cdot exp(\frac{17.3 \cdot T_{ss}}{T_{ss} + 273.3}) \tag{41}$$

3.2.4 Ground heat conduction

The ground heat flux, G, is modelled as a small constant (Walter et al. 2005, Corps of Engineers 1956):

$$G = \frac{173}{86400} \tag{42}$$

3.2.5 Heat induced by precipitation

A way of calculating the heat added by precipitation, R, is (Hock 2005):

$$R = \rho_w c_w P_r T_r \tag{43}$$

where c_w is the heat capacity of water (4.19 $kJ\ kg^{-1}K^{-1}$), P_r is the rainfall rate [$m\ s^{-1}$] and T_r is the rain temperature [℃] and assumed equal to T_a.

3.2.6 Cold content

It is estimates as (Skaugen and Saloranta 2015):

$$CC = \rho_w\ c_s\ SWE \cdot \bar{T_N} \tag{44}$$

where c_s is the heat capacity of snow (2.102 $kJ\ kg^{-1}\ K^{-1}$) and $\bar{T_N}$ is the average snow pack temperature [℃].

3.3 Calculation of snow pack- and snow surface temperatures

$\bar{T_N}$ in Eq. 44 is calculated as a weighted average of the air temperature N time steps prior to the current time step. It is assumed that the ground temperature below the snow pack hols 0 ℃.

$$\bar{T_N} = \sum_{i=1}^{N} Y_i T_{a,i} \tag{45}$$

In Eq. 45 the weights Y decrease linearly with time and are calculated as:

$$Y_i = \frac{N - i + 1}{N} \tag{46}$$

The snow surface temperature, T_{ss}, is estimated as the double of $\bar{T_N}$ (Eq. 47).

$$T_{ss} = 2\bar{T_N} \tag{47}$$

During cold days there are often situations where the simulated snow pack temperature is estimated to be much colder than the air temperature and an energy transfer, directed from the air to the snow pack, produces melt (Skaugen and Saloranta 2015). In order to avoid that the model predicts melt in such situations, the net energy change, E, is converted into a snow pack temperature change, $\Delta\bar{T}$ (Dingman 2002):

$$E = \frac{\Delta h_m \rho_w \lambda_f}{\Delta t} \tag{48}$$

$$\Delta\bar{T} = \frac{\Delta t E}{c_s \rho_w SWE} = \frac{\Delta h_m \lambda_f}{SWE c_s} \tag{49}$$

$\bar{T_N}$ is then raised by adding $\Delta\bar{T}$, that in turn involves an increase in T_{ss}. The energy balance is recalculated and the temperature difference between the snow surface and the air is reduced. Moreover, the energy flow direction is changed, from the snow pack to the air. Thus undesired melting under cold conditions does not occur.

4 Data

4.1 Field observations

During a period of 5 days in the snow melt season 2014, 15.05.-20.05, a field campaign was conducted at Filefjell. At NVEs research station there is a 420 m snow course with snow stakes made of bamboo (Stranden and Grønsten 2011). During autumn 2009, 45 snow stakes were placed along the stretch at distances approximately 10 m between them. In spring there were only 34 stakes left, probably due to harsh weather conditions. The 11 lost stakes had not been replaced at the time of the field campaign.

Measurements were performed every 12 hours, starting 15.05 20:00 with the last measurement 20.05 08:00. It took 1-1.5 hours to perform the measurements. The time labelling for each measurement is thus sat to 09:00 or 21:00.

At each stake the snow depth, h_s, was recorded. Density measurements were performed at four stakes by means of the U.S. Federal snow sampler (FS). FS is a long hollow pole that is used to extract snow. The height of the snow is first recorded, and the snow from the FS is weighted.The snow density, ρ_s, is then the mass divided by the volume. The snow water equivalent was computed with

$$SWE\ [mm] = \frac{\rho_s\ [kg\ m^{-3}]}{\rho_w\ [kg\ m^{-3}]} \cdot h_s\ [mm] \tag{50}$$

where the water density, ρ_w, was assumed to be 1000 $kg\ m^{-3}$. The SWE at each stake was found by multiplying the snow height with the average relative density, $\frac{\rho_s}{\rho_w}$, over the four density measurements. The SWE for each time of measurement was taken as the average SWE of the 34 stakes.

In addition to snow measurements temperature profile of the snow was recorded by digging a shaft and measuring the temperature at 10 cm intervals. Cloud cover was recorded by the means of subjective observations of the cloud cover on an international scale classified in eights (Store norske leksikon 2009). Table 3 explains cloud conditions and their corresponding cloud cover value.

Table 3: *Cloud cover scale (Store norske leksikon 2009)*

Cloud cover	Weather condition
$0/8 - 1/8$	Clear
$1/8 - 3/8$	Lightly cloudy
$3/8 - 5/8$	Partly cloudy
$5/8 - 8/8$	Cloudy

The SWE from field measurements were evaluated against the SWE automatically recorded by the snow weight Møen2525 (described in section 4.2.3). The SWE obtained from manual snow measurements with FS has an accuracy of ± 10 %. When comparing the results with automatically recorded values ± 10 % of the deviations can be explained with the uncertainty in the manual measurements (Fjeldheim and Barfod 2013). Results of the field campaign are given in ch. 5.

4.2 Data and model evaluation

seNorge_eb was evaluated in two steps, following the same procedure for both 3 hour and 24 hour resolution. seNorge_eb was first run as it was set up, with precipitation and temperature as the only input data. The snow pack temperature was calculated with N set to 8 time steps (i.e. 24 hours) on 3 hour resolution and 5 time steps (i.e. 5 days) on 24 hour resolution. The performance of seNorge_eb was evaluated with observed data in terms of its ability to simulate both melt rates and individual components (i.e. incoming solar radiation, atmospheric and terrestrial long-wave radiation, wind, snow surface temperature and air vapour pressure). Due to low data quality of the outgoing solar radiation the albedo could not be evaluated (explained in section 4.2.2).

In the second step parametrizations and variables were, one at the time, substituted with automatically observed data from Filefjell with the aim of assessing the effect each replacement had on simulated snow melt rates. Finally all additional input data, except for relative humidity that did not cover the 2011-melt season as did the others, were simultaneously included as input data.

4.2.1 Data

The data used and their function (input and/or evaluation) together with the instrument they were recorded and corresponding accuracy as stated by the manufacturer are given in table 4. The data were retrieved from NVEs database Hydra II, and their assigned database number and archive are specified in appendix A.

Table 4: *Accuracy and source of automatically observed variables used as input (In.) and/or evaluation (Ev.) of the model on 3 hour and 24 hour resolution. RH: relative humidity, L_a: atmospheric long-wave radiation, L_t: terrestrial long-wave radiation, $S\downarrow$: incoming solar radiation, SWE: snow water equivalent, T_{ss}: snow surface temperature.*

Measured variable	Use	Instrument	Accuracy	Height	Source
Meteo. data					
Precipitation [mm]	In.	Geonor T200B	± 0.3 mm	2 m	MET
Temperature [℃]	In.	Pt100-element	± 0.3 ℃	2 m	MET
Wind [$m\ s^{-1}$]	Ev./In	Gill Windobserver II	±2 %, 12 $m\ s^{-1}$	10 m	MET
RH [%]	Ev./In.	Campbell Scientific CS215	±4 %, 0-100 %	3.3 m	NVE
Radiation data					
L_a [$W\ m^{-2}$]	Ev./In.	Kipp & Zonen CNR4	±10 %	2.7 m	NVE
L_t [$W\ m^{-2}$]	Ev./In	Kipp & Zonen CNR4	±10 %	2.7 m	NVE
$S\downarrow$ [$W\ m^{-2}$]	Ev./In	Kipp & Zonen CNR4	±10 %	2.7 m	NVE
Snow data					
SWE [m]	Ev.	Møen2525	± 0.2 mm	0 m	NVE
T_{ss} [℃]	Ev./In	Kipp & Zonen CNR4	±10 %	2.7 m	L_t/NVE

Data of 24 hour resolution were aggregated from hourly data and averaged from 00:00 to 00:00. The value of a certain day is thus the average from the previous 24 hours. For precipitation the daily values are accumulated precipitation from the previous 24 hour. The same principle applies to the 3 hour resolution data and they have time labels 00:00, 03:00, 06:00, 09:00, 12:00, 15:00, 18:00 and 21:00. All data used were checked

for outliers and missing data. Missing data occur when more than 80 % of the data in a given time step are missing, meaning that for a 3 hour interval 3/3 hourly data must be present, and 20/24 for a 24 hour interval, in order to not have missing data for a given event. Continuity was a requirement for the data that were used as input. In cases were only a few consecutive time steps (generally from 1 to 5) had missing data the average value from the 2 closest observations was used as substitution. The time periods of the data used as input and/or evaluation (Table 4) are given in Table 5. Due to gaps of missing values in the data sets the data series cover different periods. The effect of the data uncertainty on the model results are discussed in section 7.1.

Table 5: *Time period of the data given in Table 4.*

Measured variable	**Period - 3 hour resolution**	**Period - 24 hour resolution**
Precipitation	06-10-2010 03:00 - 30-06-2014 21:00	01-10-2010 00:00 - 30-06-2014 00:00
Temperature	06-10-2010 03:00 - 30-06-2014 21:00	01-10-2010 00:00 - 30-06-2014 00:00
Relative humidity	06-10-2011 03:00 - 30.06.2012 21:00	01-10-2011 00:00 - 30.06.2012 00:00
Wind	06-10-2010 03:00 - 30-06-2014 21:00	01-10-2010 00:00 - 30-06-2014 00:00
$S\downarrow$	06-10-2010 03:00 - 25-05-2011 09:00	01-10-2010 00:00 - 25-05-2011 00:00
L_a	06-10-2010 03:00 - 25-05-2011 09:00	01-10-2010 00:00 - 30-06-2011 00:00
L_t	06-10-2010 03:00 - 25-05-2011 09:00	01-10-2010 00:00 - 30-06-2011 00:00
SWE	06-10-2010 03:00 - 30-06-2014 21:00	01-10-2010 00:00 - 30-06-2014 00:00
T_{ss}	06-10-2010 03:00 - 25-05-2011 09:00	01-10-2010 00:00 - 30-06-2011 00:00

4.2.2 Remarks to data

This section addresses how the input data in Table 4 were included in seNorge_eb. As mentioned earlier turbulent fluxes can be measured by eddy-correlation techniques. At Filefjell, however, there is no such installation due to the difficulty of operating the equipment. Therefore these fluxes are expressed in terms of parametrizations and evaluated by substituting meteorological components of the parametrizations with observed data (i.e. snow surface temperature, wind and relative humidity).

Correcting for undercatch
Undercatch of precipitation in the form of snow has long been reported as a problem at Filefjell, already in 1975 by Furmyr and after NVEs station was upgraded (Furmyr 1975; Fjeldheim and Barfod 2013). The precipitation data used in this thesis are affected by undercatch. Upon correcting the precipitation data, Furmyr's (1975) recommendations of a correction factor of 2.2 for snow was used as a guidance. Each season was tuned individually with the aim that the simulated and observed SWE at the start of each melting season should be equal in value.

Solar radiation
Outgoing solar radiation is measured at Filefjell but was not used in this thesis due to obvious errors in the data set; In too many cases the outgoing solar radiation was larger than the incoming solar radiation. Thus the observed albedo (i.e. ratio of incoming to outgoing solar radiation) could nor be used to evaluate the model.

Upon calculating snow melt seNorge_eb considers the net solar radiation and not incoming and reflected radiation as individual components (Eq. 10). When observed incoming solar radiation was included as input data, net incident solar radiation was calculated from observed incoming solar radiation, $S\downarrow_{obs}$, and simulated albedo, A:

$$S = S\downarrow_{obs}(1 - A) \tag{51}$$

Snow surface temperature
At NVEs station at Filefjell there is installed a rod with temperature loggers at different heights, 0, 0.05, 0.15, 0.30, 0.55 m above the ground. From previous analysis of the temperature sensors on the rod it had been concluded that not until the snow depths reaches $0.65 - 0.70$ m the sensor at height 0.55 m is unaffected by the air temperature (Ree and Stranden 2014). Because there must be layer of snow above the upper most logger such that it is the snow temperature and not the air temperature that is being recorded, the temperature data from these loggers are not suitable for evaluating the snow surface temperature, T_{ss}, calculated by seNorge_eb. Due to this issue the simulated T_{ss} was evaluated using observed T_{ss} derived from automatically observed terrestrial long-wave radiation, L_t). In the parametrization of L_t) (Eq. 37), T_{ss} is included. An observed variable of T_{ss} [°C] was thus derived from Eq. 37:

$$T_{ss} = (\frac{L_t}{\varepsilon_s \sigma})^{1/4} - 273.2 \tag{52}$$

Wind speed
Wind speed is being recorded at both MET and NVE stations. Upon evaluating the turbulent fluxes the constant wind speed of 1.75 $m\ s^{-1}$ was replaced with observed wind data from METs station, since both precipitation and temperature data were from this station. At METs station wind speed is measured 10 m above the ground. In the model, however, it is assumed a measuring height of 2 m. When running the simulations with observed wind the height of wind measurement, z_a, was thus changed from 2 m to 10 m.

Relative humidity
seNorge_eb assumes that the atmospheric vapour pressure included in the latent heat flux (LE) is saturated at all times. Thus, except for situations where the air temperature, T_a, is less than the snow surface temperature, T_{ss}, there will be no energy transfer from the snow to the atmosphere and no evaporation on dry days. Observed relative humidity (RH) data were included with the aim of evaluating how it affects the latent heat flux.

The vapour pressure was evaluated by including observed RH in Eq. 39, multiplying e_a with RH:

$$LE = (\lambda_V + \lambda_F) \cdot 0.622(\frac{\rho_a}{P_a})\frac{k^2}{(log(\frac{z_a - z_d}{z_0}))^2} u \cdot (RH \cdot e_a - e_s) \tag{53}$$

4.2.3 Model evaluation criteria

At NVEs station there are several instruments that record SWE: a gamma sensor, various snow pillows and the snow weight Møen2525 (shown in Fig. 2). In reports about the snow data from the research station published by staff at the section for glaciers, ice and snow, Møen2525 has, however, in all the evaluated snow seasons proven to be the most reliable automatically observation of SWE at the station (Stranden and Grønsten 2011,

Fjeldheim and Barfod 2013, Ree and Stranden 2014) and thus it is throughout this thesis regarded as the "true" SWE. Møen2525 is designed by Knut Møen at NVE, and it is a squared 5 m X 5 m snow weight made out of a decking installed on top of 4 weighing cells (Stranden and Grønsten 2011). seNorge_eb's ability to simulate melt rates during the spring melt seasons of 2011-2014 was evaluated against snow melt rates derived from observed SWE recorded by Møen2525.

The model was run with all seasons in one run. The snow melt rates were only evaluated for events in the main snow melt season in April/May.

The following conditions defined the events in the main ablation period for which the simulated snow melt rates were to be evaluated:
− both simulated and observed SWE were larger than zero
− melt was predicted by seNorge_eb and/or observed

The start of the evaluation period was defined as the date on which the observed SWE had its maximum value before it entered a period of continuously decrease towards 0 mm. The first day on which the observed SWE was 0 mm defined the end on the snow melt season and the evaluation period. We wanted the simulated and observed SWE to have equal starting points and to be equal in value at the start of the melt season. Therefore, seNorge_eb was modified so that at each defined start date of the melt season, the simulated SWE was set equal to the observed SWE. All other simulated variables remained unchanged. The snow melt rates were evaluated according to a set of criteria described in the following.

Assessing the performance of a hydrological model requires the hydrologist to make estimates of how close the simulation results are to observations (Krause et al. 2005). These estimates can be subjective and/or objective, of which the most fundamental approach of the former is visual inspection and for the latter quantitative estimates of the error term (i.e. objective efficiency criteria). Upon assessing the performance of the energy balance model used in this thesis both subjective and objective estimates were used. The development of the simulated and observed SWE throughout the melt season was visually inspected with the aim of detecting how possible deviations behaved. Moreover, three objective efficiency criteria were used to evaluate the melt rates: mean error (ME), root mean squared error (RMSE) and Nash-Sutcliffe model efficiency criteria (NS). Their respective formula are given in eqs. 54,55 56, with observed O and predicted P values and number N of events. ME and RMSE were also used to assess how well the model simulated incoming solar radiation, atmospheric and terrestrial long-wave radiation and snow surface temperature.

ME, or bias, is a measure of the systematic error in the simulations and indicates to what degree the simulations consistently over or underestimate relative to the observations (Han 2011). RMSE includes both systematic and random errors and avoids the cancellation of errors of opposite sign, thus larger errors are being emphasised and smaller errors tend to be neglected (Krause et al. 2005: Han 2011) . NS has a range of $(-\infty, 1)$ with 1 as perfect fit. If the efficiency is lower than zero (i.e. $NS < 1$) the mean value of the observations would have been a better predictor than the model, and with $NS = 0$ the simulated values are as accurate at he mean of the observations (Krause et al. 2005: Han 2011) .

$$ME = \frac{1}{N}\sum_{i=1}^{N} P_i - O_i \tag{54}$$

$$RMSE = \sqrt{\frac{1}{N}\sum_{i=1}^{N}(P_i - O_i)^2} \tag{55}$$

$$NS = 1 - \frac{\sum_{i=1}^{N}(O_i - P_i)^2}{\sum_{i=1}^{N}(O_i - \bar{O}_i)^2} \tag{56}$$

In addition to visual inspection and the quantitative model efficiency criteria, simple linear regression were performed with temperatures above -3 ℃ as predictor and residuals (i.e. simulated melt rates minus observed melt rates) to see if temperature could explain any deviations. The same was done for day numbers .

In the next chapters, 5 and 6, the results from the field campaign and simulations are presented.

5 Results: Field campaign

The snow melt season of 2014 at Filefjell was well underway when we started the field campaign 15 May around 20:00. During five days of field work, 15-20 May, there was a noticeable decrease in the amount of snow in the study area (Fig. 5).

The snow melted more rapidly around the bamboo stakes compared to the rest of the terrain, caused by the light brown colour of the stakes The same pattern was observed wherever there was some vegetation sticking up from the ground. Snow temperatures were zero at all depths in the snow shaft.

Snow depth was measured along the snow stakes according to the method described in section 4.1. Resulting SWE and automatically observed (Møen2525) SWE are seen in Fig. 6, corresponding values and melt rates are given in Table 6. Data manually collected in the field gave a lower SWE compared to automatically observed SWE at all times of measurement. In spite the differences between manually and automatically observed SWE, their corresponding melt rates were, however, quite consistent with coinciding high and low values (Table 6).

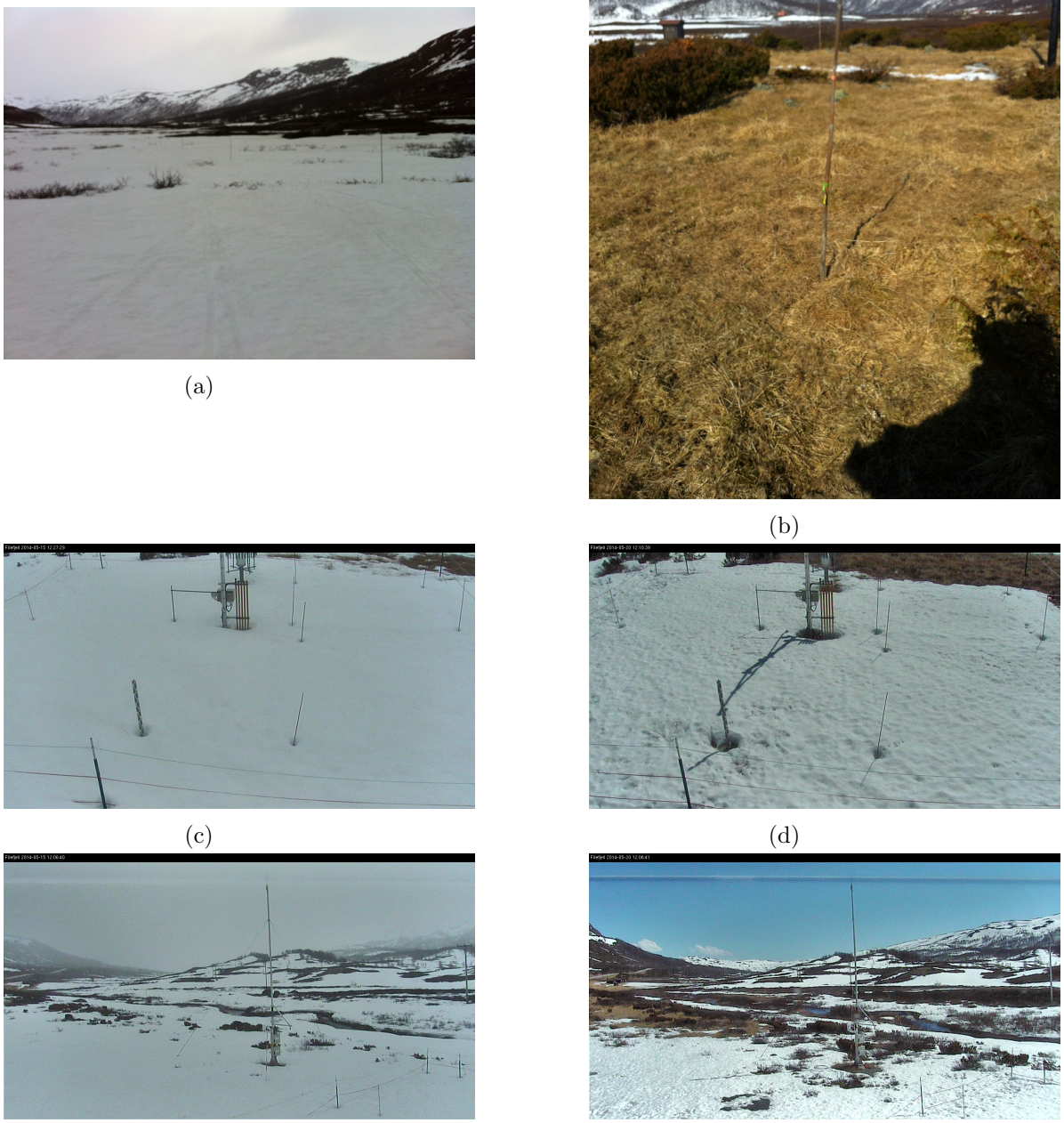

(a) (b) (c) (d) (e) (f)

Figure 5: *End and start of field campaign, Filefjell May 2014. a) Snow stakes 15.05.2014 20:00, b) Snow stakes 20.05.2014 09:00, c) NVEs measuring station 15.05.2014 13:00 (NVE), d) NVEs measuring station 20.05.2014 13:00 (NVE), e) View from METs mast 15.05.2014 12:00 (NVE), f) View from METs mast 20.05.2014 12:00 (NVE).*

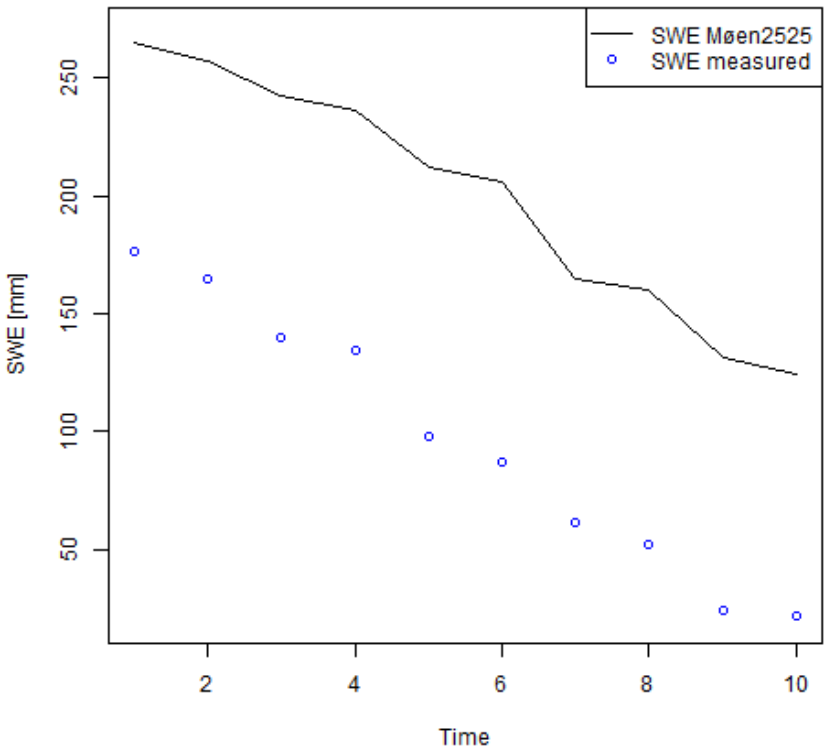

Figure 6: *SWE Filefjell 15.05.2014 21:00 - 20.05.2014 09:00, at 12 hour intervals. SWE Møen2525 are point observations and SWE measured are averaged values from the snow stakes.*

Table 6: *Results from field campaign. Snow depth (SD) and SWE given in mm at 12 hours intervals, thus melt is in mm/12 hour. MO: Manually observed (average of 34 stakes), AO: automatically observed with snow weight Møen2525.*

Date	Cloud cover	ρ_s/ρ_w	SD MO	SWE MO	Melt MO	SWE AO	Melt AO
15.05.2006 21:00		0.47	373	176		265	
16.05.2006 09:00	8/8	0.47	349	165	11	257	8
16.05.2006 21:00	6/8	0.44	316	140	26	242	15
17.05.2006 09:00	7/8	0.45	296	134	5	236	6
17.05.2006 21:00	4/8	0.41	240	98	36	212	24
18.05.2006 09:00	4/8	0.41	211	87	11	206	6
18.05.2006 21:00	0/8	0.50	122	61	27	165	41
19.05.2006 09:00	7/8	0.49	106	52	9	160	5
19.05.2006 21:00	4/8	0.45	53	24	28	131	29
20.05.2006 09:00	1/8	0.49	45	22	2	124	7

6 Results: Model simulations

The precision of seNorge_eb was evaluated in terms of snow melt rates for the snow melt seasons 2011-2014 and in terms of its parametrizations of the radiation elements and selected parameters. The evaluation period of the two latter varied according to the data quality of the observed time series.

The start of the snow melt season was defined as the date on which the SWE (from Møen2525) had its maximum value before the main ablation period started. When SWE was 0 mm, the snow melt season was said to halt. The corresponding periods for the snow melt seasons 2011-2014 are given in Table 7.

Table 7: *Start and end of melt snow melt seasons.*

	2011	2012	2013	2014
Start	9.04	27.04	5.05	19.04
End	1.05	30.05	20.05	25.05

In the following the simulation results are presented first for the 3 hour resolution and then for the 24 hour resolution (sections 6.1-6.2). Both sections start with the simulation results with precipitation and temperature as only input data, followed by seNorge_eb's ability to simulate radiation fluxes (i.e. incoming solar radiation, atmospheric and terrestrial long-wave radiation) or different parameters (wind, snow surface temperatures and vapour pressure). Then follows the results from the simulations with additional input data, where observed radiation fluxes and parameters substitute parametrizations or variables one at the time (sections 6.3-6.4).

Table 8 explains the abbreviations used for the different input data in the simulations. In all simulations precipitation and temperature are included (e.g. SimSinn includes both precipitation, temperature and observed incoming solar radiation), but additional input vary.

Table 8: *Abbreviations used with input data in the simulations. P: precipitation, T: air temperature, $S\downarrow$: incoming solar radiation, L_a: atmpospheric long-wave radiation, L_t: terrestrial long-wave radiation, T_{ss}: snow surface temperature, RH: relative humidity.*

Abbreviation	Input data
SimPT	P, T
SimSinn	P, T, $S\downarrow$
SimL	P, T, L_a, L_t
SimW	P, T, wind
SimTss	P, T, T_{ss}
SimRH	P, T, RH
SimAll	P, T, $S\downarrow$, L_a, L_t, wind, T_{ss}

T_{ss} is included in the terrestrial long-wave radiation, L_t, (Eq. 37) and in the turbulent fluxes (SE and LE, eqs. 38 and 39). In this section the simulated SWE where observed T_{ss} is included (i.e. SimTss) is thus affected by a change in these fluxes. The individual fluxes are analysed only in terms of changes in SH and LE due to the small effect the observed T_{ss} has on L_t.

6.1 Precipitation and temperature - 3 hour resolution

In this section the results of seNorge_eb's precision in predicting snow melt rates are presented, along with its ability to simulate individual components. Input and output data are on 3 hour resolution.

6.1.1 Correcting for undercatch

The 3 hour resolution precipitation data used as input were corrected for undercatch. Before correcting the precipitation data for undercatch of snow seNorge_eb predicted a too low SWE (Sim P untuned) compared to observed SWE (Fig. 7). After having tuned the correction factor individually for each snow season (Sim P tuned) the observed and simulated SWE were more consistent.

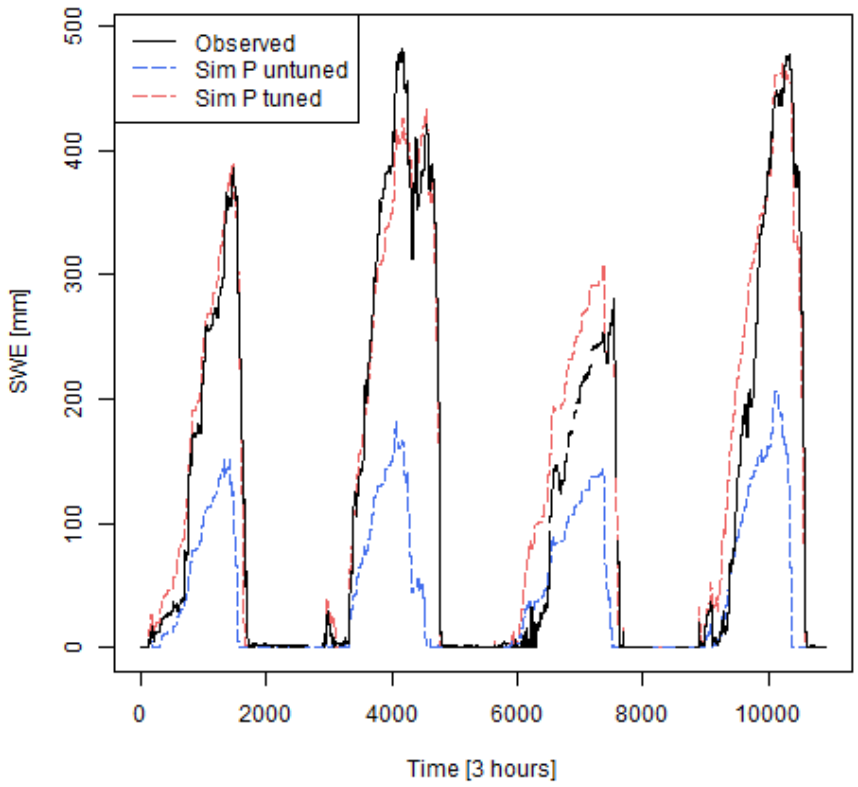

Figure 7: *Oct. 2010-June 2014:, 3 hour resolution: Observed SWE and SWE before and after having corrected the precipitation data for undercatch of snow (P untuned/ P tuned).*

The snow correction factor for each season are given in Table 9. Each season ended up with an unique value so that the SWE at the start of the melt season was roughly the same. There are, however, deviations between simulated SWE with tuned precipitation and observed SWE during the snow season as a whole. For 3 hour resolution this is

most evident for the seasons 2011-2012 and 2012-2013 (second and third snow season in Fig. 7).

Table 9: *Snow correction factor, 3 hour resolution.*

	2010-2011	2011-2012	2012-2013	2013-2014
Snow correction factor	2.2	2.15	1.85	1.922

6.1.2 Model performance

seNorge_eb was run with temperature and precipitation on 3 hour resolution. The simulated and observed SWE are given in Fig. 8. By visual inspection the model managed to reproduce the SWE in the main melt seasons (i.e. periods stated in Table 7) of 2012-2014. In 2011 the simulated SWE deviated the most from the observed values, and underestimated in the start and overestimated at the end of the season. This impression fits with the evaluation of the snow melt rates, for which 2011 is clearly the worst season.

By looking at the distribution of the energy fluxes throughout the melt seasons 2011-2014 (Fig. 9) net solar radiation was the largest contributor to melt, and the total energy followed its cycle. Long-wave radiation was mainly negative and had a mean negative value (Table 10) thus counteracting melt. The turbulent fluxes (SH and LE) were the second largest fluxes. Ground heat (G) and heat input by rain (R) were negligible. Events where the cold content (CC) was negative coincide with a halt in melt (figs. 8 and 9). In 2014 CC exceeded SH and LE in terms of average values in the melt season (Table 10).

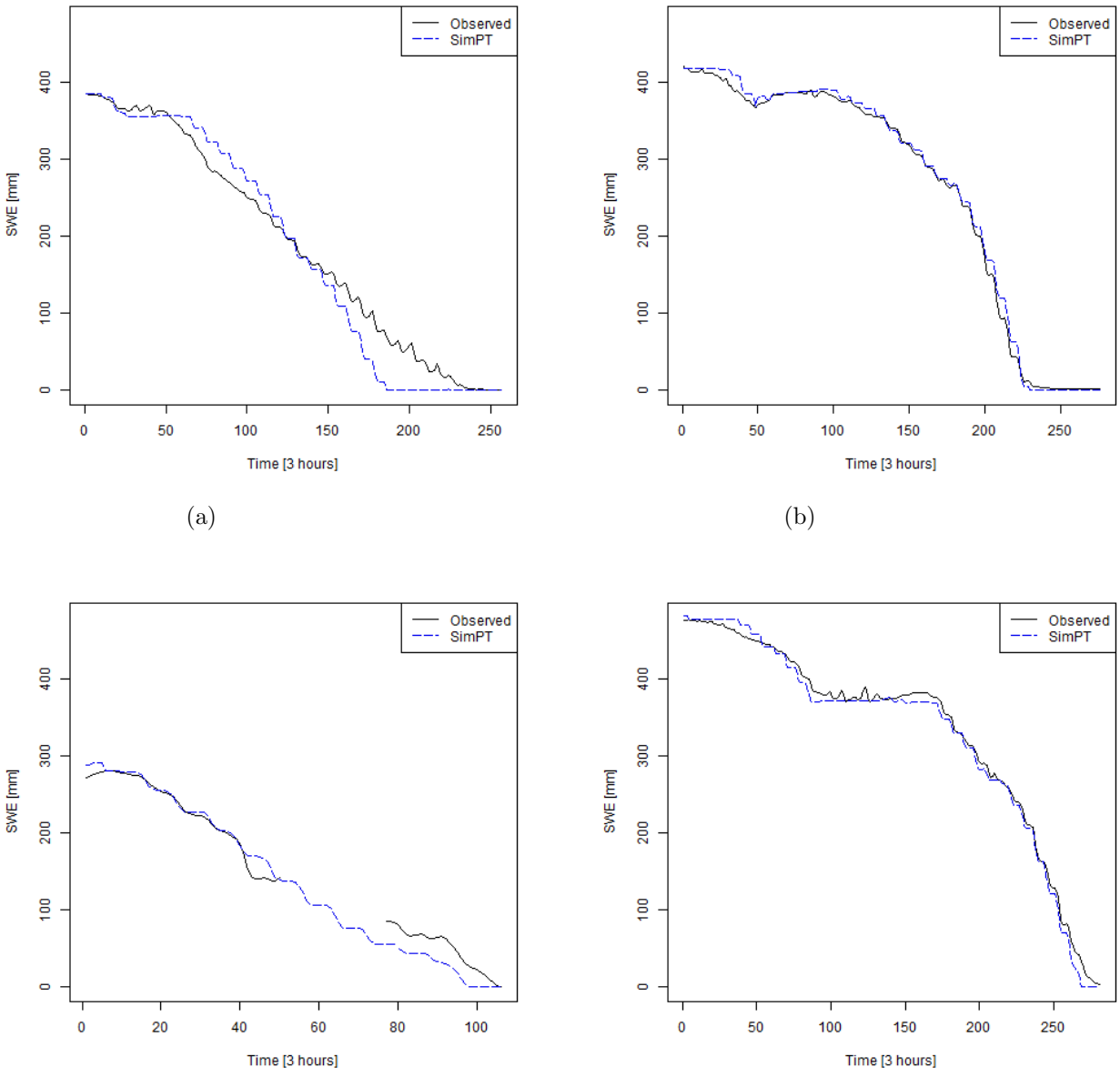

Figure 8: *SWE during melt seasons of 2011-2014, 3 hour resolution. Observed SWE is from Møen2525. a) 2011, b) 2012, c) 2013, d) 2014.*

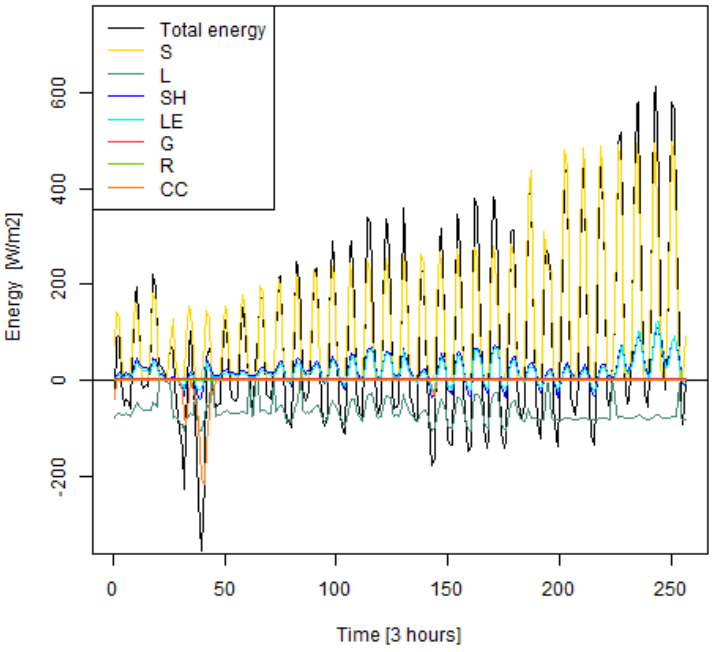
Total energy
S
L
SH
LE
G
R
CC
Energy [W/m2]
-200
0
200
400
600
0
50
100
150
200
250
Time [3 hours]

(a)

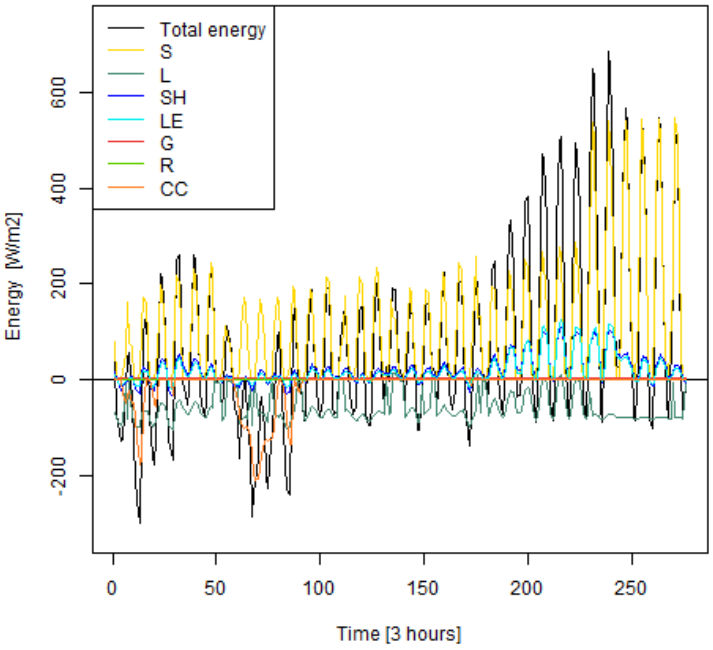
Total energy
S
L
SH
LE
G
R
CC
Energy [W/m2]
-200
0
200
400
600
0
50
100
150
200
250
Time [3 hours]

(b)

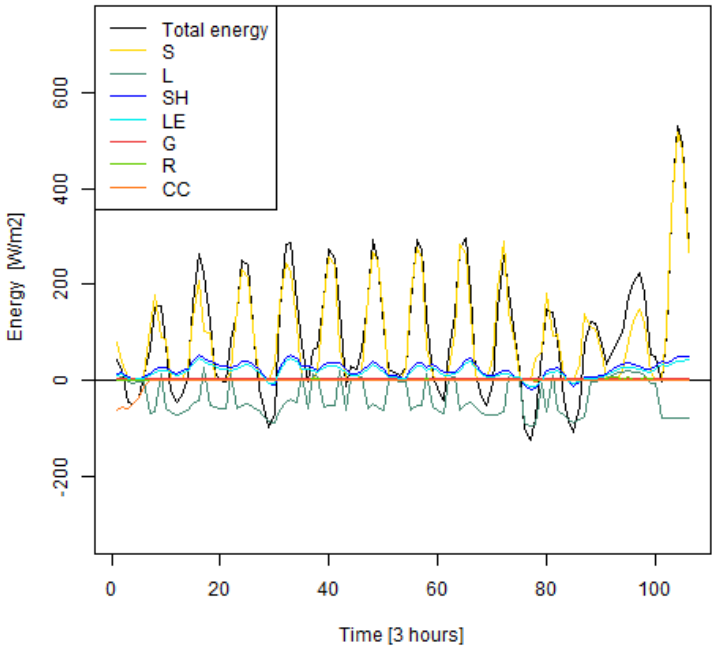

(c)

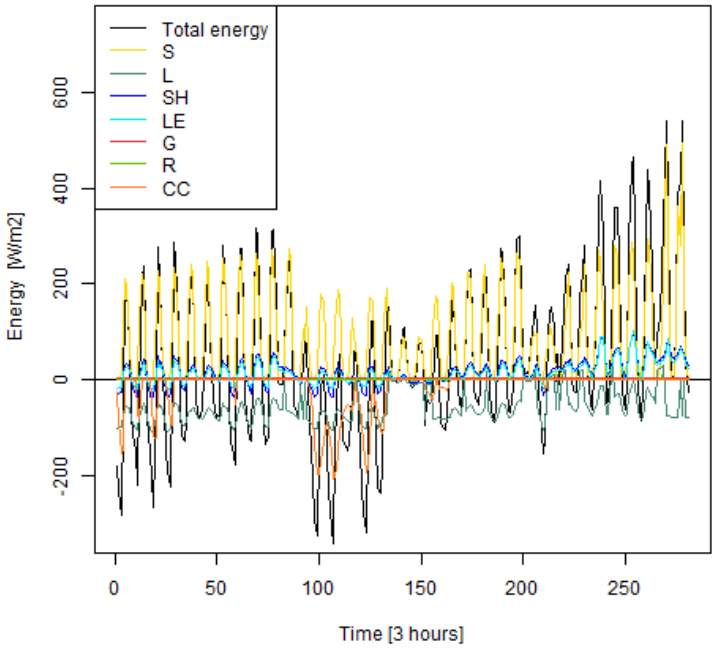

(d)

Figure 9: *Distribution of energy fluxes and total energy available for melt during melt season. 3 hour resolution. a) 2011, b) 2012, c) 2013, d) 2014.*

Table 10: *Mean values of energy fluxes in Fig. 9, melt season of 2011, 3 hour resolution.*

Energy flux	2011	2012	2013	2014
Total energy	81.60	74.90	95.40	45.70
S	110.50	108.30	92.80	86.20
L	-65.00	-59.40	-37.60	-55.70
SH	20.60	20.10	22.60	16.70
LE	18.40	18.50	17.80	14.90
G	2.00	2.00	2.00	2.00
R	0.00	0.00	0.50	0.10
CC	-5.00	-14.60	-2.60	-18.50

seNorge_eb predicted the melt rates with highest precision in 2012 in terms of NS and RMSE, followed by 2013 with the best ME (Table 11).

Table 11: *Model evaluation snow melt rates,3 hour resolutions. Events were both simulated and observed $SWE > 0$ mm and simulation and/or observation indicate melt are evaluated.*

	All seasons	2011	2012	2013	2014
No. of residuals	587	148	179	63	197
NS	-0.17	-0.99	0.35	0.03	-0.60
ME [mm]	0.89	1.10	0.81	0.22	1.10
RMSE [mm]	3.20	3.10	2.80	3.40	3.70

seNorge_eb overestimated the snow melt rates (Fig. 10). This is in accordance with the values of ME in Table 11. The largest portion of the residual melt rates falls within the range $-0.5 - 0.0$ mm (Fig. 10b), but the majority of the residuals are positive.

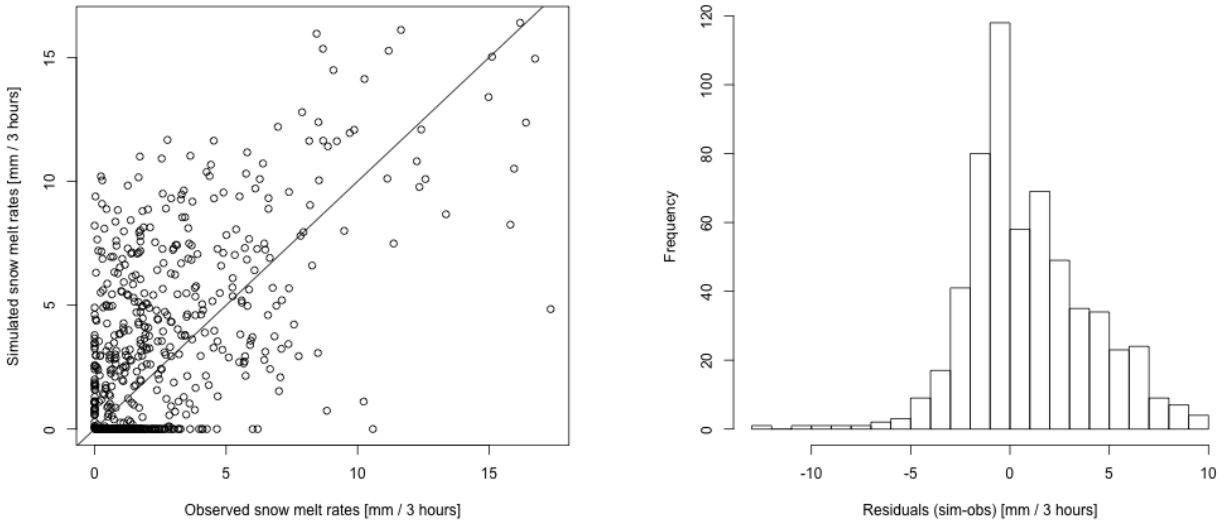

(a) (b)

Figure 10: *Melt rates 2011-2014, 3 hour resolution. a) Observed vs. simulated melt rates, b) Histogram of residuals (sim-obs) of melt rates melt.*

Simple linear regression indicated that temperature was significant in explaining the residual values, however day number was not (Fig. 11).

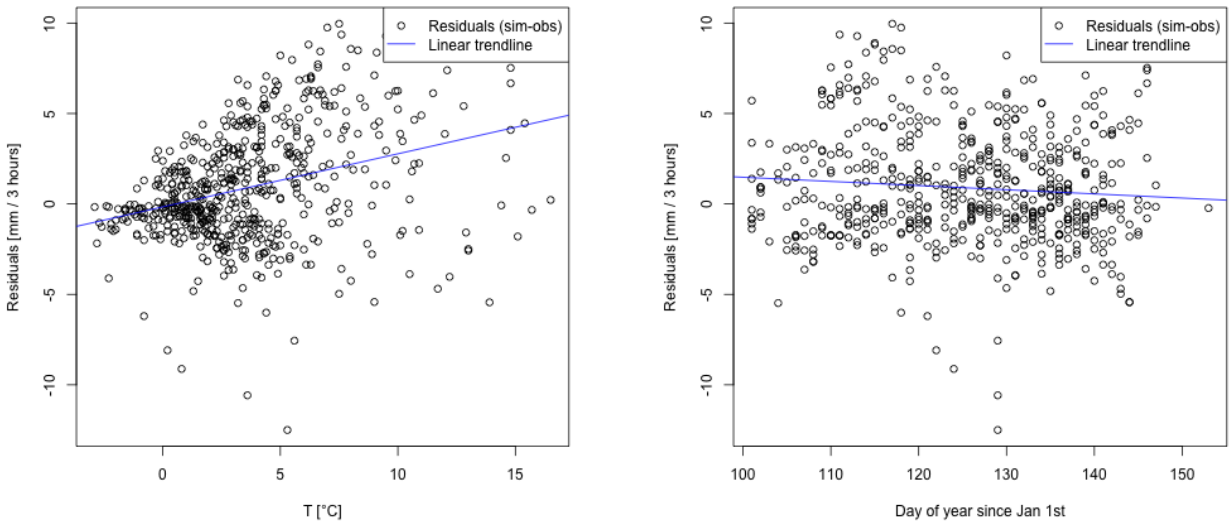

(a) (b)

Figure 11: *a) Temperature vs. residuals, p-value* $2.20 \cdot 10^{-16}$. *b) Day number vs. residuals, p-value 0.039. 3 hour resolution.*

6.1.3 Incoming solar radiation

Observed data of incoming solar radiation was for 3 hour resolution continuous only for the snow season 2010-2011 (i.e. October to May). seNorge_eb consistently underestimated incoming solar radiation on cloudy events and overestimated on clear events (Fig. 12 and Table 12). Clear and cloudy events combined gave a slight overestimation of 5.64 $W\ m^{-2}$. The maximum simulated values were slightly larger than the observed values, although few in number (Fig. 12).

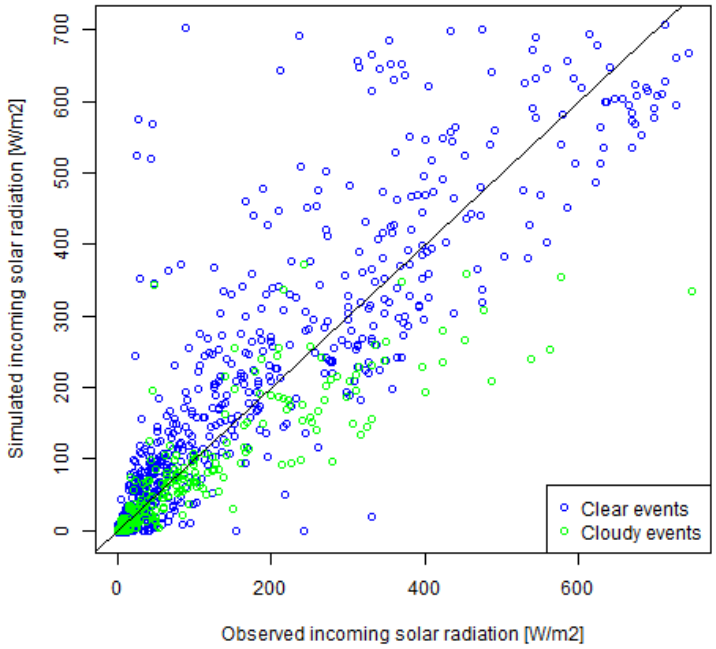

Figure 12: *Snow season 2010-2011, 3 hour resolution. Observed vs. simulated incoming solar radiation (Eq. 10).*

Table 12: *Error of events in Fig. 12, simulated vs. observed incoming solar radiation, 3 hour resolution.*

	All events	Cloudy events	Clear events
ME $[W\ m^{-2}]$	5.46	-11.20	12.50
RMSE $[W\ m^{-2}]$	65.60	49.40	71.50

6.1.4 Long-wave radiation

Observed data of atmospheric and terrestrial long-wave radiation was for 3 hour resolution continuous only for the snow season 2010-2011. Atmospheric long-wave radiation, L_a, was clearly underestimated by the model on clear events and slightly overestimated on cloudy events (Fig. 13 and Table 13). In sum, seNorge_eb underestimated L_a with a mean error (ME) of $-37.40\ W\ m^{-2}$.

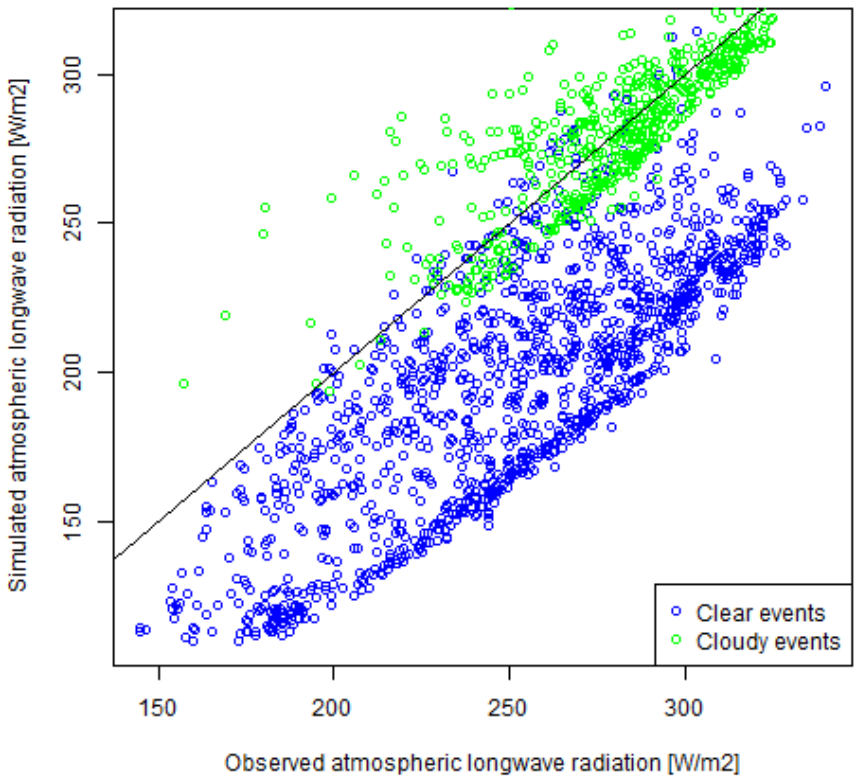

Figure 13: *Snow season 2010-2011, 3 hour resolution. Observed vs. simulated atmospheric long-wave radiation (Eq. 36).*

Table 13: *Error of events in Fig. 13, simulated vs. observed atmospheric long-wave radiation, 3 hour resolution.*

	All events	Cloudy events	Clear events
ME $[W\ m^{-2}]$	-37.40	1.32	-55.10
RMSE $[W\ m^{-2}]$	51.50	16.70	61.20

Terrestrial long-wave radiation, L_t, does not depend on cloud cover and thus ME and RMSE were not divided according to weather conditions. ME was only slightly underestimated $-0.85\ W\ m^{-2}$, and RMSE $14.50\ W\ m^{-2}$. For a number of events the simulated L_t took on a value of about $316\ W\ m^{-2}$, whereas the corresponding observed values ranged roughly between $270 - 330\ W\ m^{-2}$ (Fig. 14). These events occured during the snow melt season when a simulated snow surface temperature of 0 ℃ resulted in a constant L_t.

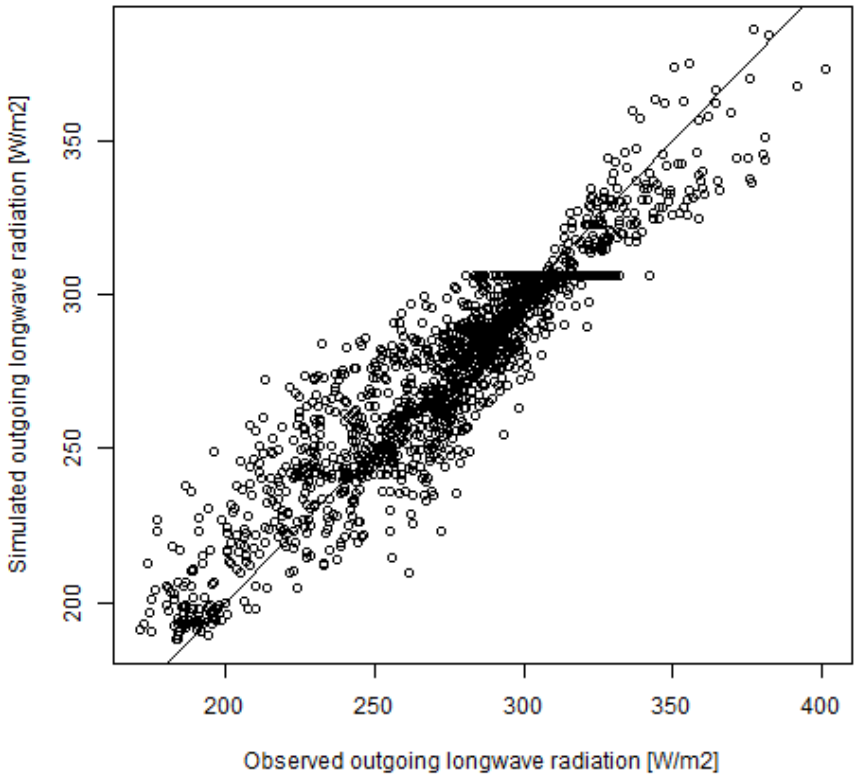

Figure 14: *Observed vs. simulated terrestrial radiation (Eq. 37) on events with SWE* > 0*, 3 hour resolution. ME:* $-0.85\ W\ m^{-2}$*, RMSE: 14.50* $W\ m^{-2}$.

The net simulated long-wave radiation (i.e. L_a, minus L_t) was underestimated due to the mean underestimation of L_a.

6.1.5 Wind

The constant wind speed in seNorge_eb of 1.75 $m\ s^{-1}$ was generally less than the observed wind speed during the period Oct. 2010 − June 2014 (Fig. 15). The mean observed wind speed was 3.74 $m\ s^{-1}$. Note that the observed values are measured at 10 m height and 1.75 $m\ s^{-1}$ is assumed to have a measuring height of 2 m.

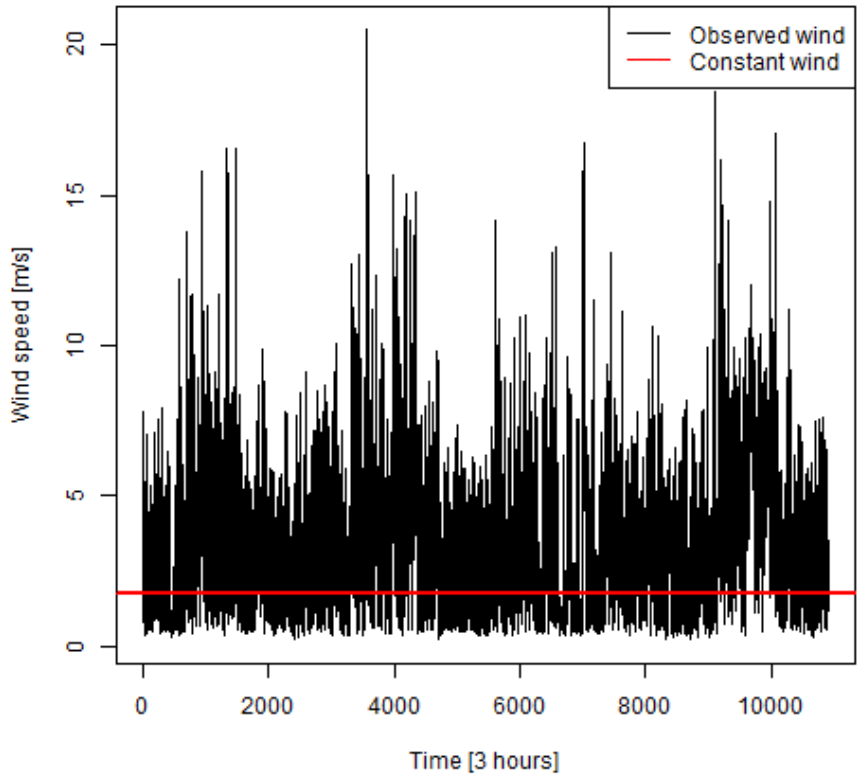

Figure 15: *Observed vs. simulated wind speed, all year Oct. 2010 − June 2014, 3 hour resolution.*

6.1.6 Snow surface temperature

The snow surface temperature, T_{ss}, simulated by seNorge_eb compared to observed values derived from terrestrial radiation had a good correspondence with a ME of -0.06 ℃ and RMSE of 3.68 ℃. Since T_{ss} theoretically cannot exceed 0 ℃, observed values of T_{ss} were capped at 0 ℃. During the melt season of 2011 observed T_{ss} was below 0 ℃ on more events than the simulated T_{ss} (Fig. 16).

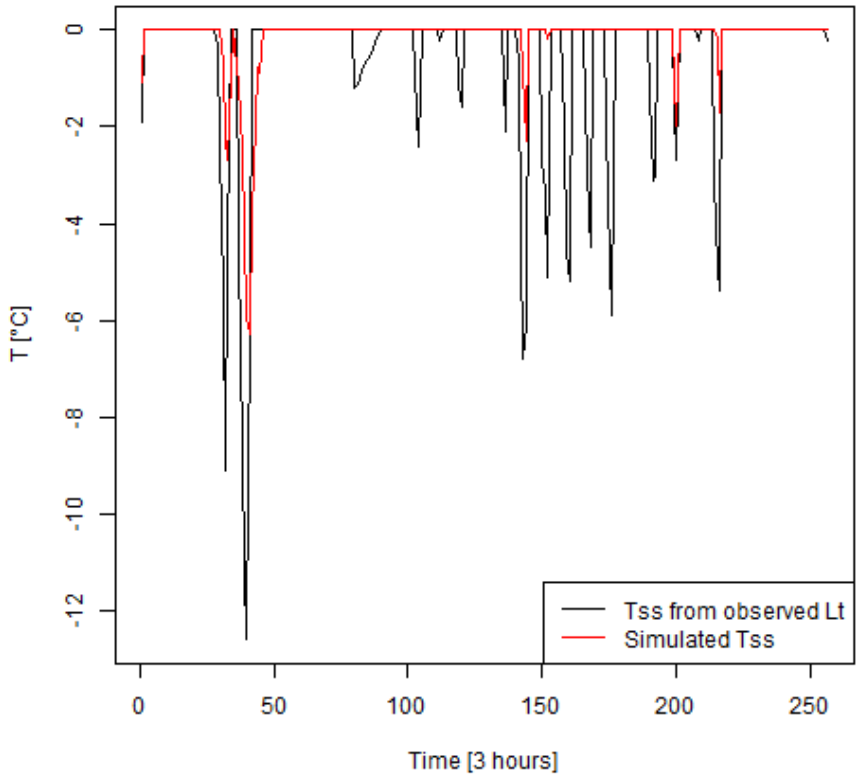

Figure 16: *Observed and simulated snow surface temperature during melt season of 2011, 3 hour resolution.*

6.1.7 Relative humidity

Observed relative humidity (RH) data were included in the parametrization of the latent heat flux to evaluate the vapour pressure. The air vapour pressure was at Filefjell almost never saturated (i.e. RH < 100 %, Fig. 17), with a mean value of 83.49 %.

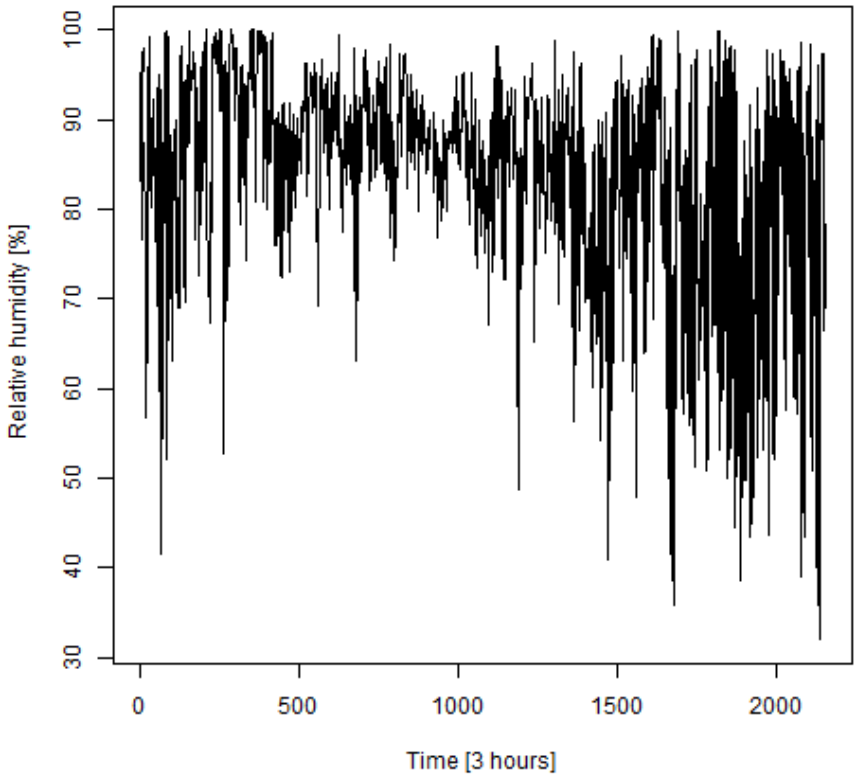

Figure 17: *Observed relative humidity Oct. 2011- May 2012, 3 hour resolution. Mean value: 83.49 %*

6.1.8 Summary: model performance - 3 hour resolution

After having run the model with 3 hour resolution precipitation and temperature data the impression was that the model performed well in predicting snow melt rates (Table 11). The main energy source for melt was net solar radiation (i.e. the sum of the net solar and long-wave radiation) . The net radiation exceeded the turbulent fluxes, which were the second largest contributors to snow melt. By looking at how seNorge_eb simulated individual fluxes deviations were discovered. Incoming solar radiation was on average slightly overestimated and underestimated on cloudy events. Net long-wave radiation was highly underestimated caused by underestimation of the atmospheric long-wave radiation. The constant wind speed of 1.75 $m\ s^{-1}$ was for the majority of the events an underestimation compared to observed wind data (note that the measuring height differ). Observed and simulated snow surface temperatures, T_{ss}, showed on average good agreement. When observed T_{ss} was capped at 0 °C it was in the ablation period of 2011 more often negative than simulated T_{ss} or more negative when both were negative. Relative humidity was for the majority of events less than 100 %.

6.2 Precipitation and temperature - 24 hour resolution

In this section the results of the investigations of seNorge_eb precision in predicting snow melt rates and individual parameters on 24 hour resolution are presented.

6.2.1 Correcting for undercatch

The precipitation data were corrected for snow undercatch. The correction factor for each season are given in Table 14, and they are all close to 2. The simulated SWE before and after the correction (untuned/tuned P) is shown in Fig. 18 together with observed SWE.

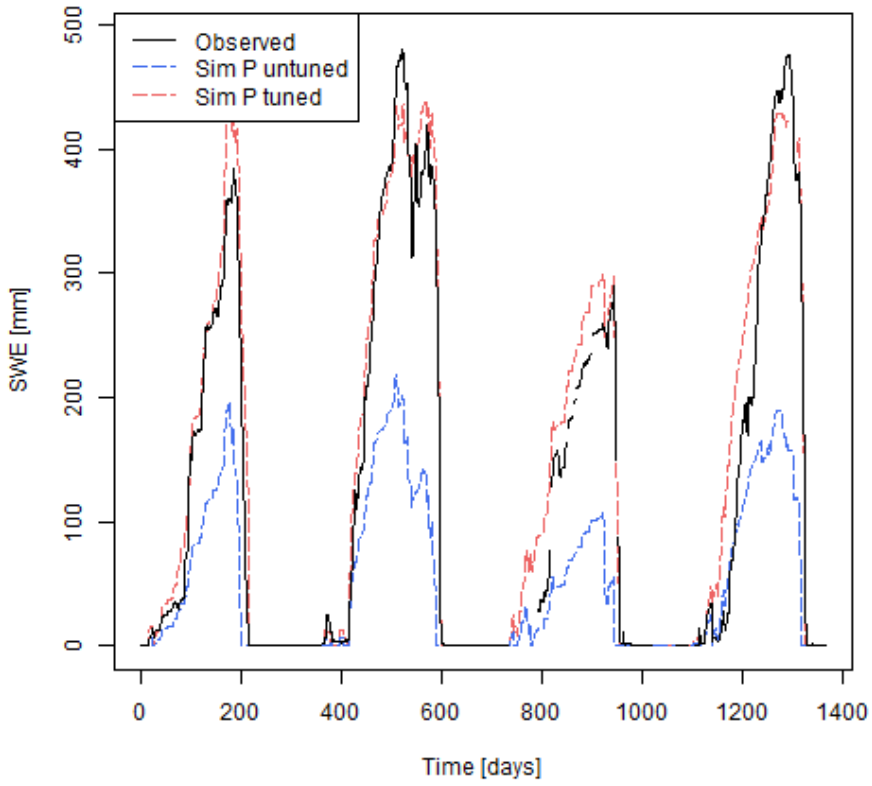

Figure 18: *Oct. 2010-June 2014:, 24 hour resolution: Observed SWE and SWE before and after having corrected the precipitation data for undercatch of snow (P untuned/ P tuned).*

The snow correction factor for each season is given in Table 14. Each season ended up with an unique value so that the SWE at the start of the melting season was roughly the same.

Table 14: *Start and end of melt snow melt seasons.*

	2010-2011	2011-2012	2012-2013	2013-2014
Snow correction factor	2.2	1.9	2.1	1.75

6.2.2 Model performance

By visual inspection of Fig. 19 the simulated SWE had the best fit compared to observed values from snow weight Møen2525 in the melt season of 2013. For the other seasons seNorge_eb simulated a higher SWE compared to observed values.

The total energy available for melt increased as the melt seasons proceed due to the increase in solar radiation (S) (Fig. 20). Cold content (CC) heat input by rain (R) and ground heat flux (G) were all negligible (Fig. 20 and Table 15). In terms of mean simulated values throughout the melt periods 2011-2014 (Table 15) S was the largest contributor to snow melt, followed by the turbulent fluxes (SH and LE), whereas L counteracted melt.

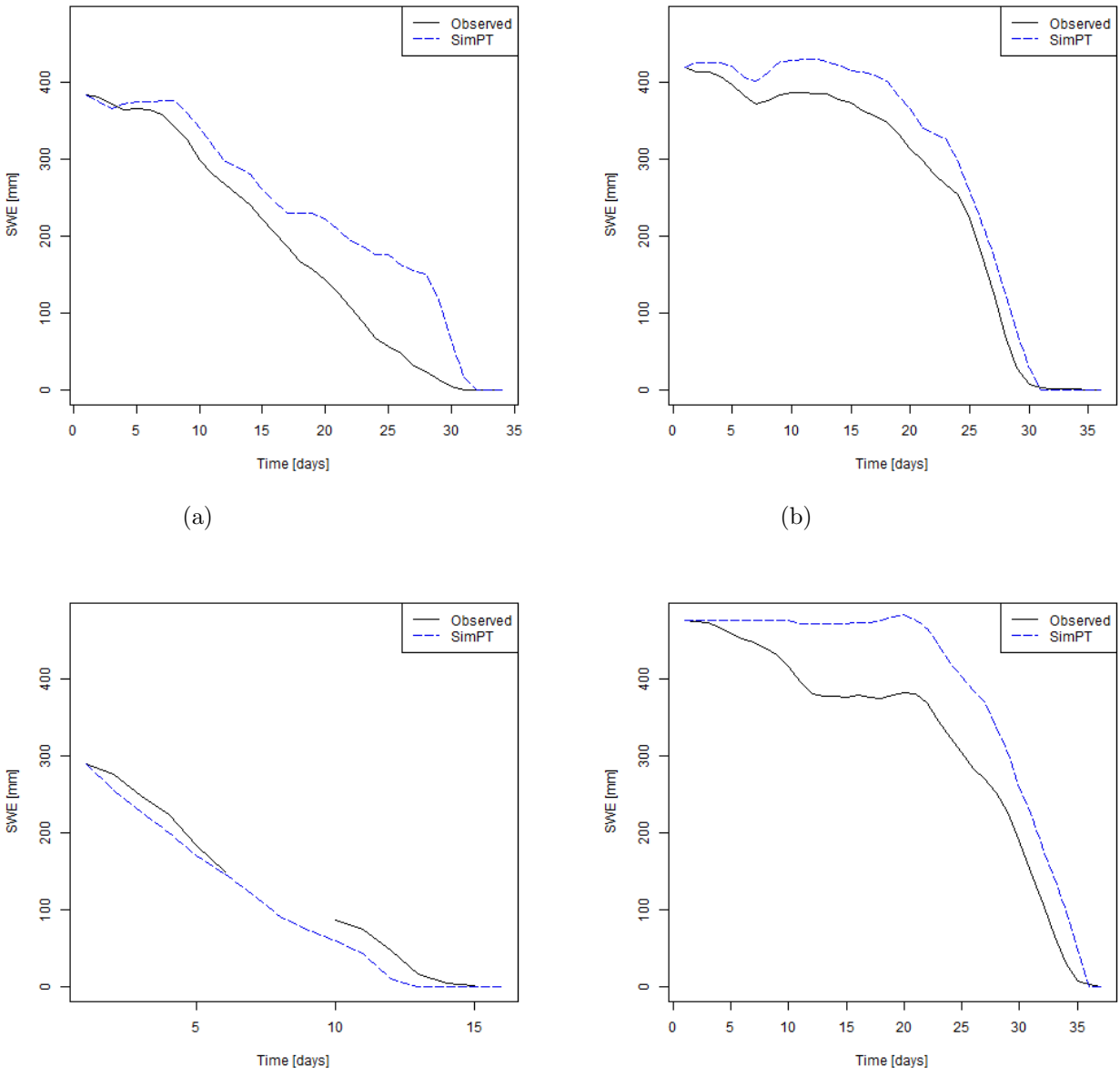

Figure 19: *Observed and simulated SWE during melt seasons of 2011-2014, 24 hour resolution. a) 2011, b) 2012, c) 2013, d) 2014.*

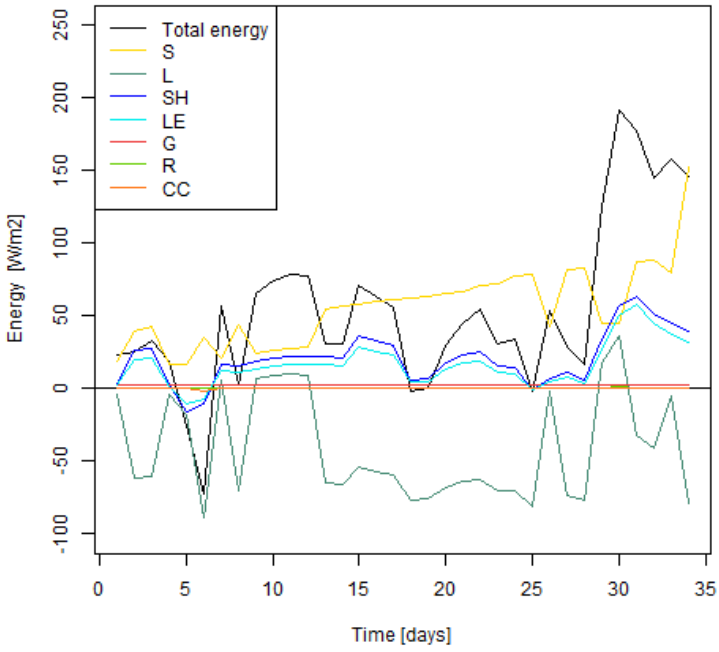
Total energy
S
L
SH
LE
G
R
CC
Energy [W/m2]
250
200
150
100
50
0
-50
-100
0
5
10
15
20
25
30
35
Time [days]

(a)

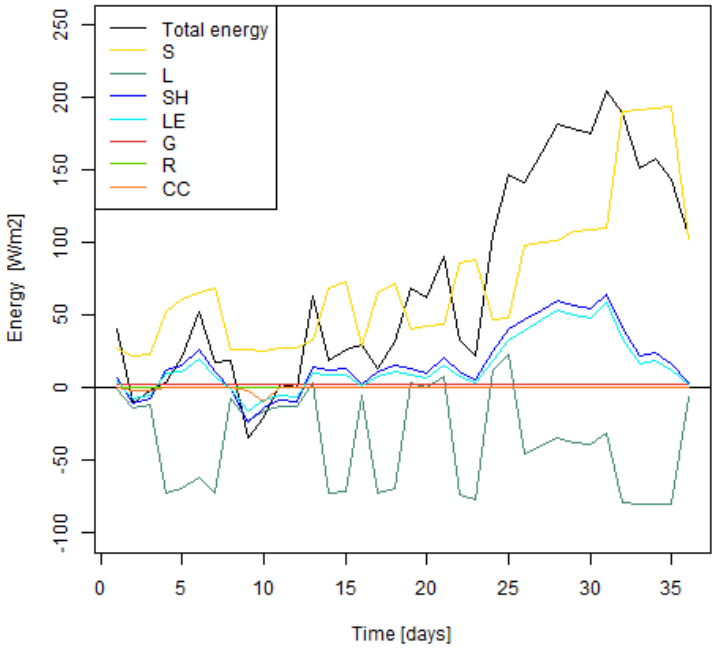
Total energy
S
L
SH
LE
G
R
CC
Energy [W/m2]
250
200
150
100
50
0
-50
-100
0
5
10
15
20
25
30
35
Time [days]

(b)

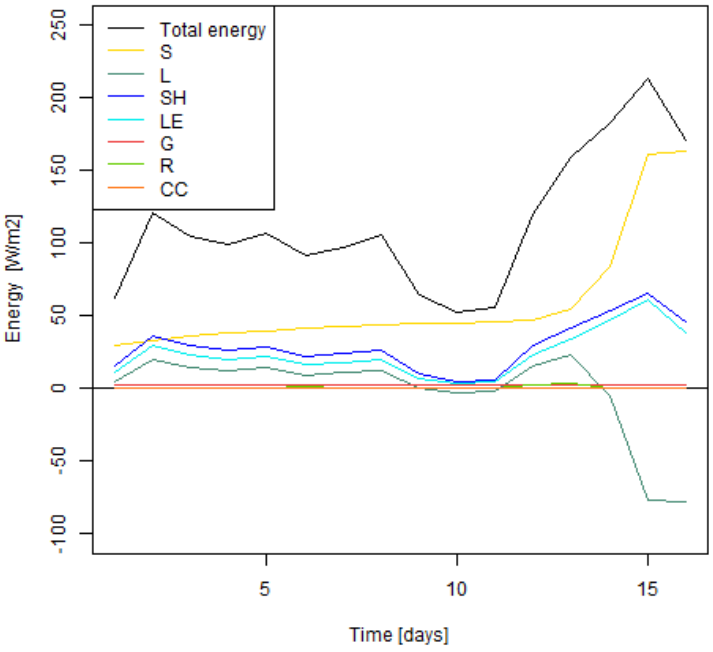

(c)

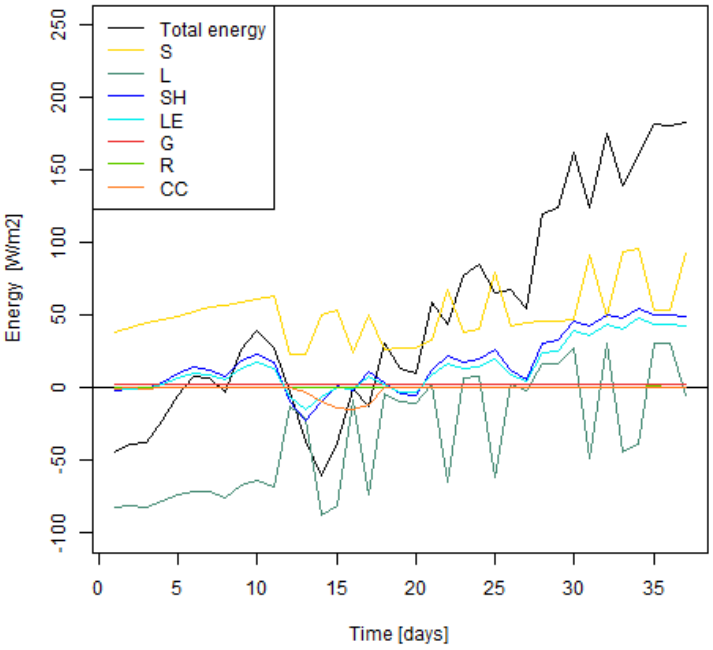

(d)

Figure 20: *Distribution of simulated energy fluxes during melt seasons of 2011-2014, 24 hour resolution. a) 2011, b) 2012, c) 2013, d) 2014.*

Table 15: *Mean value of simulated energy fluxes in snow melt seasons 2011-2014 (Fig. 20), 24 hour resolution.*

	2011	2012	2013	2014
Total energy	54.20	72.10	113.00	50.30
S	55.70	74.70	59.40	51.20
L	-41.00	-36.60	-1.70	-33.00
SH	20.90	17.70	29.10	17.30
LE	16.70	14.80	23.60	14.20
G	2.00	2.00	2.00	2.00
R	0.10	0.00	0.60	0.10
CC	-0.10	-0.40	0.00	-1.50

By evaluating the model according to the evaluation criteria defined in section 4.2.3 the model showed good performance when considering all melt seasons (Table 16), with 2012 being the best season. The number of residuals (i.e. simulated minus observed melt rates) were 98 and thus few in number, particularly in 2013 with only 9 events. The highest frequency of the residuals were negative in value (Fig. 21b).

Table 16: *Model evaluation snow melt rates, 24 hour resolution.*

	All seasons	2011	2012	2013	2014
No. of residuals	98	30	28	9	31
NS	0.31	-3.70	0.72	0.35	0.64
ME	0.42	0.06	0.52	3.70	-0.28
RMSE	10.00	14.00	8.20	11.00	7.90

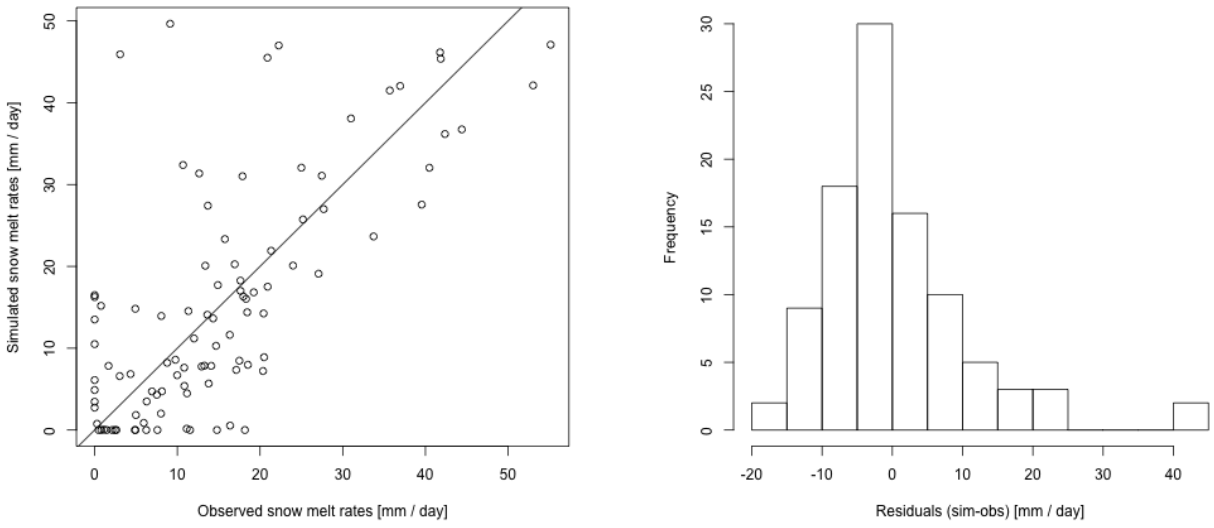

(a) (b)

Figure 21: *Melt rates 2011-2014, 24 hour resolution. a) Observed vs. simulated melt rates, b) Histogram of residuals (sim-obs) of melt rates melt.*

From simple linear regression temperature was found significant in explaining the residual error (i.e. simulated-observed values), whereas day number was not (Fig. 22).

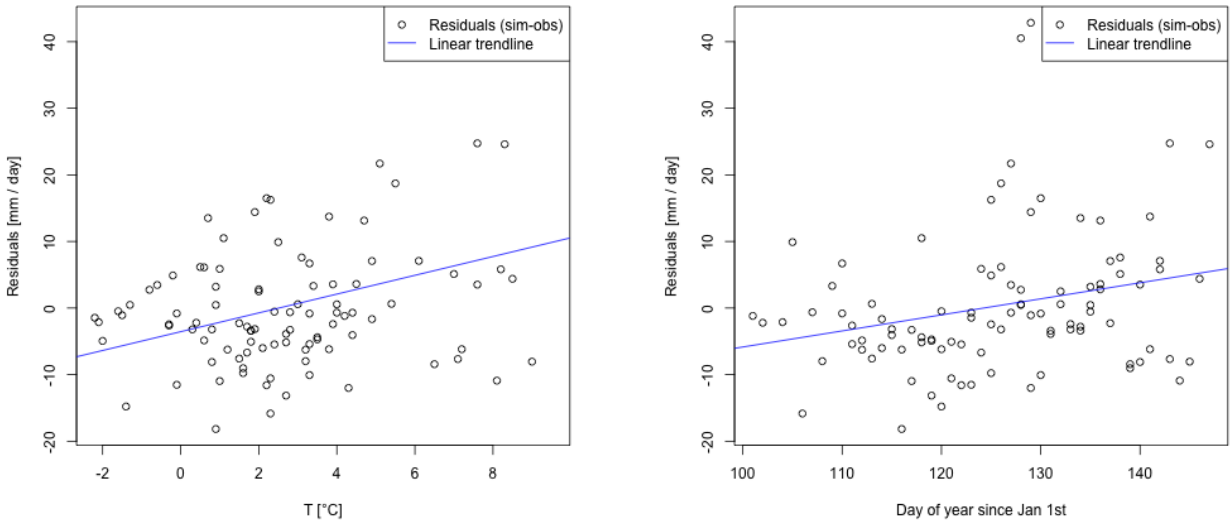

(a) (b)

Figure 22: *a) Temperature vs. residuals, p-value* $1.97 \cdot 10^{-4}$. *b) Day number vs. residuals, p-value 0.011. 24 hour resolution.*

6.2.3 Incoming solar radiation

For all events from October 2010 to May 2011, the simulated incoming solar radiation, $S\downarrow$, was less than the observed values with an upper limit of around 260 $W\ m^{-2}$ on clear events and 150 $W\ m^{-2}$ on cloudy events (Fig. 23). Cloudy events had the highest underestimation with a mean deviation of $-36.10\ W\ m^{-2}$ (Table 17).

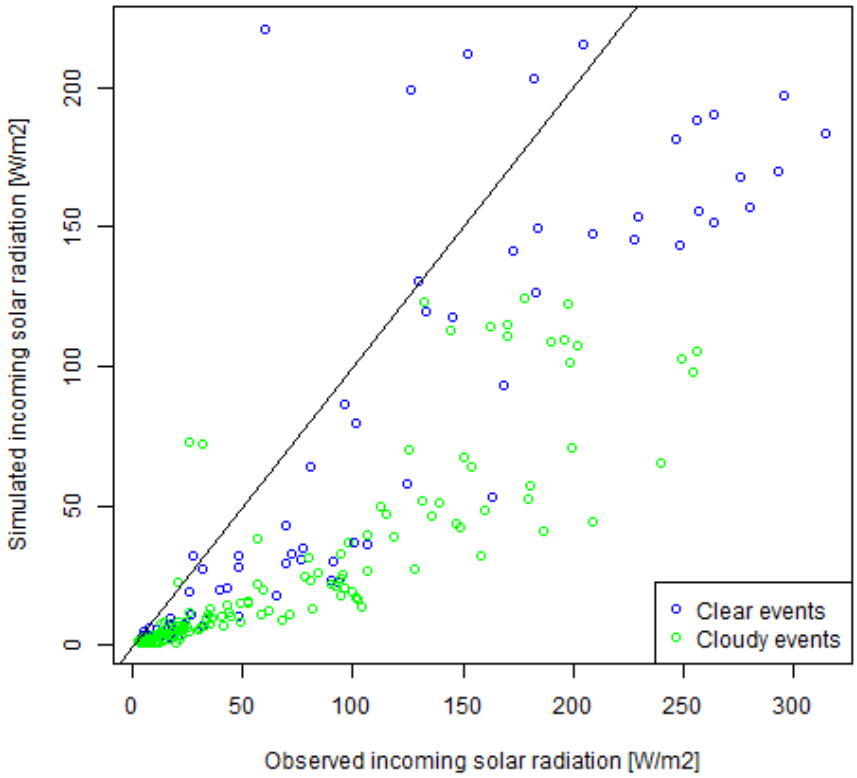

Figure 23: *Observed vs. simulated incoming solar radiation (Eq. 10) Oct. 2010 - May 2011, 24 hour resolution.*

Table 17: *Error of simulated vs. observed incoming solar radiation (Fig. 23), 24 hour resolution.*

	All events	Cloudy events	Clear events
ME [$W\ m^{-2}$]	-36.30	-39.10	-30,70
RMSE [$W\ m^{-2}$]	56.30	57.10	54.70

6.2.4 Long-wave radiation

Atmospheric long-wave radiation, L_a, was underestimated by seNorge_eb with a mean error (ME) of -7.38 $W\ m^{-2}$ and RMSE of 35.10 $W\ m^{-2}$, compared to observed L_a. Taking into account the weather condition revealed that L_a was underestimated on clear events and overestimated on cloudy events (Fig. 24 and Table 18).

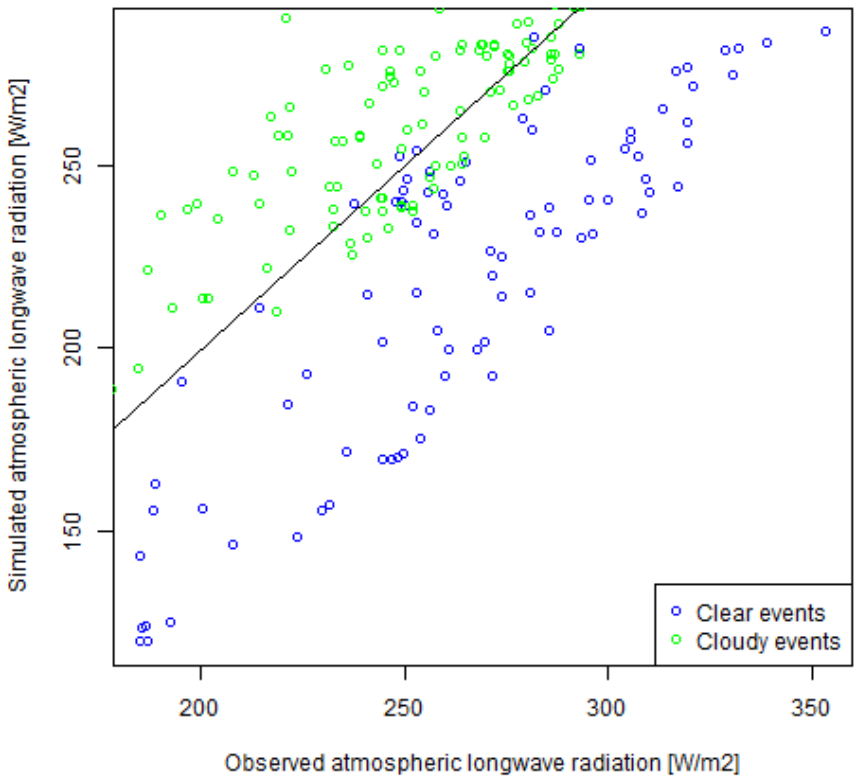

Figure 24: *Observed vs. simulated atmospheric long-wave radiation (Eq. 36), 24 hour resolution*

Table 18: *Error of simulated vs. observed atmospheric long-wave radiation (Fig. 24), 24 hour resolution*

	All events	Cloudy events	Clear events
ME $[W\ m^{-2}]$	-7.38	11.50	-47.80
RMSE $[W\ m^{-2}]$	35.10	21.10	53.90

Terrestrial long-wave radiation, L_t, was slightly overestimated by 5.52 $W\ m^{-2}$ on events with observed snow cover (Fig. 25). The simulated values were 316 $W\ m^{-2}$ for a number of events whereas the observed values varied between approximately 150 $W\ m^{-2}$ to 340 $W\ m^{-2}$. These events took place during the ablation period.

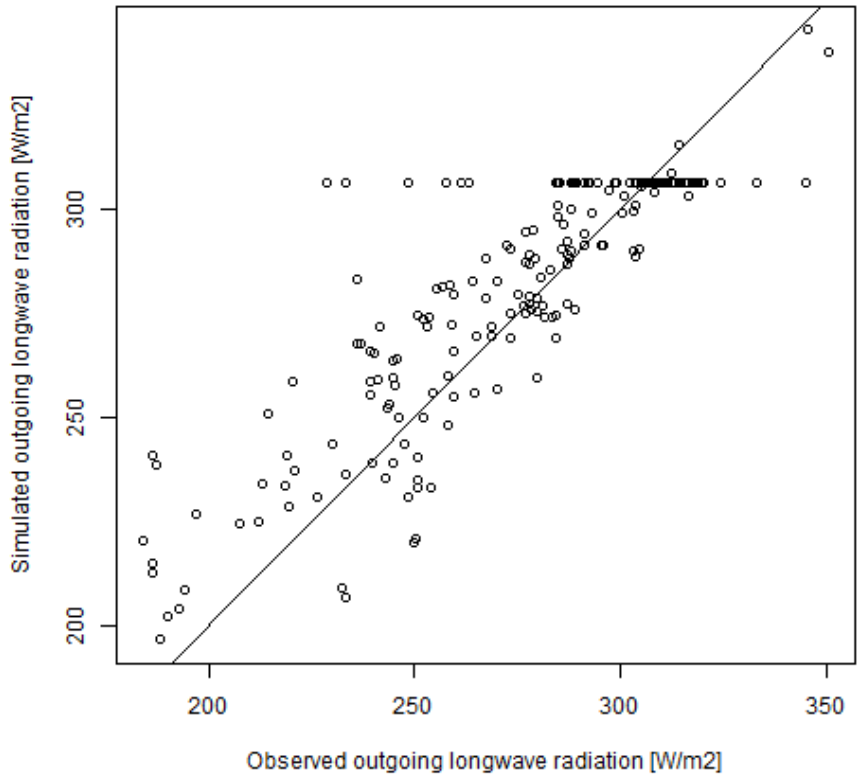

Figure 25: *Observed vs. simulated terrestrial radiation (Eq. 37) on events with observed* $SWE > 0$*, 24 hour resolution. ME: 5.52* $W\ m^{-2}$*, RMSE: 18.40* $W\ m^{-2}$*.*

6.2.5 Wind

The constant wind speed in seNorge_eb of 1.75 $m\ s^{-2}$ was generally less than the observed wind speed during the period Oct. 2010 − June 2014 (Fig. 26) where the mean observed wind speed was 3.75 $m\ s^{-2}$ from daily values. As already mentioned, the observed values are measured at 10 m height and the constant value of 1.75 $m\ s^{-2}$ has in seNorge_eb a measuring height of 2 m.

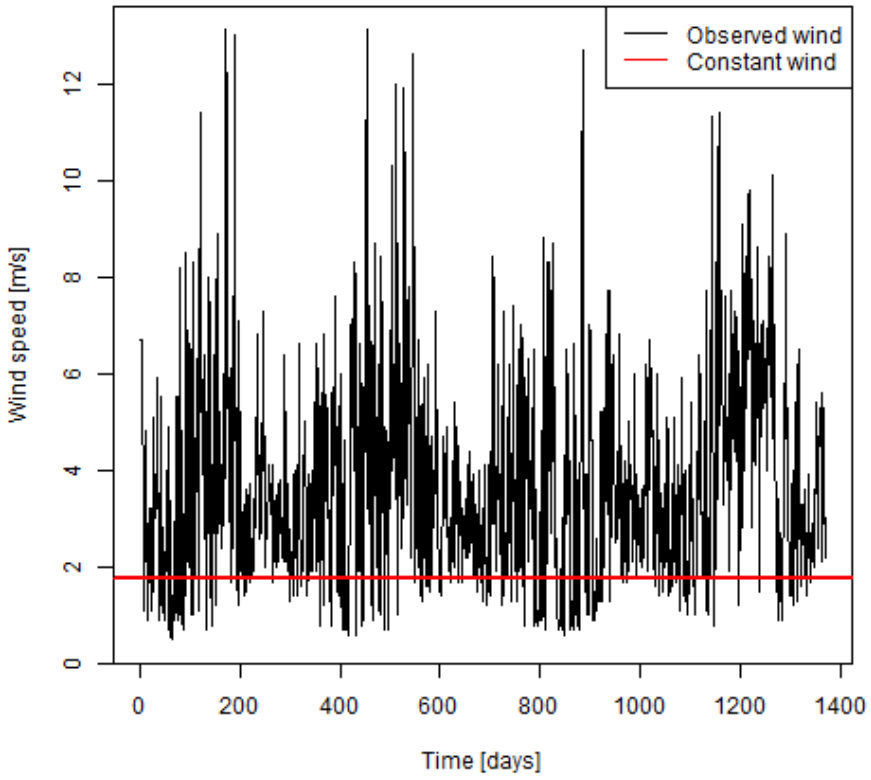

Figure 26: *Wind speed 2011-2014, 24 hour resolution. Constant wind speed of 1.75 m s^{-2} indicated in red.*

6.2.6 Snow surface temperature

Simulated snow surface temperatures, T_{ss}, compared to T_{ss} derived from observed L_t had a ME of 1.47 ℃ and RMSE of 4.69 ℃. Since T_{ss} theoretically cannot exceed 0 ℃ the observed values of T_{ss} were capped at this temperature. Fig. 27 includes the observed T_{ss} with an upper limit of 0 ℃ and the simulated values during the ablation period 2011. The observed T_{ss} on 24 hour resolution was below 0 ℃ on more events than the simulated T_{ss} and more negative on events where both observed and simulated T_{ss} were less than 0 ℃ (Fig. 27).

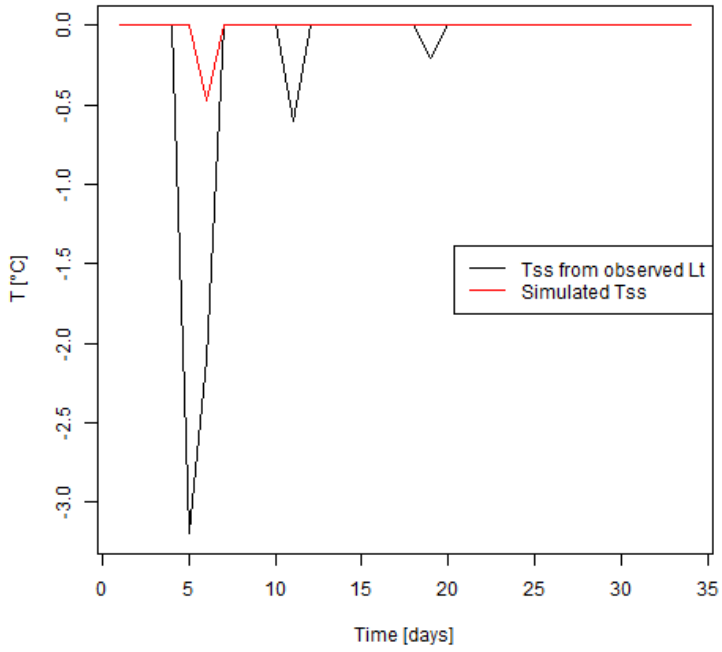

Figure 27: *Observed and simulated snow surface temperature during melt season of 2011, 24 hour resolution.*

6.2.7 Relative humidity

Observed relative humidity (RH) data were included in the parametrization of the latent heat flux to evaluate the vapour pressure. According to Fig. 28 the 24 hour resolution air vapour pressure was at Filefjell never saturated (i.e. RH less than 100 %), with a mean observed RH of 83.55 %.

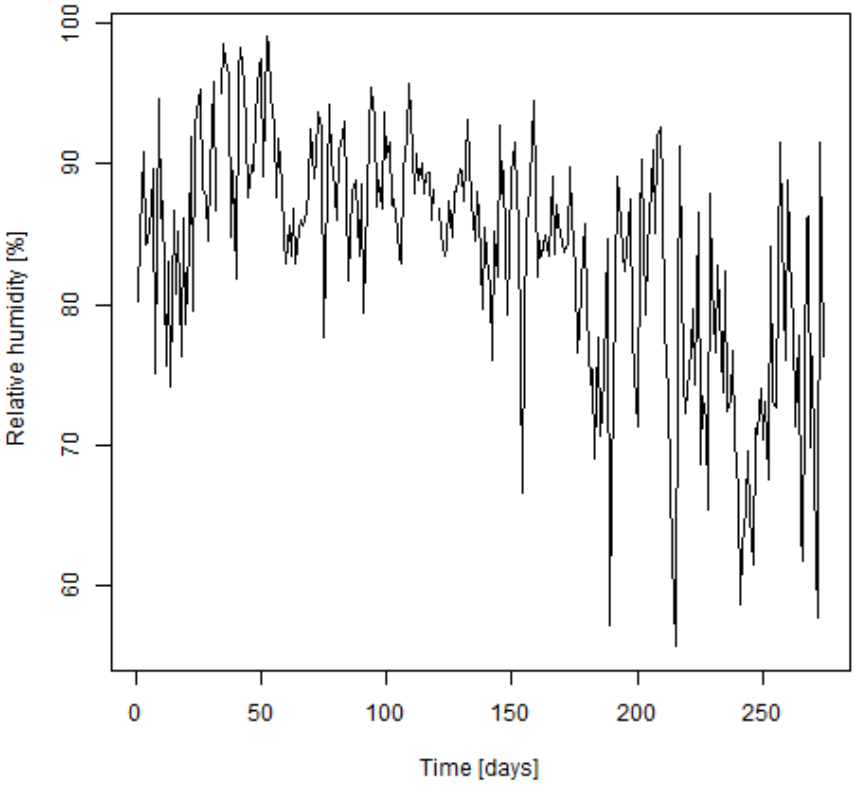

Figure 28: *Observed relative humidity Oct. 2011-May 2012, 24 hour resolution. Mean value: 83.55 %.*

6.2.8 Summary: model performance - 24 hour resolution

After having run seNorge_eb with 24 hour resolution precipitation and temperature data the impression was that the model performed well in predicting snow melt rates (Table 16). The main energy source for melt was net solar radiation (S) that exceeded the the turbulent fluxes (SH and LE), which were the second largest contributors to snow melt.

By looking at how the model simulated individual fluxes and variables large deviations were found. Incoming solar radiation was on average highly underestimated, both on cloudy and clear events. Net long-wave radiation was underestimated (-7.38 $W\ m^{-2}$) in total and overestimated on cloudy events and highly underestimated on clear events. Observed wind was generally larger than the constant wind speed of 1.75 $m\ s^{-1}$ (note that the measuring height differ). Observed and simulated snow surface temperatures, T_{ss}, were only slightly overestimated. When observed T_{ss} values were capped at 0 ℃ the observed values were negative on more events that what was predicted by the model and more negative when both were less than 0 ℃. The relative humidity showed that the air was not saturated at all times.

6.3 Additional input data - 3 hour resolution

In this section the results from simulations on 3 hour resolution with additional input data are presented. The additional input data were included one at the time by substituting the parametrizations of incoming solar radiation, $S\downarrow$, atmospheric and terrestrial radiation, L_a and L_t, and variables of the turbulent fluxes (wind, snow surface temperature, T_{ss}, and relative humidity, RH). One simulation also includes all the additional data, except RH that did not cover the period Oct. 2010- May 2011.

6.3.1 Incoming solar radiation

Observed incoming solar radiation, $S\downarrow$, substituted the part of the parametrization of net incident solar radiation that represents $S\downarrow$ (Eq. 51). The simulated SWE for the snow melt season of 2011, with input data precipitation, temperature and $S\downarrow$, is given in Fig. 29 (SimSinn). Compared to the observed SWE and SimPT, SimSinn underestimated melt in the start of the melt season and overestimated towards the end. Thus, from a visual inspection, including observed $S\downarrow$ did not improve the melt rates.

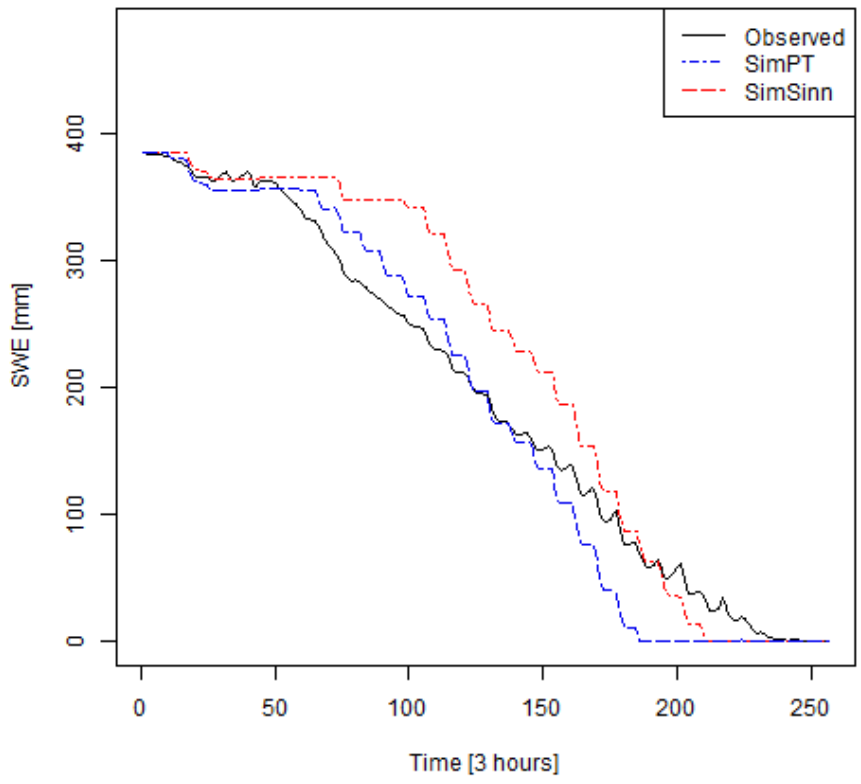

Figure 29: *SWE, snow melt season of 2011, 3 hour resolution. SimPT: precipitation and temperature, SimSinn: precipitation, temperature and incoming solar radiation.*

The distribution of the net solar radiation flux (S) throughout the melt season is shown in Fig. 30, where Ssim is parametrized S, and Sobs includes observed incoming solar

radiation. Ssim underestimated in the middle of the melt season (event 100-180) and was clearly higher than Sobs on other events (e.g. events around 70-80 and 250. Mean values were 110.5 $W\ m^{-2}$ and 94.20 $W\ m^{-2}$ for Ssim and Sobs respectively.

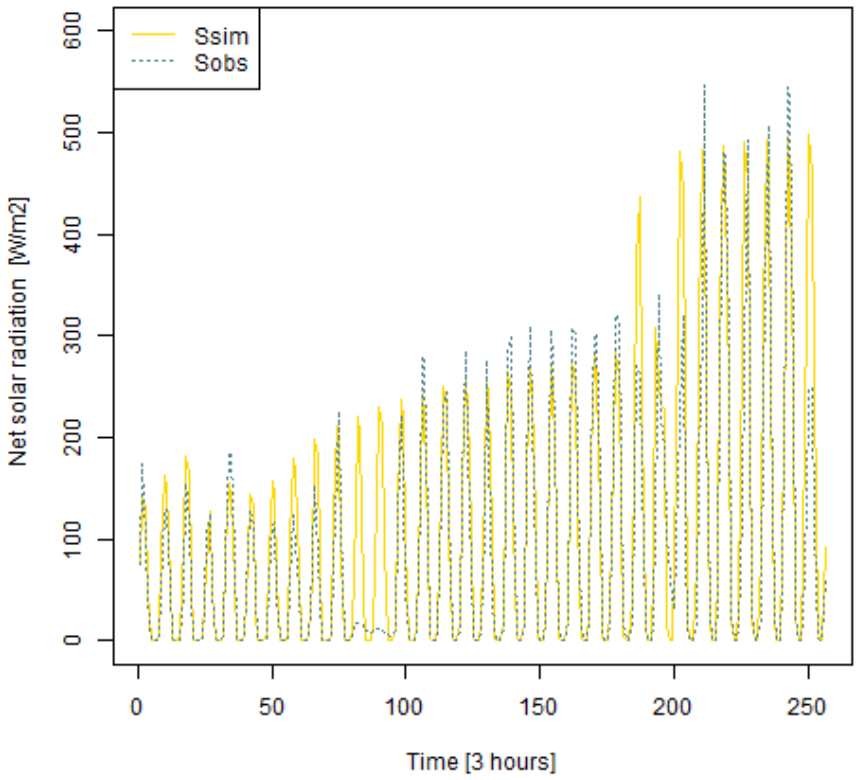

Figure 30: *Distribution of energy fluxes, melt season of 2011, 3 hour resolution. Ssim: parametrized S, Sobs: includes observed incoming solar radiation. Mean Ssim: 110.5 $W\ m^{-2}$, mean Sobs: 94.20 $W\ m^{-2}$.*

Table 19 gives the results of the model evaluation for the snow melt rates for the period in Fig. 29, 9 April - 1 May. All the efficiency criteria (NS, ME, RMSE) showed a slightly increase in the melt rated predicted by seNorge_eb with observed $S\downarrow$ included in the simulations. The simulated snow melt rates were slightly overestimated with a ME of 0.78 mm (Table 19 and Fig. 31). Both temperature and day number were found significant in explaining the residual error (Fig. 32).

Table 19: *Model evaluation of snow melt rates. Snow melt season of 2011 with observed $S\downarrow$ as additional input, 3 hour resolution. Events were both simulated and observed $SWE > 0$ mm and simulation and/or observation indicate melt are evaluated.*

	SimSinn	SimPT
No. of. residuals	160	148
NS	-0.62	-0.99
ME [mm]	0.78	1.10
RMSE [mm]	3.00	3.10

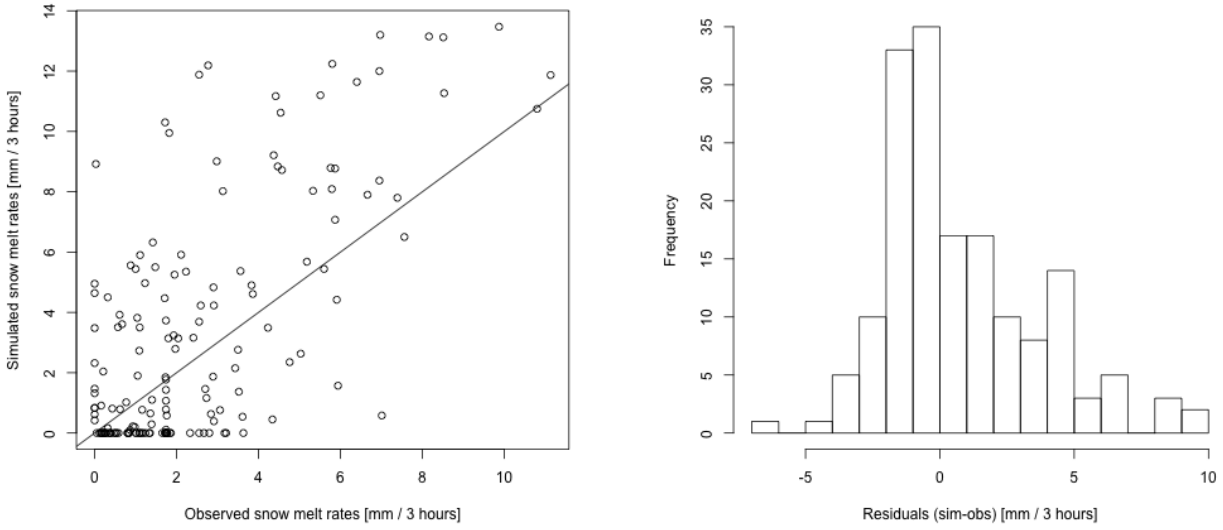

(a) (b)

Figure 31: *a) Observed vs. simulated melt rates, b) Histogram of residuals (sim-obs) of melt rates melt. Snow melt season of 2011 with observed $S\downarrow$ as additional input, 3 hour resolution.*

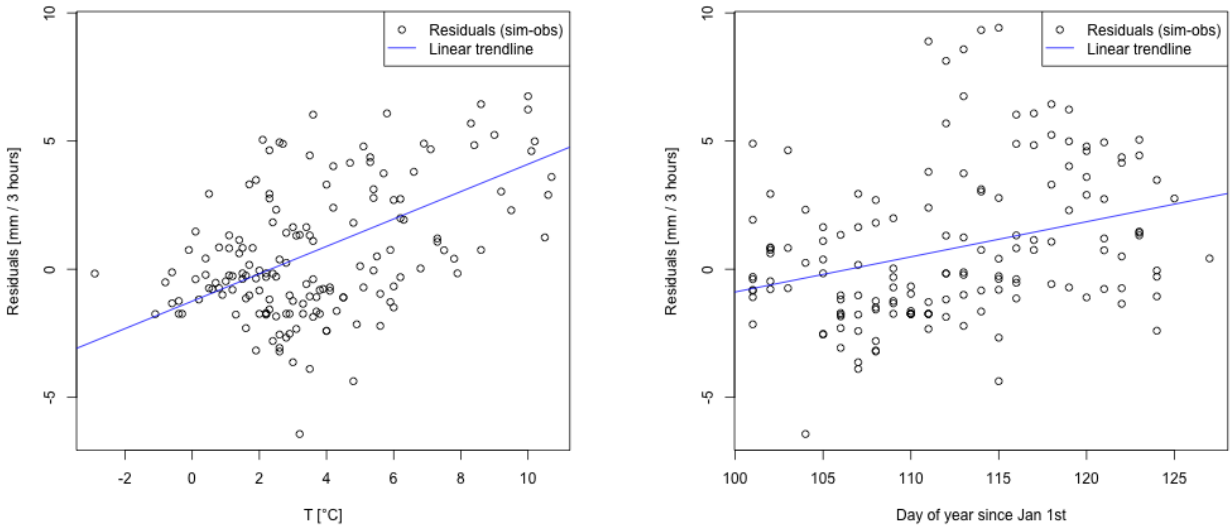

(a) (b)

Figure 32: *a) Temperature vs. residuals, p-value* $5.13 \cdot 10^{-13}$. *b) Day number vs. residuals, p-value* $9.1 \cdot 10^{-5}$. *Observed* $S\downarrow$ *included as input data, 3 hour resolution.*

6.3.2 Long-wave radiation

The substitution of the parametrizations of L_a and L_t (eq. 36 and 37) with observed data help increase the snow melt rates such that the ablation period was markedly reduced (Fig. 33). This was due to the observed L_a being larger i value than the simulated L_a (as seen in section 6.1).

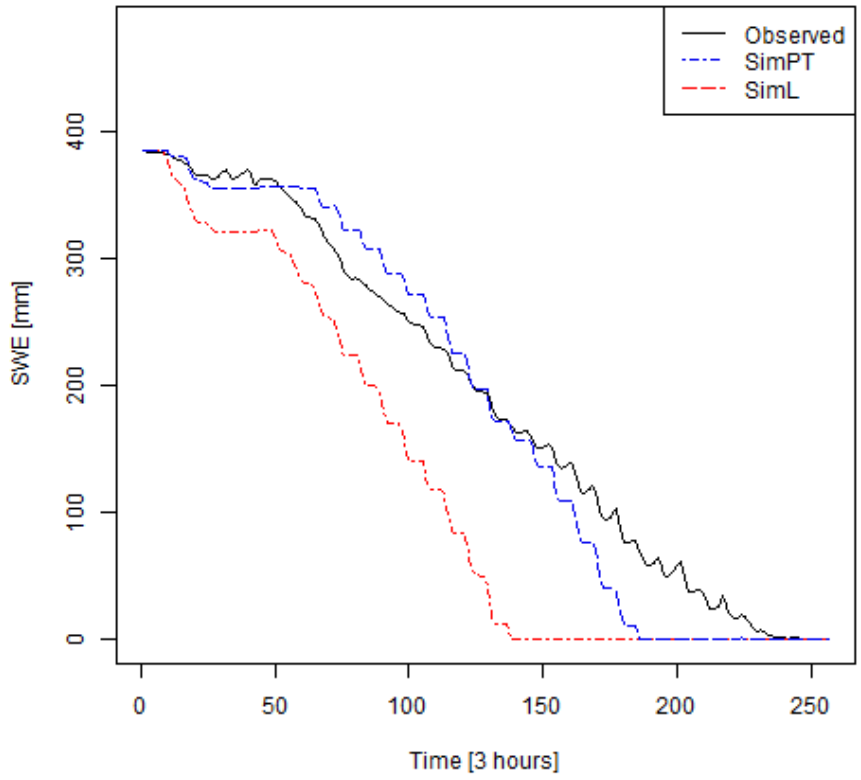

Figure 33: *SWE during melt season of 2011, 3 hour resolution. SimPT: precipitation and temperature, SimL: precipitation, temperature atmospheric and terrestrial long-wave radiation.*

The distribution of the net long-wave radiation flux, L, during the ablation period of 2011, from parametrization (Lsim) and observed data (Lobs) is shown in Fig. 34. Lobs was generally higher in value, with a mean value of -37.10 $W\ m^{-2}$, compared to -65.0 $W\ m^{-2}$ for Lsim.

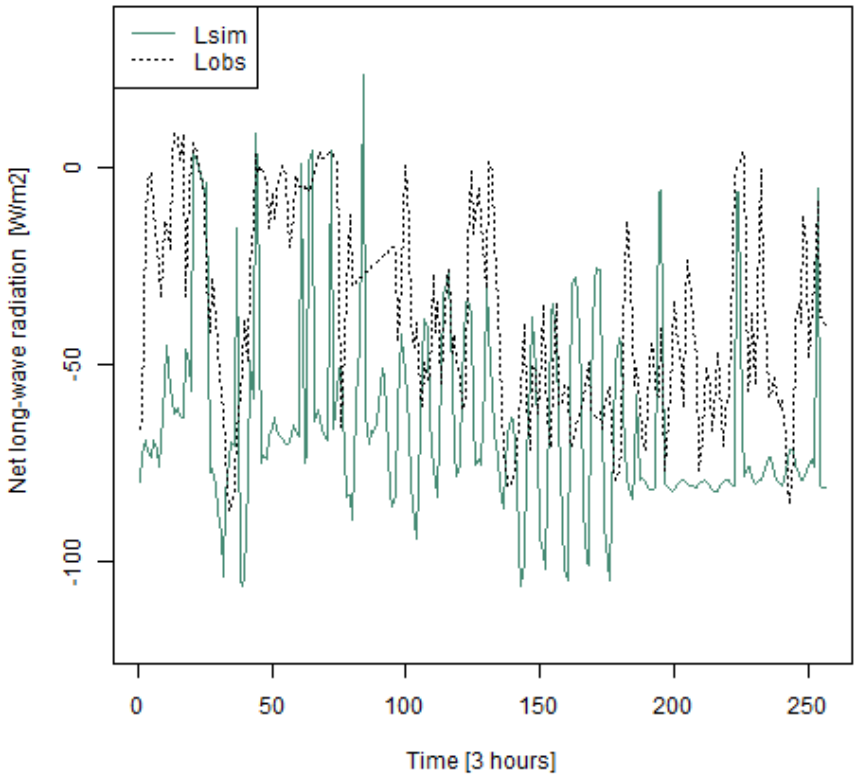

Figure 34: *Distribution of the net long-wave radiation flux, melt season of 2011, 3 hour resolution. Lobs: observed net long-wave radiation, Lsim: parametrized net long-wave radiation (eqs. 36 and 37). Mean Lobs: -37.10 W* m^{-2}*, mean Lsim: -65.0 W* m^{-2}.

Table 20 informs that, according to the objective model evaluation criteria, the snow melt rates were not improved by including observed L_a and L_t. Fig. 35 illustrates that the snow melt rates were in general overestimated.

Table 20: *Model evaluation of melting season 2011 on 3 hour resolutions. Events were both simulated and observed SWE* > 0 *mm and simulation and/or observation indicate melt are evaluated.*

	SimL	SimPT
No. of. residuals	120	148
NS	-3.30	-0.99
ME [mm]	1.50	1.10
RMSE [mm]	3.40	3.10

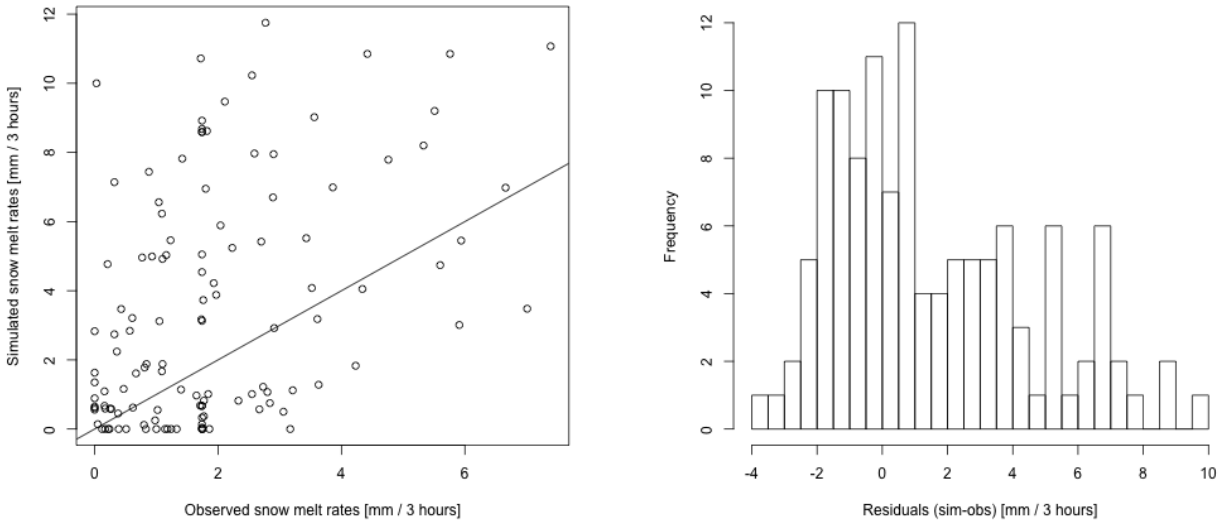

(a) (b)

Figure 35: *a) Observed vs. simulated melt rates, b) Histogram of residuals (sim-obs) of melt rates melt. Snow melt season of 2011 with observed L_a and L_t as additional input data, 3 hour resolution*

Temperature was found significant in explaining the error, whereas day number was not (Fig. 36).

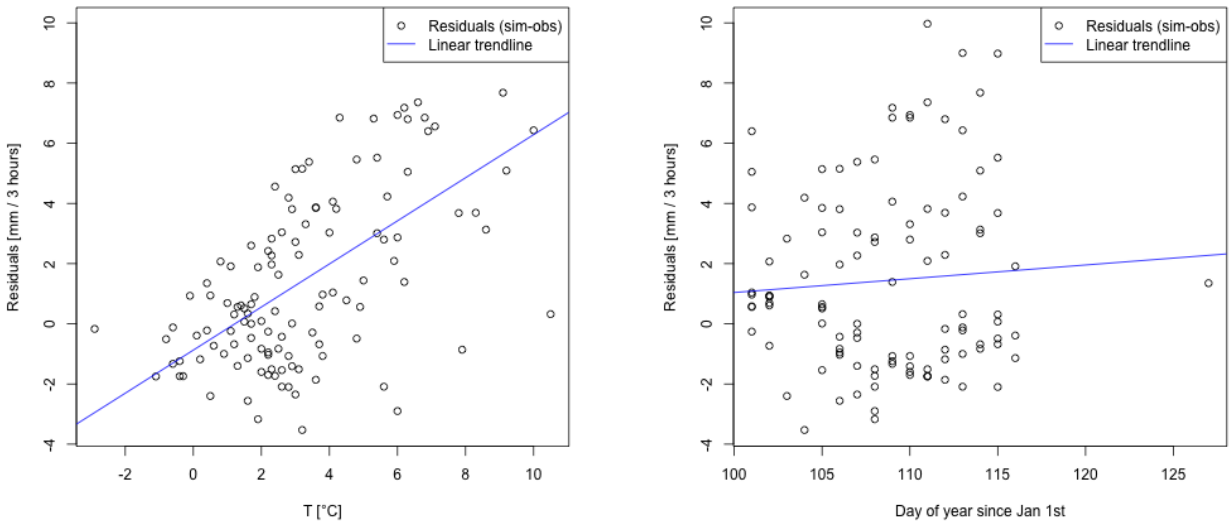

(a) (b)

Figure 36: *a) Temperature vs. residuals, p-value* $2.65 \cdot 10^{-14}$. *b) Day number vs. residuals, p-value 0.47. 3 hour resolution. Observed L_a and L_t included in simulations.*

6.3.3 Wind

When the constant wind speed of 1.75 $m\ s^{-1}$ in the turbulent fluxes (sensible heat flux, SH, and latent heat flux, LE) was substituted with observed wind data there was a reduction in the length of the snow season, most noticeable in 2011 and 2013 (Fig. 37).

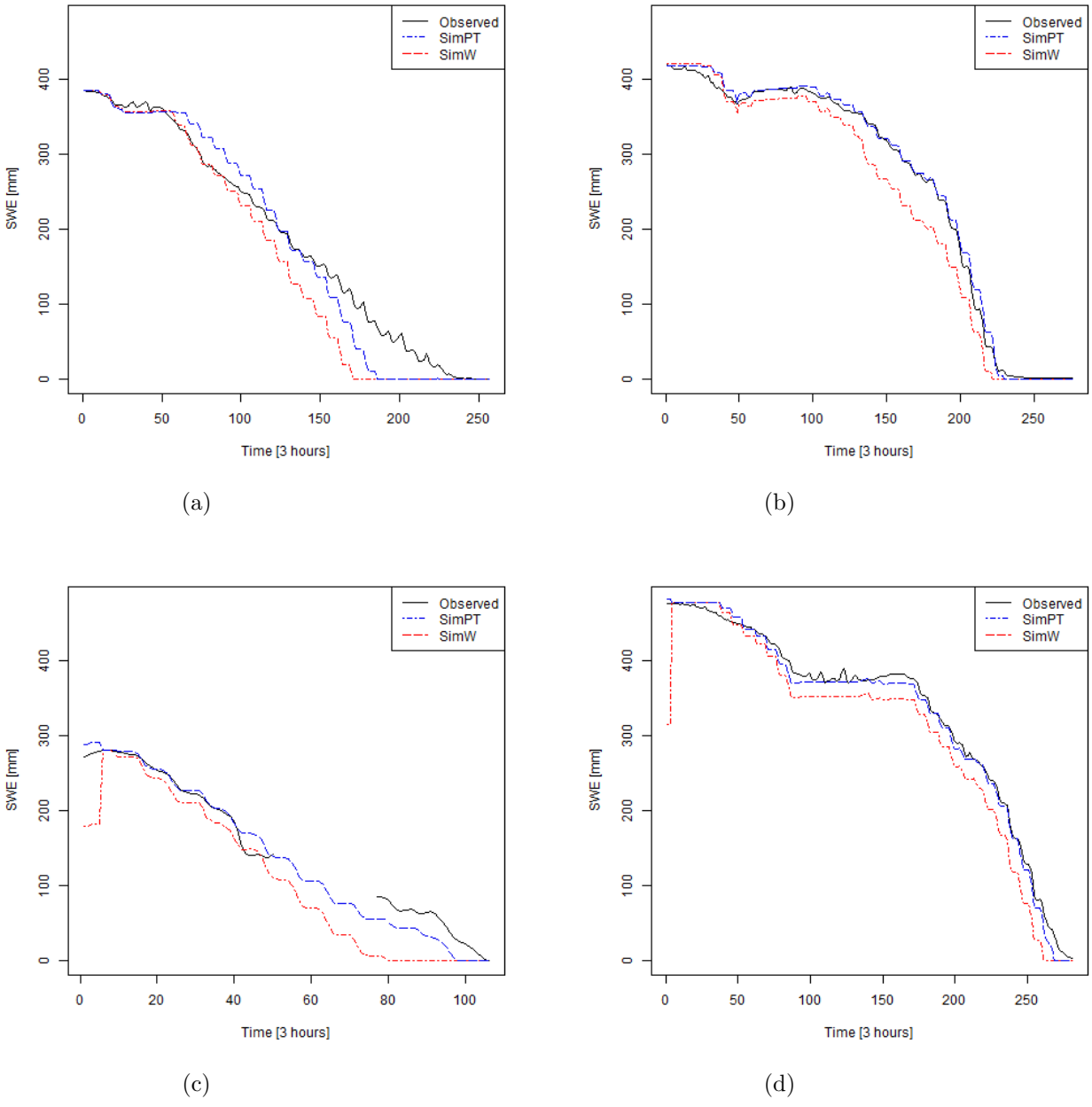

Figure 37: *SWE during melt seasons. a) 2011, b) 2012, c) 2013, d) 2014. SimPT: precipitation and temperature, SimW: precipitation, temperature and wind. 3 hour resolution.*

SH and LE were increased in all melt seasons 2011-2014 due to the introduction of observed wind data (Fig. 38 and Table 21), thus increasing the snow melt rates.

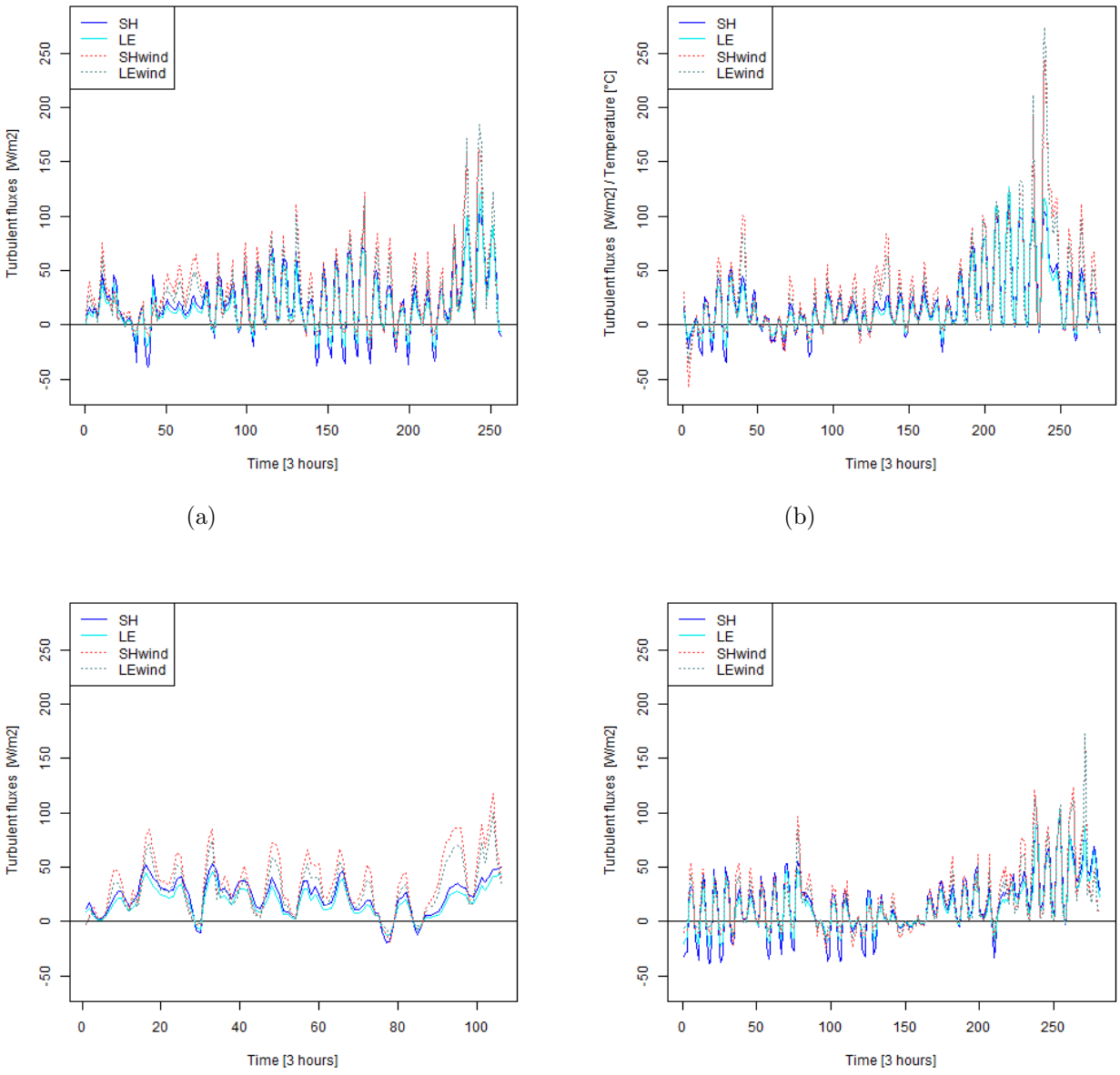

Figure 38: *a) 2011, b) 2012, c) 2013, d) 2014. Distribution turbulent energy fluxes during snow melt seasons. SH and LE: precipitation and temperature, SEwind and LEwind: precipitation, temperature, and wind. 3 hour resolution.*

Table 21: *Mean values* $[W\ m^{-2}]$ *of energy fluxes in Fig.* **??**, *3 hour resolution.*

Energy flux	2011	2012	2013	2014
SHwind	29.50	27.80	35.60	21.40
SH	20.60	20.10	22.60	16.70
LEwind	25.30	25.10	28.00	18.40
LE	18.40	18.50	17.80	14.90

The objective model evaluation criteria did not show any improvements in the melt rates by looking at all seasons or individual seasons, except for season 2013 (Table 11 in section 6.1 compared to Table 22). Fig. 39 illustrates that the melt rates were overestimated.

Table 22: *Model evaluation of snow melt rates, melt seasons 2011-2014, 3 hour resolutions. Wind additional input data. Events were both simulated and observed SWE* > 0 *mm and simulation and/or observation indicate melt are evaluated.*

	All seasons	2011	2012	2013	2014
No. of residuals	550	140	170	48	192
NS	-0.53	-2.50	0.16	-0.39	-0.86
ME [mm]	1.20	1.30	0.96	1.00	1.30
RMSE [mm]	3.60	3.50	3.10	4.30	3.90

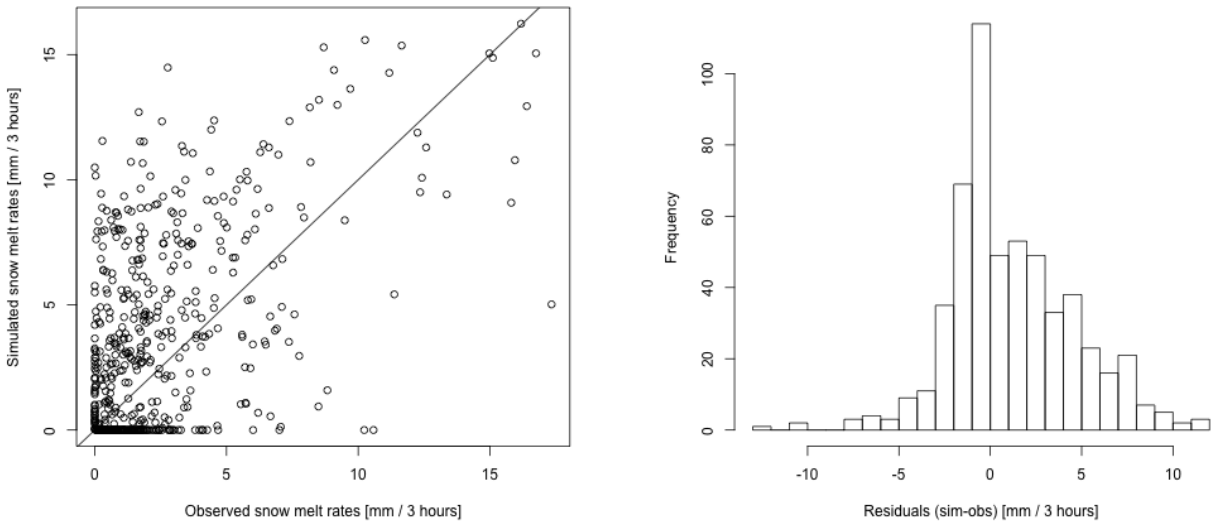

(a) (b)

Figure 39: *a) Observed vs. simulated melt rates, b) Histogram of residuals (sim-obs) of melt rates melt. Snow melt season of 2011, with observed wind as additional input data. 3 hour resolution.*

Temperature was significant in explaining the residual error when wind was included in the simulations, whereas day number was not (Fig. 40).

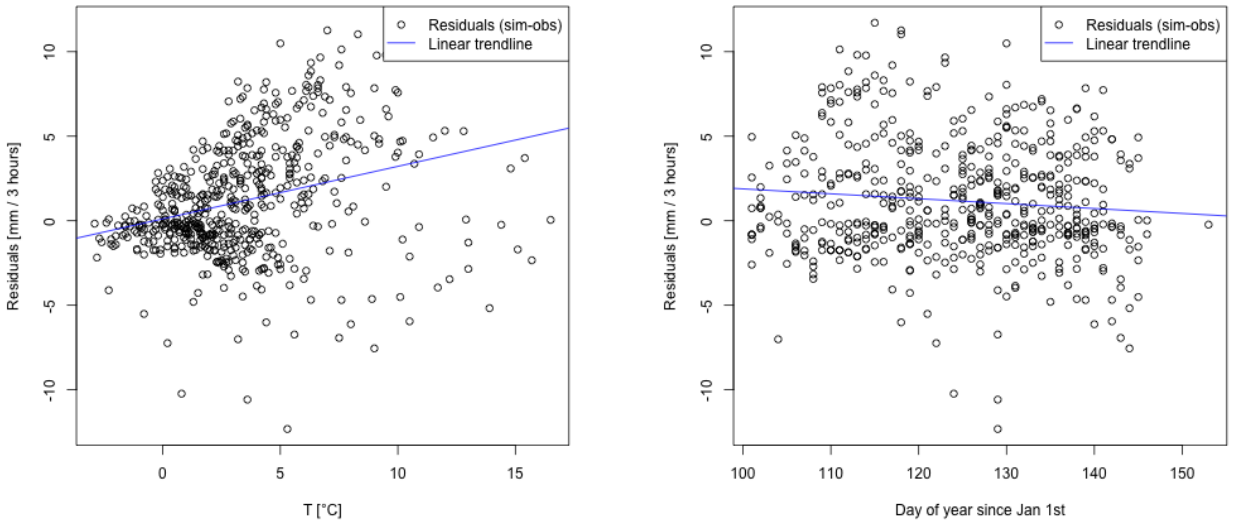

(a) (b)

Figure 40: *a) Temperature vs. residuals, p-value* $1.3 \cdot 10^{-12}$*. b) Day number vs. residuals, p-value 0.024. Snow melt seasons 2011-2014, 3 hour resolution.*

6.3.4 Snow surface temperature

T_{ss}, derived from observed long-wave radiation, L_t, resulted in a longer snow season compared to simulations where T_{ss} was calculated by seNorge_eb itself (SimTss vs. SimPT in Fig. 41). Compared to observed SWE, SimTss underestimated in the start of the melt season and overestimated towards the end.

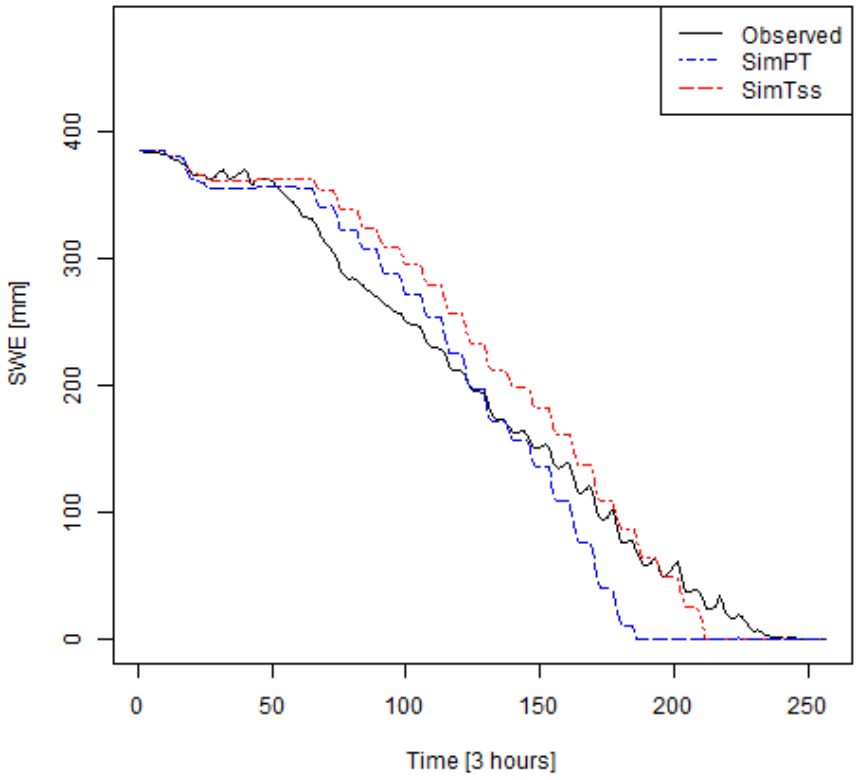

Figure 41: *Snow melt season of 2011, 3 hour resolution. SimPT: precipitation and temperature, SimTss: precipitation, temperature and* T_{ss}.

The turbulent fluxes, SH and LE, decreased as a result of including observed T_{ss} as input data (Fig. 42 and Table 23). Net long-wave radiation showed a small increase, but changed by a smaller amount than SH and LE. Observed T_{ss} thus had largest effect on the turbulent fluxes.

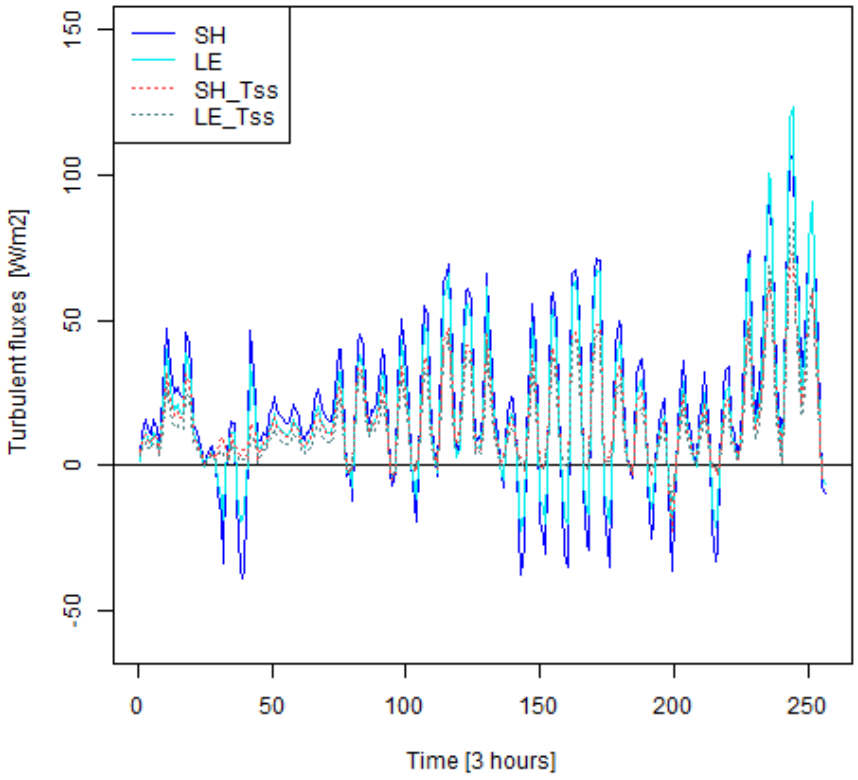

Figure 42: *Distribution turbulent energy fluxes during melt season of 2011, 3 hour resolution. SH and LE: precipitation and temperature, LE_Tss: precipitation, temperature and* T_{ss}.

Table 23: *Mean values* $[W\ m^{-2}]$ *of energy fluxes during ablation period 2011, 3 hour resolution.*

	SimT_{ss}	SimPT
L	-62.40	-65.00
SH	16.30	20.60
LE	13.90	18.40

According to all of the objective model evaluation criteria the simulated snow melt rates were improved compared to simulations with only precipitation and temperature (SimPT) when observed T_{ss} was included in seNorge_eb (Table 24).

Table 24: *Model evaluation of snow melt rates. Snow melt season of 2011 with T_{ss} as additional input data. Events were both simulated and observed SWE > 0 mm and simulation and/or observation indicate melt are evaluated.*

	SimT_{ss}	SimPT
No. of. residuals	163	148
NS	-0.39	-0.99
ME [mm]	0.68	0.81
RMSE [mm]	2.75	3.10

Snow melt rates were generally overestimated compared to observed snow melt rates with T_{ss} as additional input data (Fig. 43).

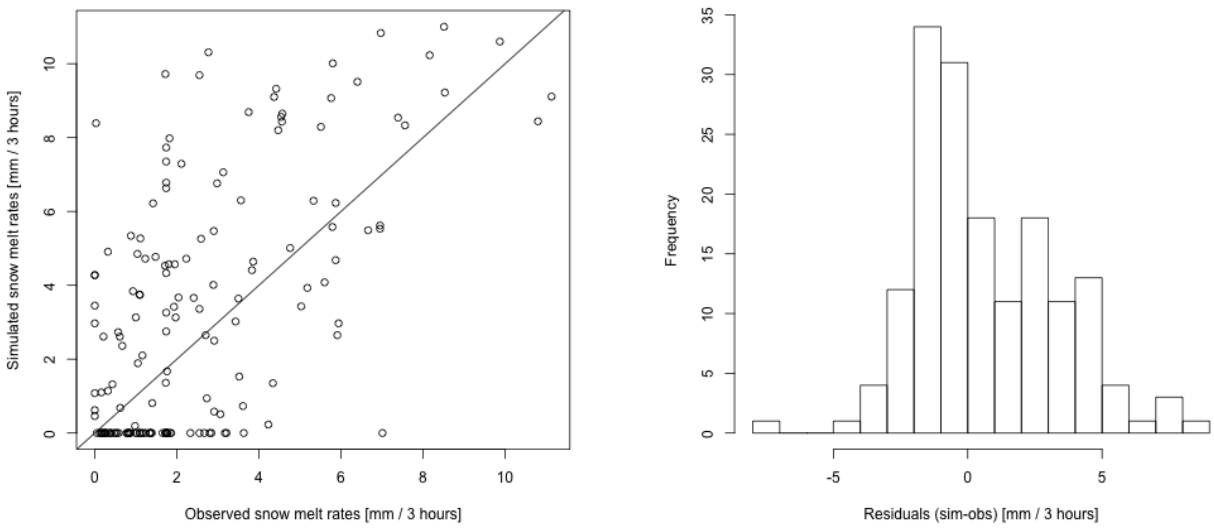

(a) (b)

Figure 43: *a) Observed vs. simulated melt rates, b) Histogram of residuals (sim-obs) of melt rates melt. Snow melt season of 2011, with observed T_{ss} as additional input data. 3 hour resolution.*

Temperature was significant in explaining the residual error when T_{ss} was included in the simulations, whereas day number was not (Fig. 44).

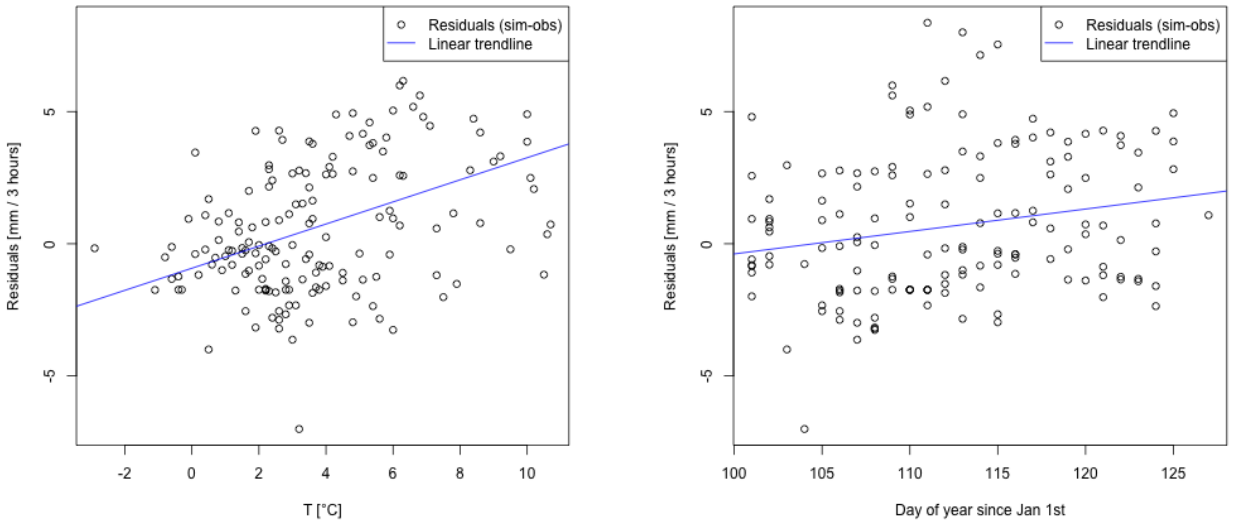

(a) (b)

Figure 44: *a) Temperature vs. residuals, p-value* $3.95 \cdot 10^{-9}$*. b) Day number vs. residuals, p-value 0.01. Observed* T_{ss} *as additional input data, 3 hour resolution.*

6.3.5 Relative humidity

SWE was reduced at a slower rate during the melt seasons 2012 as a result of introducing observed relative humidity, RH, in the latent heat flux (SimRH compared to SimPT, Fig. 45). This was caused by a reduction in the latent heat flux (LE compared to LE_RH in Fig. 46).

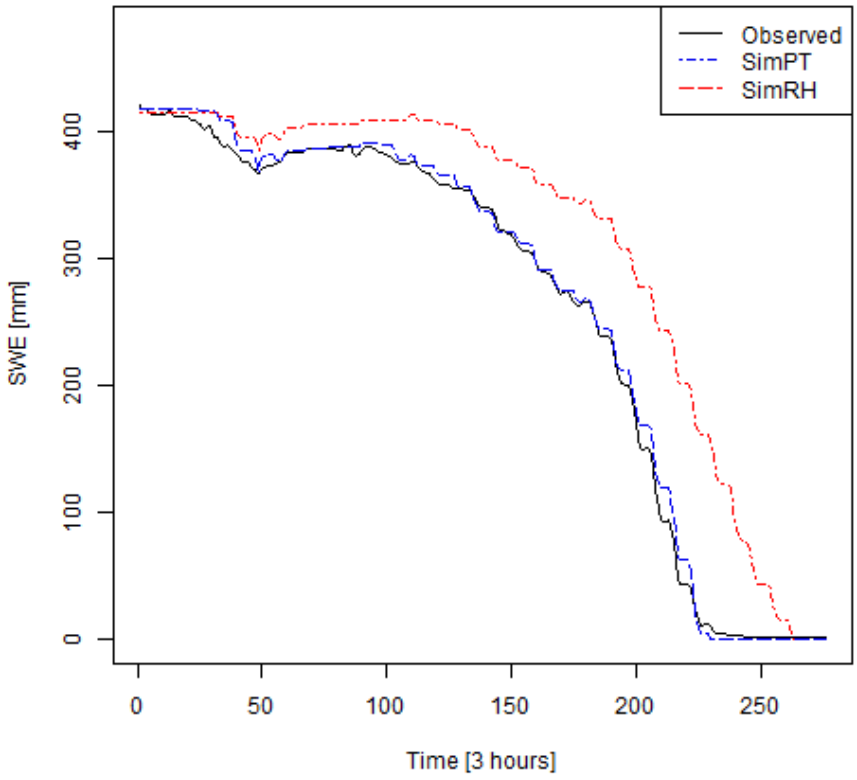

Figure 45: *Observed and simulated SWE during melt season of 2012. SimPT: precipitation and temperature, SimRH: precipitation, temperature and relative humidity. 3 hour resolution.*

With relative humidity included in the simulations LE became negative also for positive air temperatures, T_a >0 ℃ (LE_RH compared to LE in Fig. 46) meaning that evaporation also occured when $T_a > T_{ss}$. Moreover, SH and LE no longer worked in the same direction for all events.

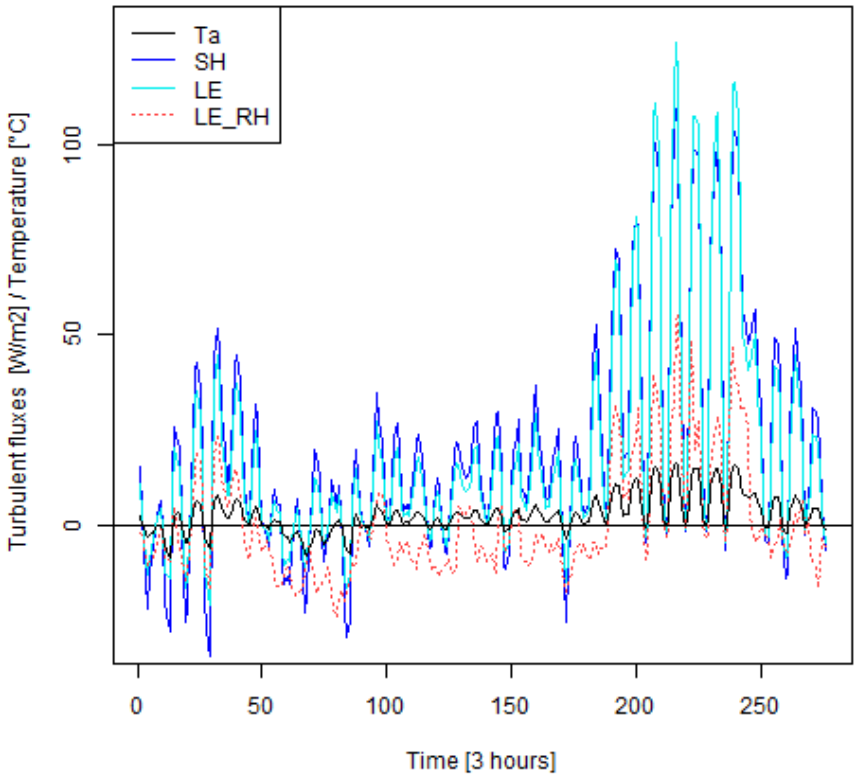

Figure 46: *Distribution turbulent energy fluxes during melt season of 2012. SH and LE: precipitation and temperature, LE_RH: precipitation, temperature and RH. T_a: observed air temperature. Mean LE_RH: -0.20 W m^{-2}, mean LE: 18.50 W m^{-2}. 3 hour resolution.*

According to the objective model evaluation criteria seNorge_eb did not improve its ability to estimate snow melt rates when observed RH was included (Table 25), except for a small reduction of 0.10 mm in the mean error (ME).

Table 25: *Model evaluation of snow melt rates. melt season of 201,2 3 hour resolutions. Events were both simulated and observed SWE > 0 mm and simulation and/or observation indicate melt are evaluated.*

	SimRH	SimPT
No. of. residuals		179
NS	-0.05	0.35
ME [mm]	0.71	0.81
RMSE [mm]	3.38	2.80

The snow melt rates were for the majority of the evaluated events overestimated with observed RH as input data (Fig. 47a), however the highest frequency of the residuals were slightly negative (Fig. 47b).

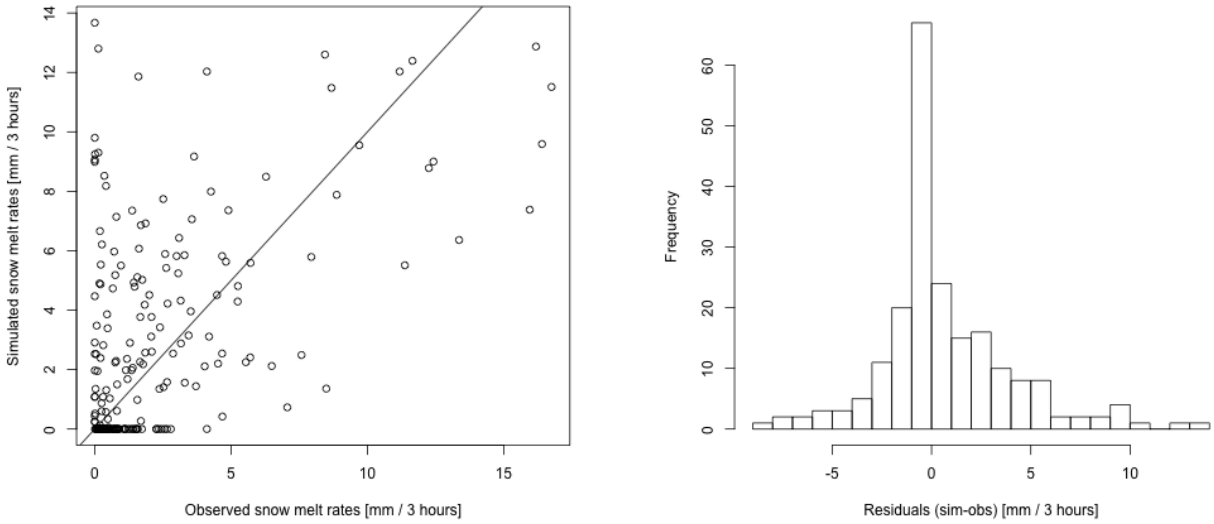

(a) (b)

Figure 47: *a) Observed vs. simulated melt rates, b) Histogram of residuals (sim-obs) of melt rates melt. Snow melt season of 2011, with observed relative humidity as additional input data. 3 hour resolution.*

Temperature was significant in explaining the residual error when observed RH was included in the simulations, whereas day number was not (Fig. 48).

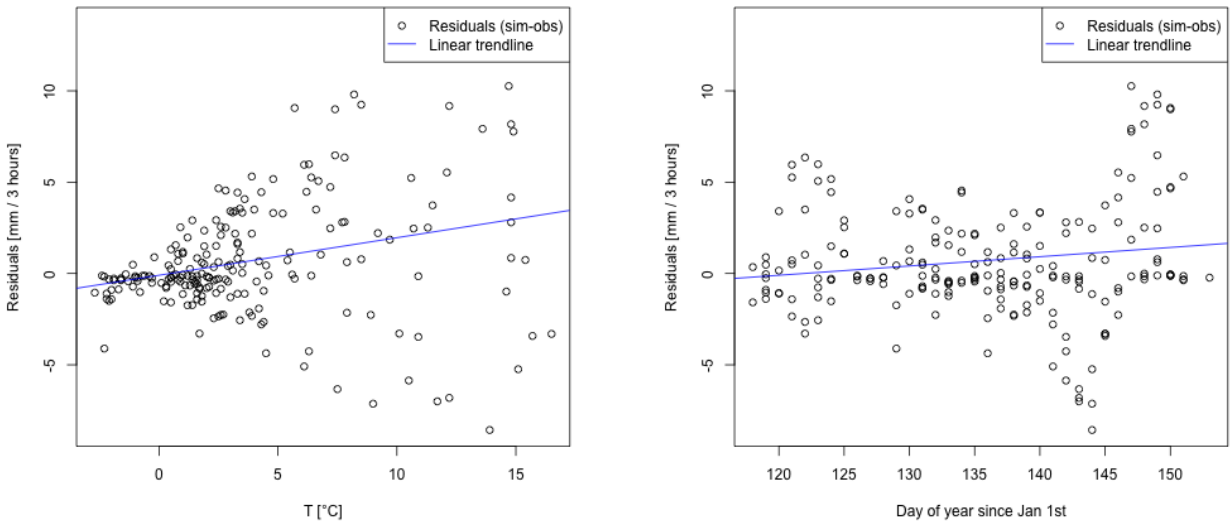

(a) (b)

Figure 48: *a) Temperature vs. residuals, p-value* $2.88 \cdot 10^{-16}$. *b) Day number vs. residuals, p-value 0.42. Observed relative humidity as additional input data, 3 hour resolution.*

6.3.6 $S\downarrow$, L, wind, T_{ss}

This section contains the model simulation results on 3 hour resolution with additional input data $S\downarrow$, L, wind, T_{ss} for the period October 2010-May 2011. The relative humidity data on 3 hour resolution could not be included due to missing data.

From a visual perspective the additional input data did not improve the results (SimAll compared with observed SWE , Fig. 49).

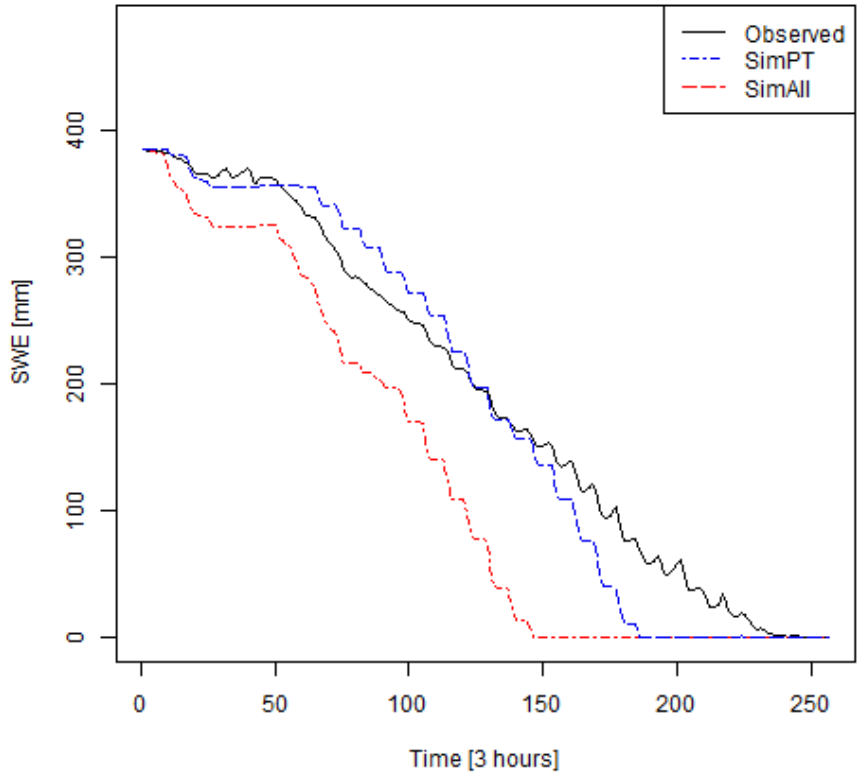

Figure 49: *Snow melt season of 2011, 3 hour resolution. SimPT: precipitation and temperature, SimAll: precipitation, temperature, $S\downarrow$, L_a and L_t, wind and T_{ss}.*

According to Table 26 the objective model evaluation criteria, the simulated snow melt rates did not improve when observed $S\downarrow$, L_a and L_t, wind and T_{ss} were included as input data. Simulated melt rates were generally overestimated compared to observed rates (Fig. 50).

Table 26: *Model evaluation of snow melt rates. Melting season 2011, 3 hour resolutions. Additional input data: $S\downarrow$, L, wind, T_{ss}. Events were both simulated and observed SWE > 0 mm and simulation and/or observation indicate melt are evaluated.*

	SimAll	SimPT
No. of. residuals	130	148
NS	-3.20	-0.99
ME [mm]	1.40	0.81
RMSE [mm]	3.30	3.10

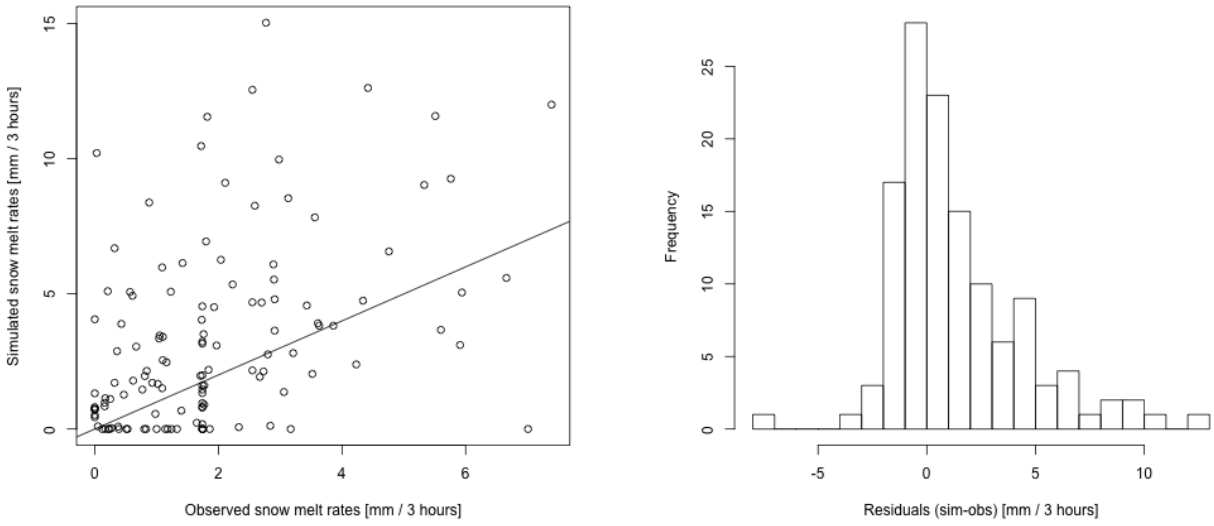

(a) (b)

Figure 50: *a) Observed vs. simulated melt rates, b) Histogram of residuals (sim-obs) of melt rates melt. Snow melt season of 2011, with observed relative humidity as additional input data. 3 hour resolution.*

Temperature was significant in explaining the residual error when observed $S\downarrow$, L_a and L_t, wind and T_{ss} were included in the simulations, whereas day number was not (Fig. 51).

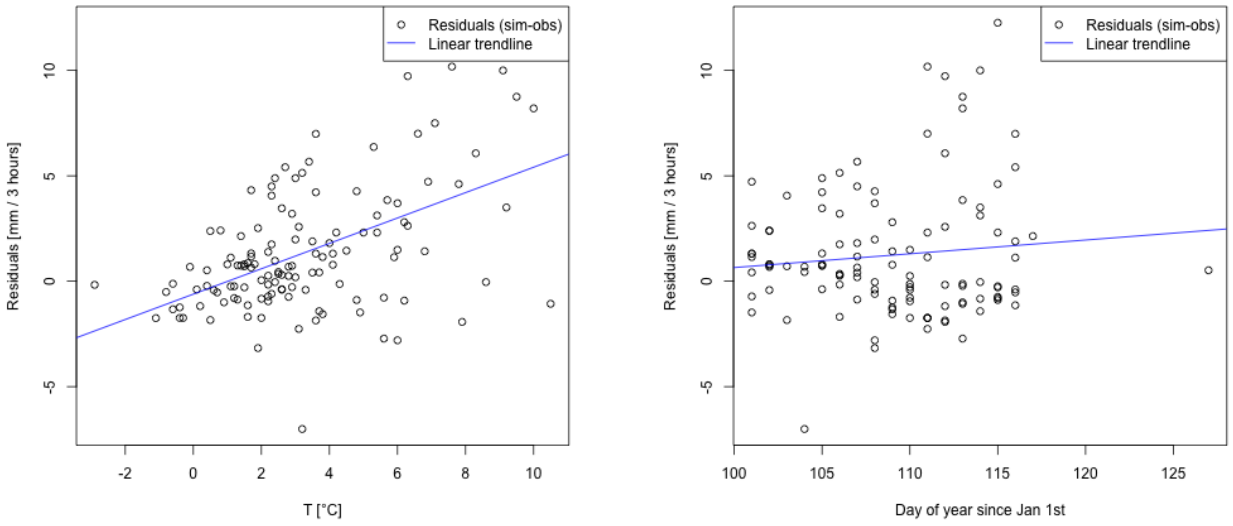

(a) (b)

Figure 51: *a) Temperature vs. residuals, p-value* $5.33 \cdot 10^{-10}$. *b) Day number vs. residuals, p-value 0.2742. Observed relative humidity as additional input data, 3 hour resolution.*

6.3.7 Summary: introducing additional data - 3 hour resolution

By simulating with observed solar radiation, $S\downarrow$, for the 2011-season the model underestimated melt in the start and overestimated towards the end. The model performance improved slightly in terms of NS (from -0.99 to -0.62), however the overall performance did not improve as the ME and RMSE both showed a slight increase.

The inclusion of observed long-wave radiation data accounted for the most noticeable change in melt; Due to more energy available for melt, the length of the ablation period was reduced. The snow melt rates were not improved.

The turbulent fluxes were affected by introducing observed wind, snow surface temperature, T_{ss} and relative humidity, RH. Observed wind had the effect of increasing the turbulent fluxes thus increasing melt rates, whereas snow surface temperature and relative humidity data worked in the opposite direction. Relative humidity had the largest effect in terms of reducing the latent hat flux and thus reducing melt, and it facilitated evaporation from the snow to the air. In terms of the objective model evaluation criteria, T_{ss} was the only observed variable that managed to improve the snow melt rates in terms of all of the 3 objective evaluation criteria.

When observed $S\downarrow$, L_a and L_t, wind and T_{ss} were included as input data for the snow season 2010-2011, the snow melt rates were, in terms of the visual and objective model evaluation criteria, not improved. The observed relative humidity data did not cover this period. However, if we compare simulated SWE with relative humidity and the SWE with observed $S\downarrow$, L_a and L_t, wind and T_{ss} as additional input data, combined they might give an acceptable result as they work in opposite directions.

6.4 Additional input data - 24 hour resolution

In this section the results from simulations with additional input data, beyond precipitation and temperature, on 24 hour resolution are presented. The additional input data were included one at the time by substituting the parametrizations of incoming solar radiation, $S\downarrow$, atmospheric and terrestrial radiation, L_a and L_t, and variables of the turbulent fluxes (wind, snow surface temperature, T_{ss}, and relative humidity, RH. One simulation also includes all the additional data, except RH that did not cover the period Oct. 2010- May 2011.

6.4.1 Incoming solar radiation

The result in terms of SWE when observed incoming solar radiation, $S\downarrow$, was included as input data in seNorge_eb, together with precipitation and temperature, is seen in Fig. 52 (SimSinn). The simulation with observed $S\downarrow$ caused the snow to melt more rapidly compared to simulations with simulated $S\downarrow$ on 24 hour resolution (SimPT in Fig. 52). The simulated SWE became closer to the observed values.

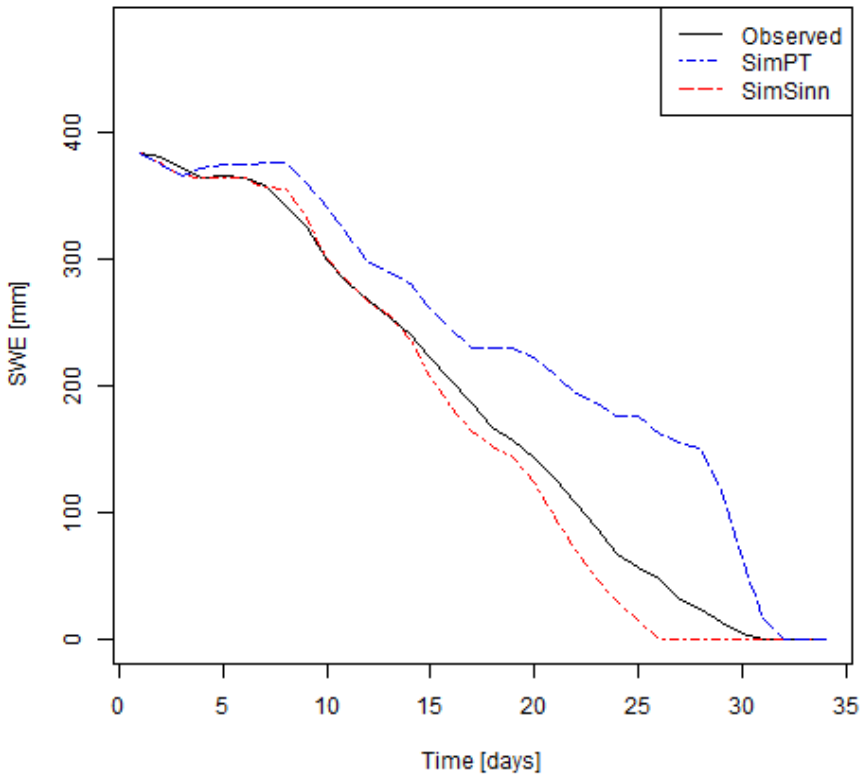

Figure 52: *SWE during melt season of 2011. SimPT: precipitation and temperature, SimSinn: precipitation, temperature and observed $S\downarrow$. 24 hour resolution.*

Observed $S\downarrow$ resulted in an increase in the net solar radiation during the snow melt season of 2011 (Sobs compared to Ssim in Fig. 53.

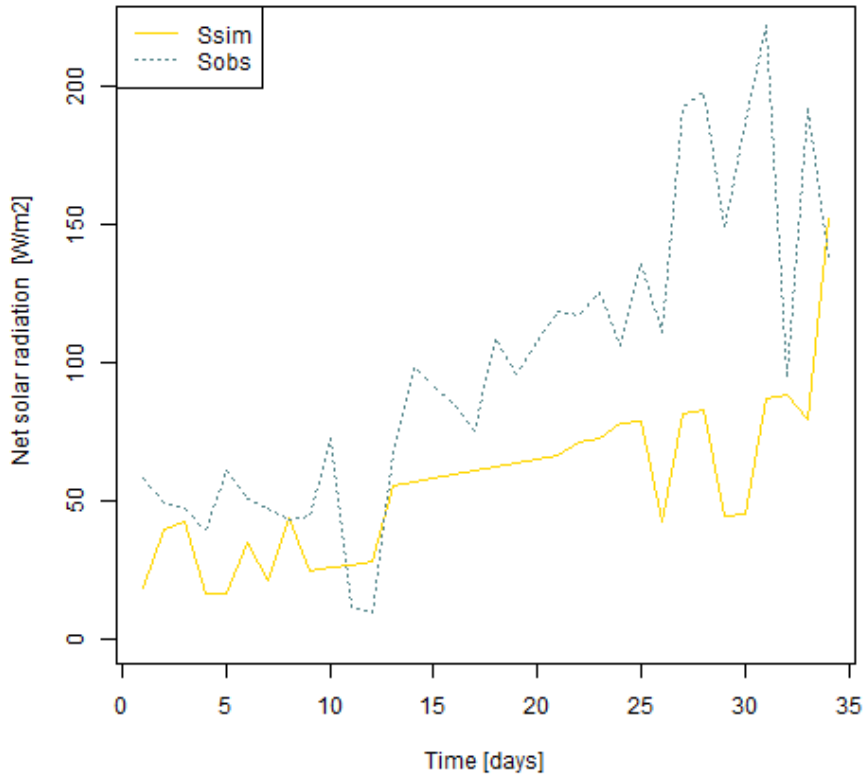

Figure 53: *Distribution of energy fluxes during melt season of 2011, Ssim: simulated net solar radiation, Sobs: net solar radiation with observed $S\downarrow$. Mean Ssim: 74.70 Wm^{-2}, mean Sobs: 116.90 Wm^{-2}.*

The objective model evaluation criteria were ambivalent regarding the improvement of the snow melt rates, and the overall impression is that the snow melt rates were not improved with the inclusion of observed $S\downarrow$ as input data (Table 27) because NS increased, ME increased and RMSE remained unchanged.

Table 27: *Model evaluation of melting season of 2011, 24 hour resolutions. Events were both simulated and observed $SWE > 0$ mm and simulation and/or observation indicate melt are evaluated.*

	SimSinn	SimPT
No. of residuals	24.00	30
NS	-0.81	-3.70
ME [mm]	7.90	0.06
RMSE [mm]	14.00	14.00

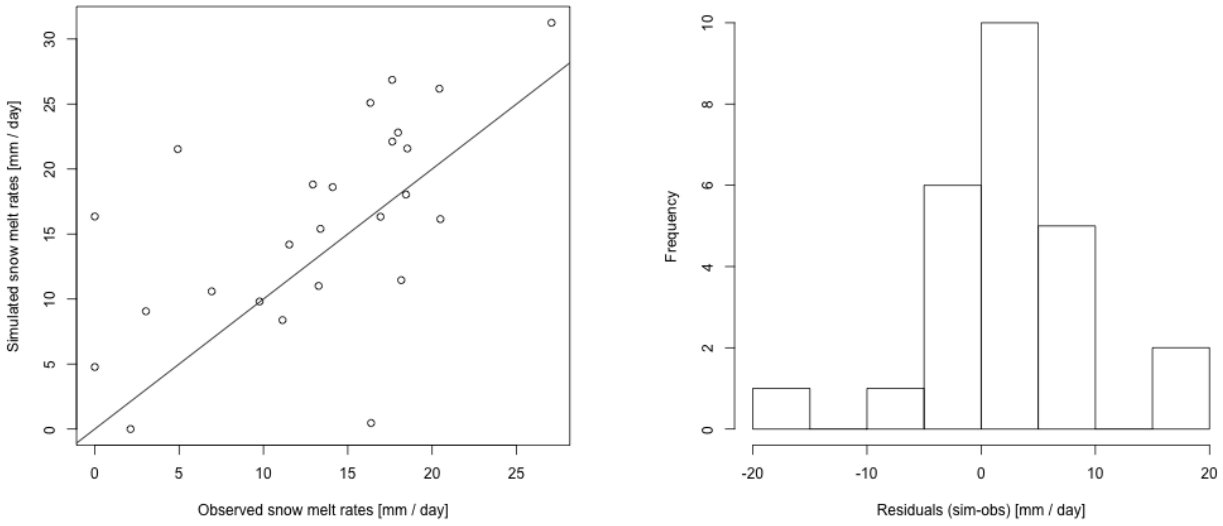

(a) (b)

Figure 54: *a) Observed vs. simulated melt rates, b) Histogram of residuals (sim-obs) of melt rates melt. Snow melt season of 2011, with observed incoming solar radiation as additional input, 24 hour resolution.*

Temperature and day number were found significant (although on the 95 % confidence interval) in explaining the residual error.

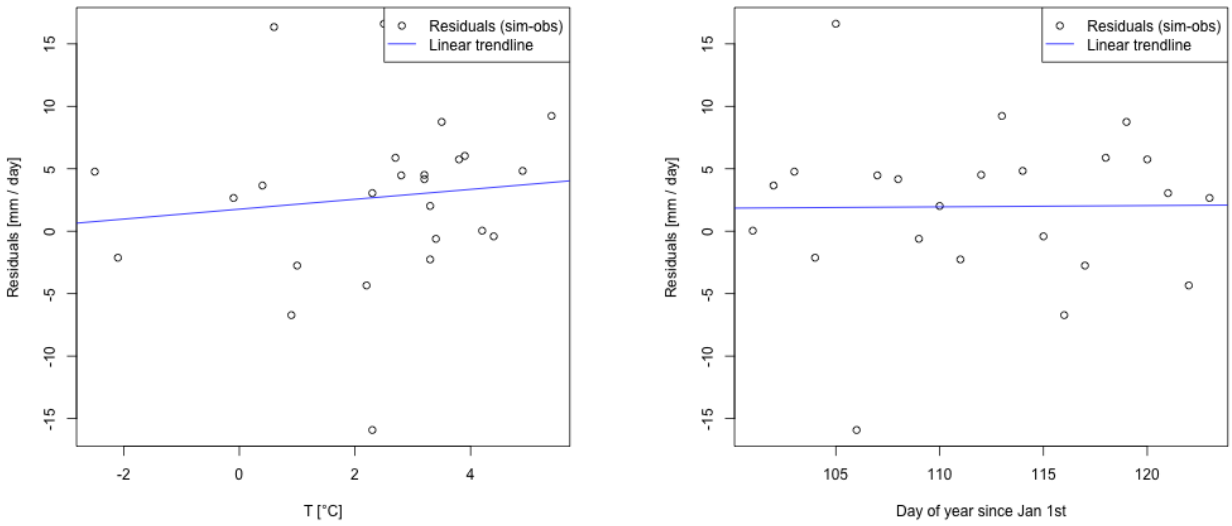

(a) (b)

Figure 55: *a) Temperature vs. residuals, p-value* 0.022. *b) Day number vs. residuals, p-value* 0.0035. *Observed S ↓ included as input data, 24 hour resolution.*

6.4.2 Long-wave radiation

The substitution of the parametrizations of L_a and L_t (eqs. 36 and 37) with observed data had little visual effect (Fig. 56).

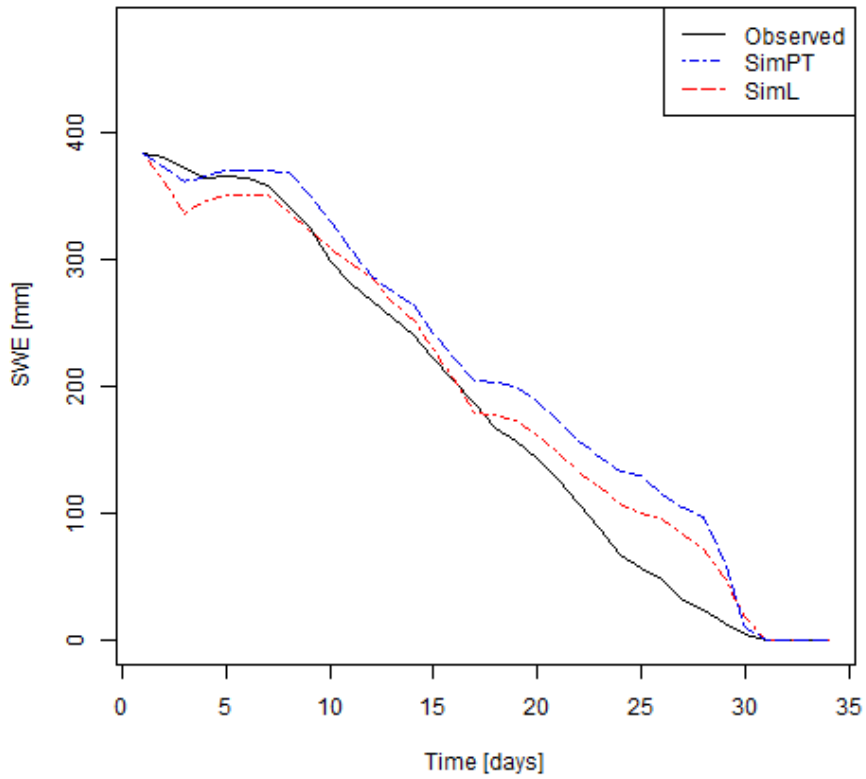

Figure 56: *SWE during melt season of 2011, 24 hour resolution. SimPT: precipitation and temperature, SimL: precipitation, temperature atmospheric and terrestrial long-wave radiation.*

The energy input from observed net long-wave radiation was close in value compared to simulated values (Fig.57), with a mean value of -37.60 $W\ m^{-2}$ and -35.00 $W\ m^{-2}$ respectively.

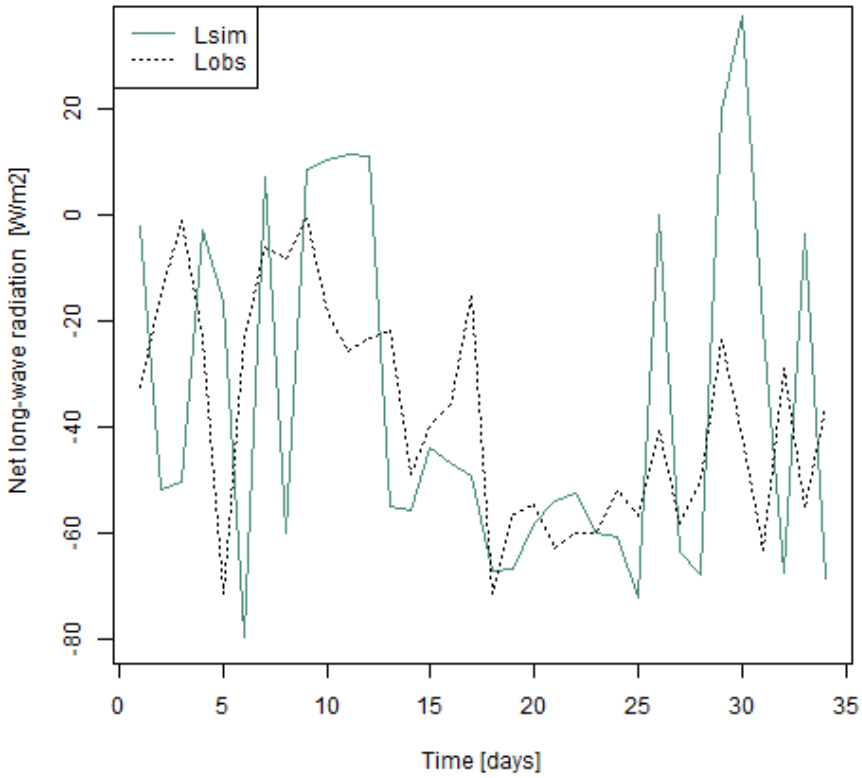

Figure 57: *Distribution of net long-wave radiation during melt season of 2011, 24 hour resolution. Lsim: precipitation and temperature, Lobs:precipitation, temperature and observed L_a and L_t. Mean Lobs, -37.60 W m^{-2} mean Lsim -35.00 W m^{-2}.*

Observed L_a and L_t improved the melt rates in terms of NS and RMSE, but not in terms of ME (Table 28). The residuals are few in number, however the majority is centred around -10 mm to 10 mm (Fig. 58). Temperature was found significant in explaining the residual error, whereas day number was not (Fig. 59).

Table 28: *Model evaluation of snow melt rates. melt season of 2011, 24 hour resolution.Observed long-wave radiation data as additional input.*

	SimL	SimPT
No. of. residuals	28	30
NS	-1.24	-3.70
ME	-0.24	0.06
RMSE	8.58	14.00

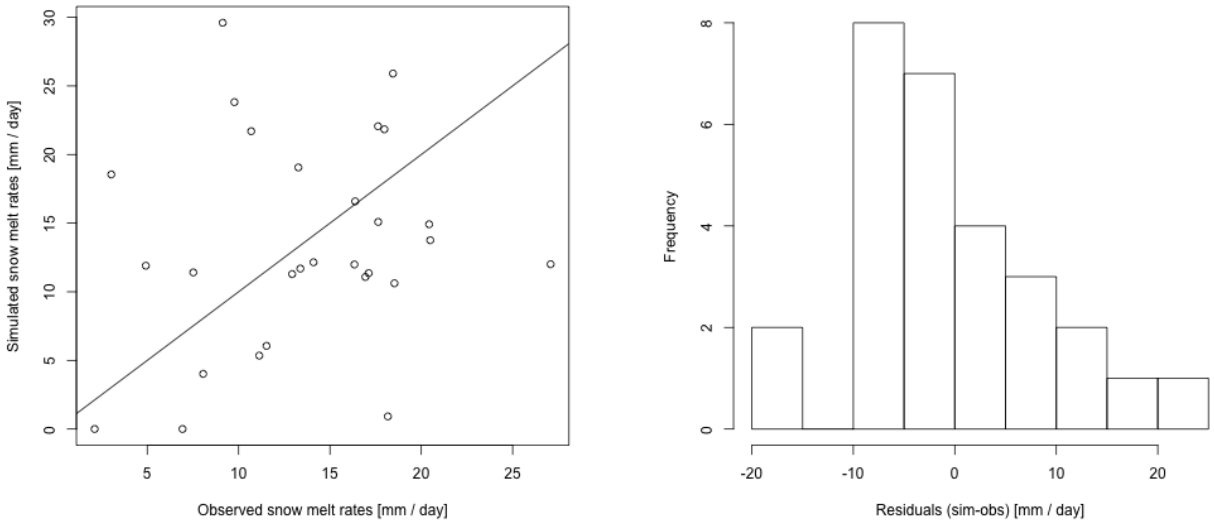

(a) (b)

Figure 58: *a) Observed vs. simulated melt rates, b) Histogram of residuals (sim-obs) of melt rates melt. Snow melt season of 2011 with observed L_a and L_t as additional input data, 24 hour resolution*

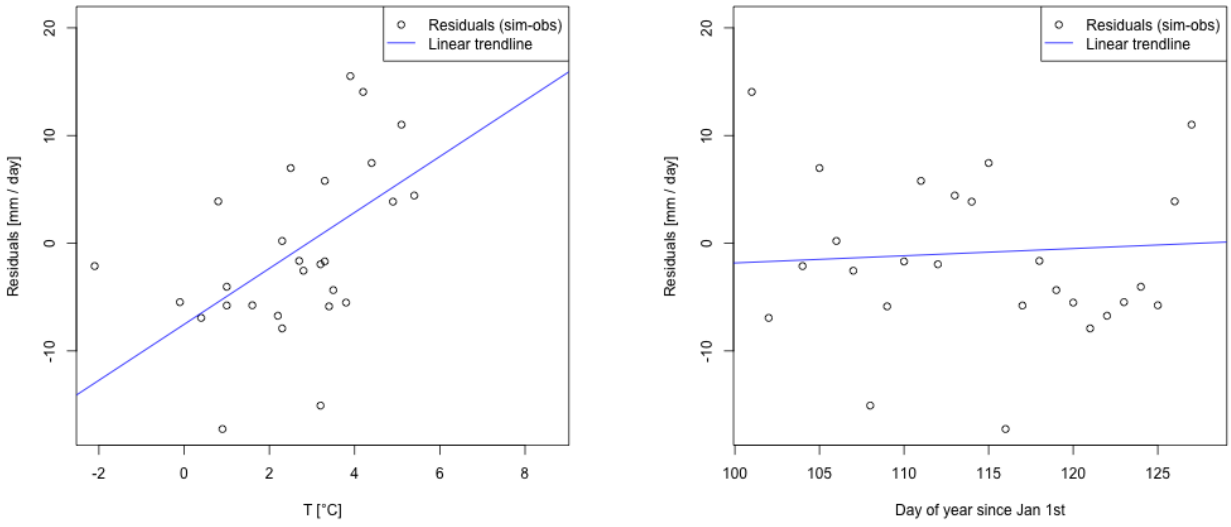

(a) (b)

Figure 59: *a) Temperature vs. residuals, p-value* $2.65 \cdot 10^{-14}$. *b) Day number vs. residuals, p-value* 0.47. *Observed L_a and L_t included as input data, 24 hour resolution.*

6.4.3 Wind

When the constant wind speed of 1.75 $m\ s^{-}$ in seNorge_eb was substituted with observed wind data there was a small change in SWE for the 2011 and 2013 melt seasons (figs. 60a and 60c) and little or no change in 2012 and 2014 (figs. 60b and 60d). Events where observed wind had an increasing effect on the snow melt coincided with an increase in SH and LE (e.g. events 5-10 in Fig. 61a and 12-14 in Fig. 61c).

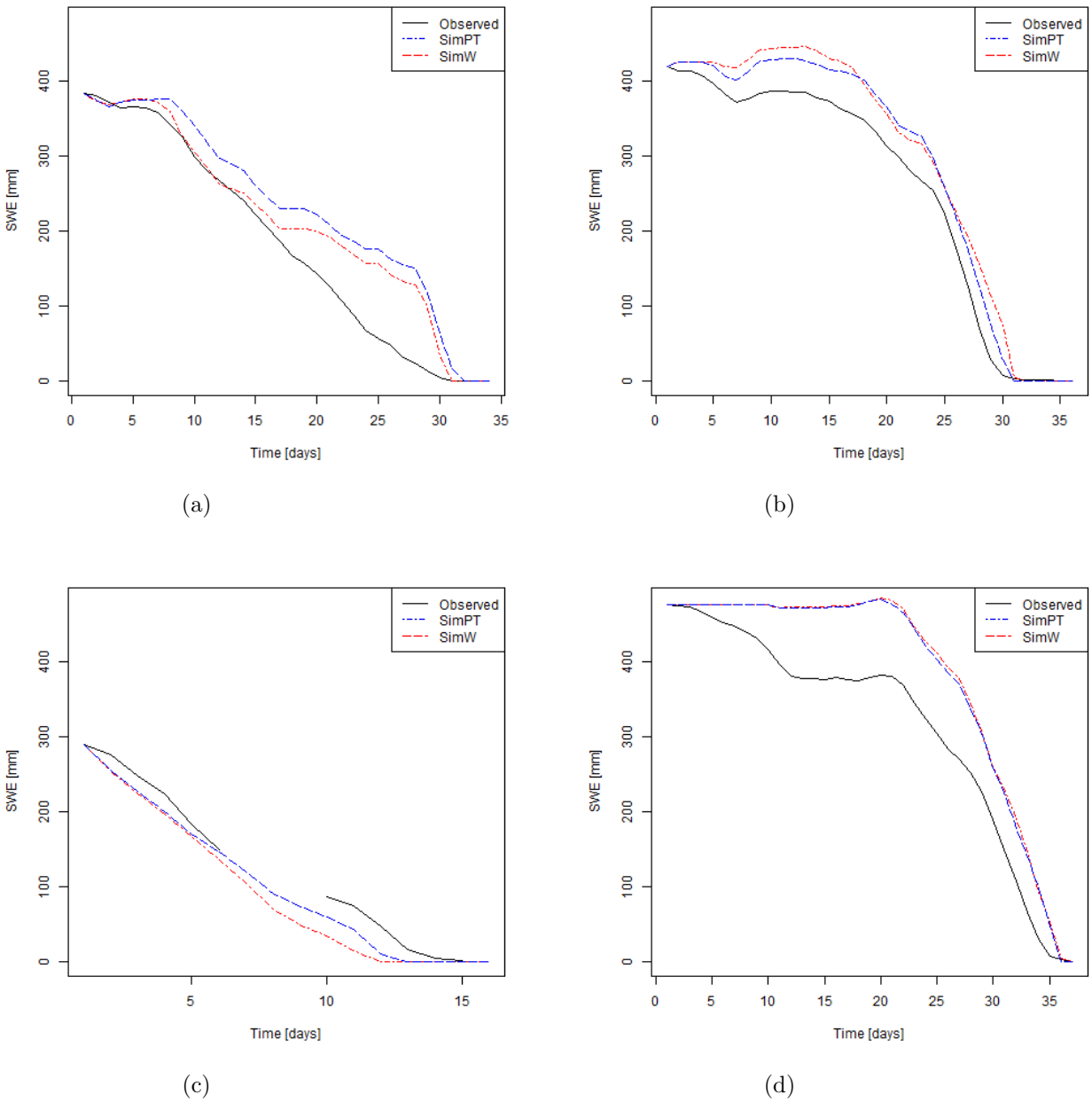

Figure 60: *Observed and simulated SWE during melt seasons. a) 2011, b) 2012, c) 2013, d) 2014. SimPT: precipitation and temperature, SimW: precipitation, temperature and wind. 24 hour resolution.*

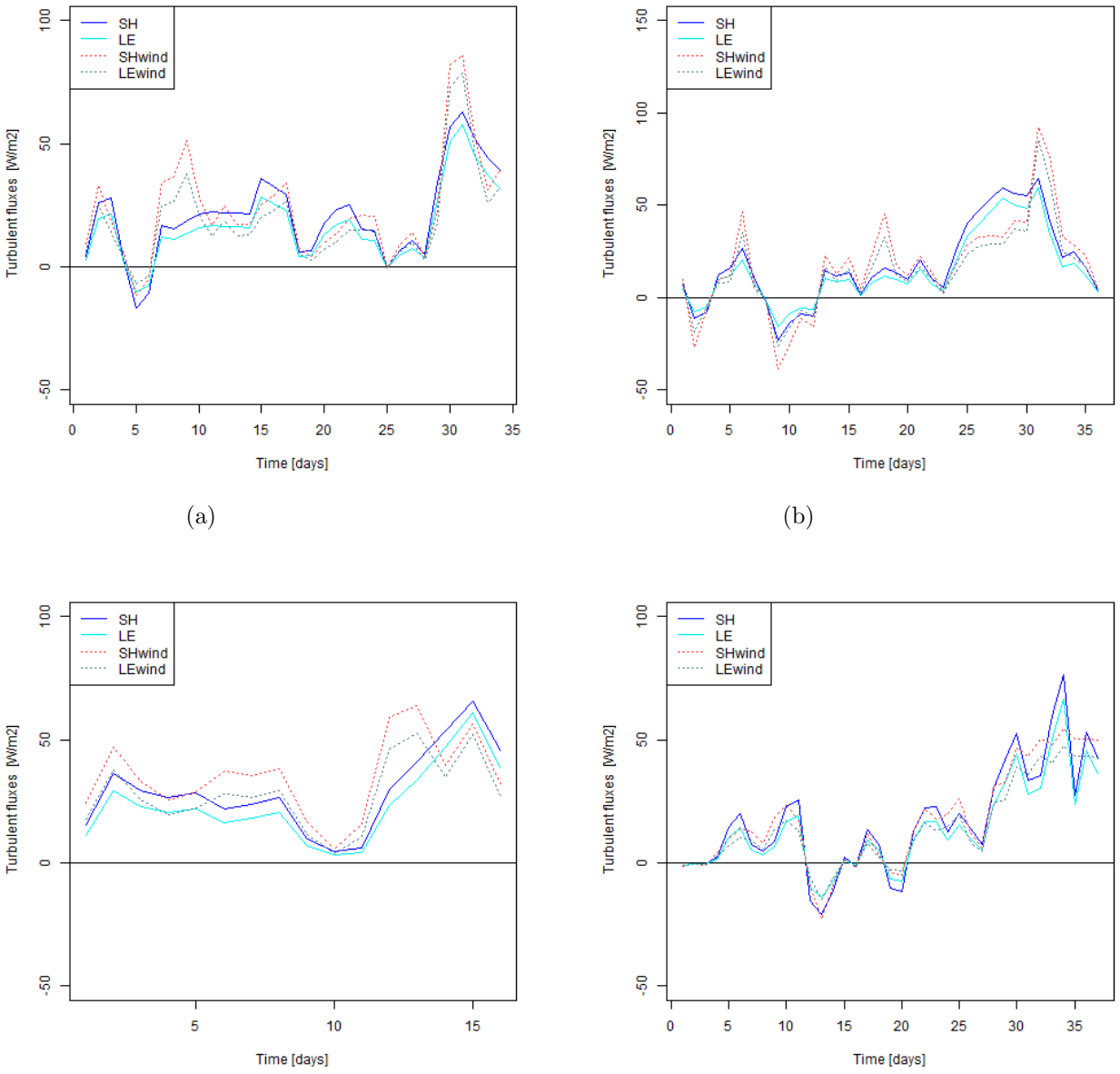

Figure 61: *a) 2011, b) 2012, c) 2013, d) 2014. Distribution of turbulent energy fluxes during melt seasons. SH and LE: precipitation and temperature, SEwind and LEwind: precipitation, temperature, and wind. 24 hour resolution.*

Table 29: *Mean values* $[W\ m^{-2}]$ *of energy fluxes in Fig. 61, 24 hour resolution.*

	2011	2012	2013	2014
SH	20.90	17.70	29.10	17.30
SHwind	23.50	17.90	34.90	16.70
LE	16.70	14.80	23.60	14.20
LEwind	18.70	14.80	27.80	13.70

The objective model evaluation criteria were ambivalent regarding the improvement of the snow melt rates with observed wind in the simulations, and the overall impression is that the snow melt rates were not improved (Table 30 compared to Table 16). seNorge_eb overestimated snow melt with a net positive mean error (ME) for all season (however negative in 2011) (Table 30 and Fig. 62). There are some residual outliers (> 40 mm) that draws the net ME in a positive direction (Fig. 62b). RMSE shows less variation between the seasons (Table 30).

Table 30: *Model evaluation of snow melt rates. Melt seasons 2011-2014, 24 hour resolutions. Wind as additional input data. Events were both simulated and observed $SWE > 0$ mm and simulation and/or observation indicate melt are evaluated.*

	All seasons	2011	2012	2013	2014
No of. residuals	98	29	29	8	32
NS	-0.12	-3.60	0.01	0.13	0.31
ME	1.40	-0.32	2.10	6.50	0.95
RMSE	13.00	13.00	15.00	13.00	11.00

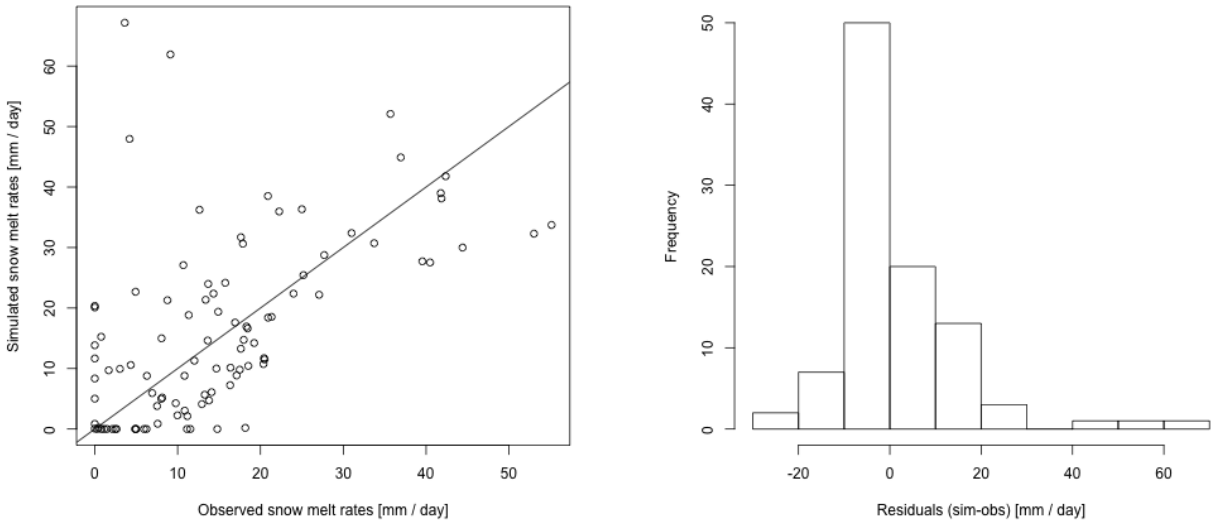

(a) (b)

Figure 62: *a) Observed vs. simulated melt rates, b) Histogram of residuals (sim-obs) of melt rates melt. Snow melt season of 2011, with observed wind as additional input data. 24 hour resolution.*

Both temperature and day number were found significant in explaining the residual error when observed wind was included as input data (Fig. 63).

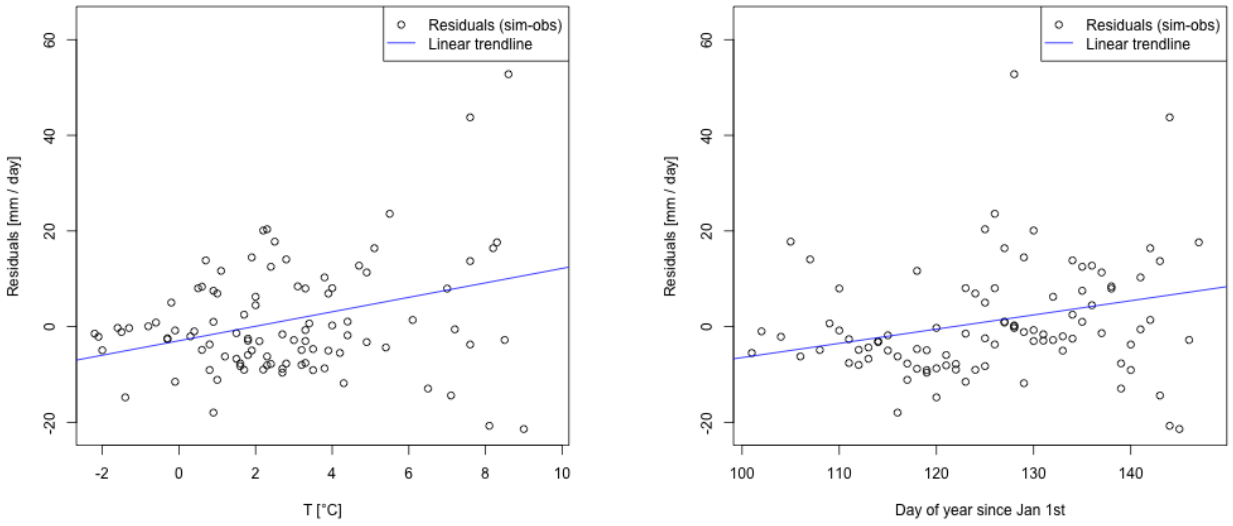

(a) (b)

Figure 63: *a) Temperature vs. residuals, p-value 0.0016. b) Day number vs. residuals, p-value 0.011. Snow melt seasons 2011-2014, 24 hour resolution.*

6.4.4 Snow surface temperature

Including snow surface temperature, T_{ss}, derived from observed 24 hour resolution long-wave radiation resulted in slower meltdown compared to simulation where T_{ss} was computed by the model (Fig. 64). By including T_{ss} from observed long-wave terrestrial radiation data the mean total energy available for snow melt decreased due to an increase in net long-wave radiation (L) and a decrease in the turbulent fluxes (SH and LE) (Table 31 and Fig. 65).

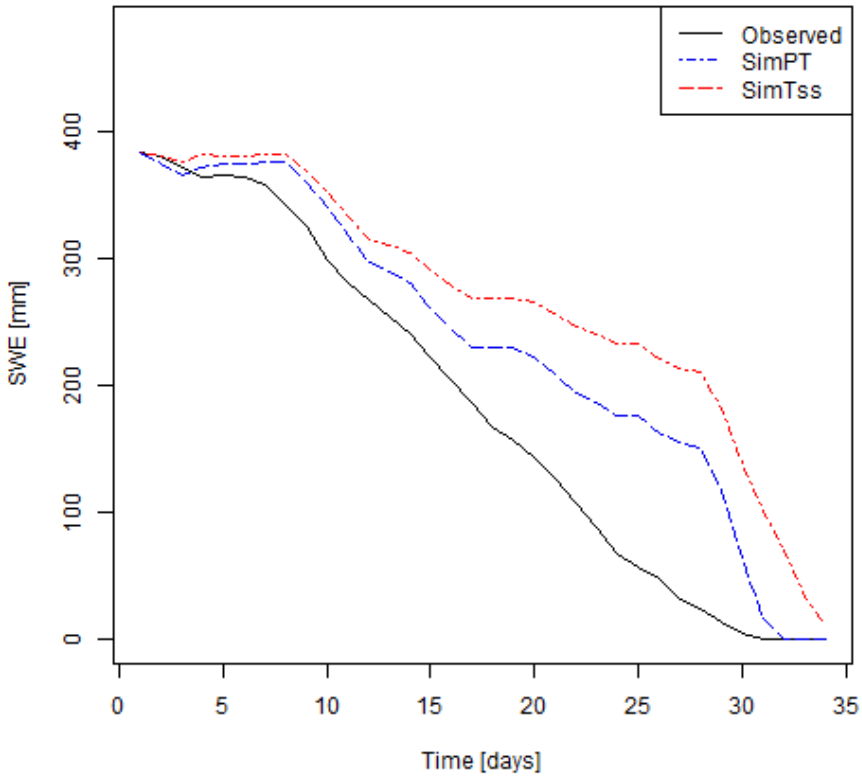

Figure 64: *Snow melt season of 2011, 24 hour resolution. SimPT: precipitation and temperature, SimTss: precipitation, temperature and* T_{ss}.

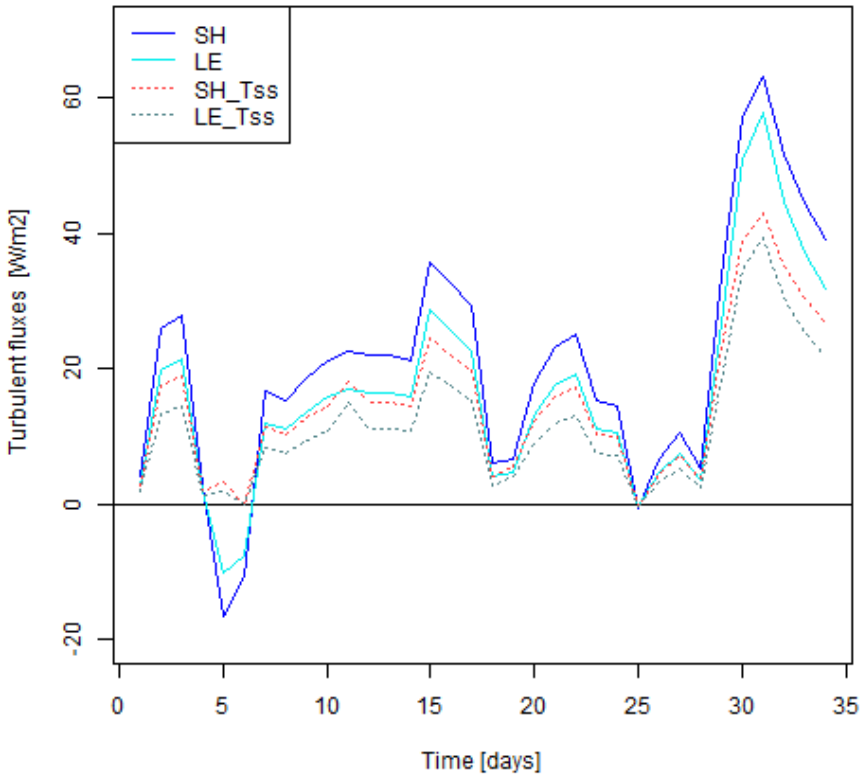

Figure 65: *Distribution of the turbulent energy fluxes during melt season of 2011, 24 hour resolution. SH and LE: precipitation and temperature, LE_Tss: precipitation, temperature and* T_{ss}.

Table 31: *Mean values* $[W\ m^{-2}]$ *of net long-wave and turbulent fluxes the during ablation period of 2011, 24 hour resolution.*

	SimT_{ss}	SimPT
L	-38.60	-41.00
SH	15.00	20.90
LE	11.90	16.70

According to the objective model evaluation criteria the snow melt were not better simulated, except for a small increase in NS, by including observed T_{ss} as input data (Table 32).

Table 32: *Model evaluation of snow melt rates. Melting season of 2011, 24 hour resolutions. Events were both simulated and observed SWE > 0 mm and simulation and/or observation indicate melt are evaluated.*

	SimT_{ss}	SimPT
No. of. residuals	33	30
NS	-2.88	-3.70
ME	-0.49	0.06
RMSE	14.10	14.00

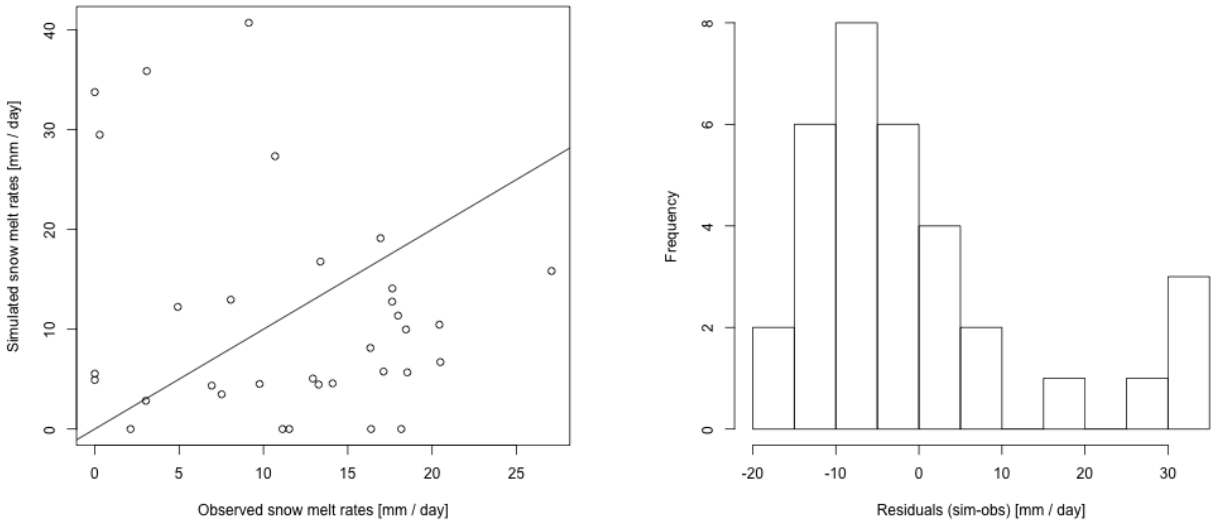

(a) (b)

Figure 66: *a) Observed vs. simulated melt rates, b) Histogram of residuals (sim-obs) of melt rates melt. Snow melt season of 2011, with observed T_{ss} as additional input data. 24 hour resolution.*

Both temperature and day number were significant in explaining the residual error when T_{ss} was included in the simulations (Fig. 67).

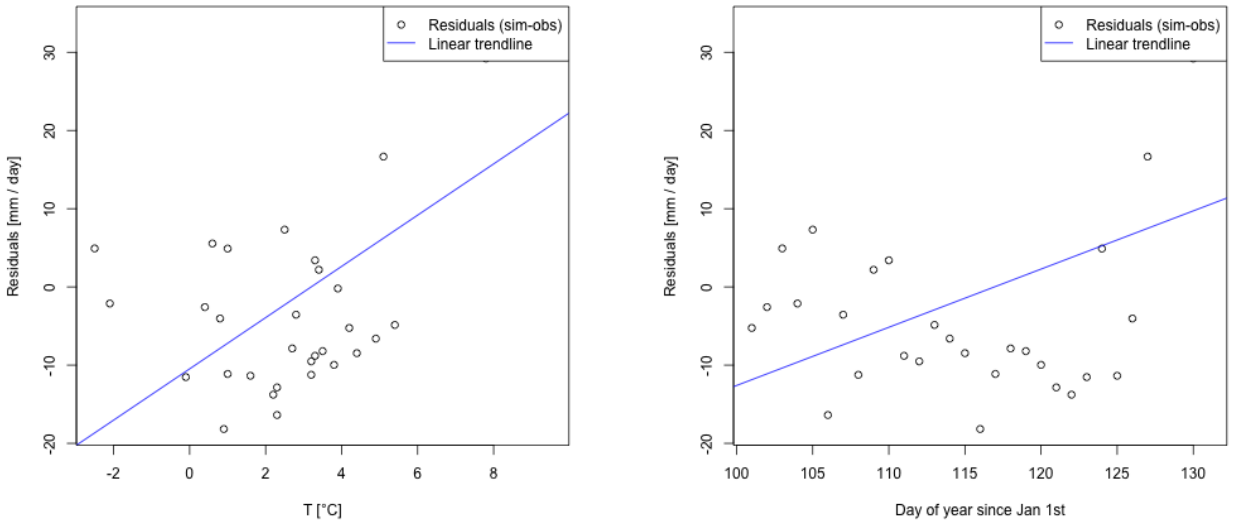

(a) (b)

Figure 67: *a) Temperature vs. residuals, p-value* $1.5 \cdot 10^{-5}$. *b) Day number vs. residuals, p-value 0.009. Observed* T_{ss} *as additional input data, 3 hour resolution.*

6.4.5 Relative humidity

As a result of including RH in the latent heat flux, the snow season was extended (SimRH in Fig. 68). This was a result of the relative humidity being less than 100 % on majority of the days. The reduction in the latent heat flux is seen in in Fig. 69 (LE compared to LE_RH).

With relative humidity included in the simulations LE became negative also for positive air temperatures ($T_a > 0$°C (LE compared to LE no data in Fig. 69). Meaning that evaporation took place for air temperatures of both negative and positive T_a. Moreover, the turbulent fluxes no longer worked in the same direction for all events. The snow melt rates were only improved in terms of NS (Table 33), and they were underestimated (Fig. 70).

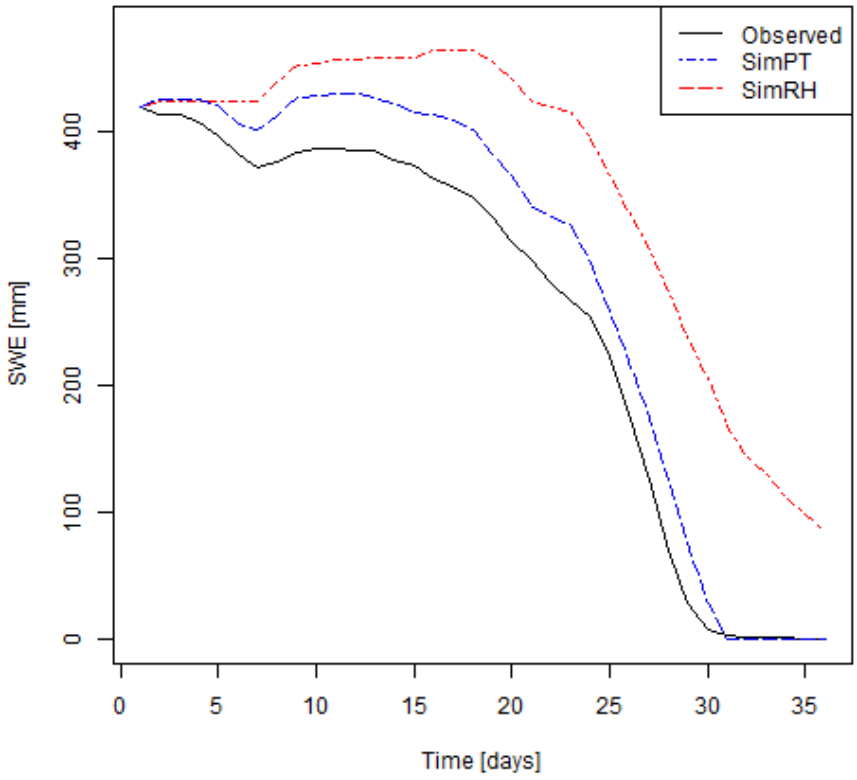

Figure 68: *Observed and simulated SWE during melt season of 2012. SimPT: precipitation and temperature, SimRH: precipitation, temperature and relative humidity. 24 hour resolution.*

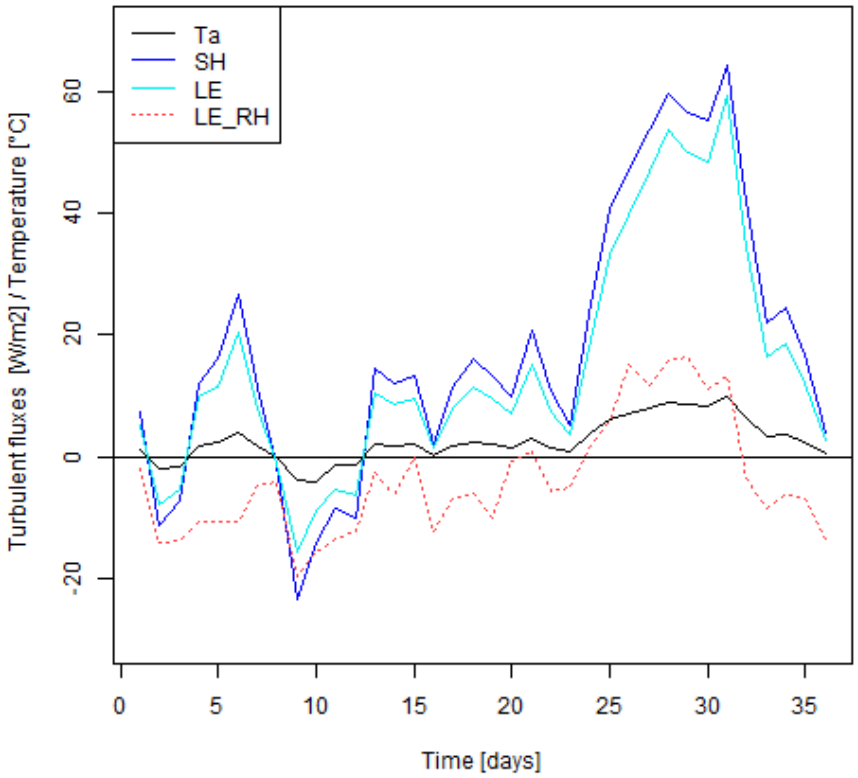

Figure 69: *Distribution turbulent energy fluxes during melt season of 2012. SH and LE: precipitation and temperature, LE_RH: precipitation, temperature and RH. T_a: observed air temperature. Mean LE_RH: -3.8 W m^{-2}, mean LE: 14.80 W m^{-2}. 24 hour resolution.*

Table 33: *Model evaluation of snow melt rates. melt season of 2012, 24 hour resolutions. Results from simulation with only precipitation and temperature data are given in parentheses. Events were both simulated and observed SWE > 0 mm and simulation and/or observation indicate melt are evaluated.*

	SimRH	SimPT
No. of residuals	33	30
NS	0.36	0.72
ME	-1.48	0.52
RMSE	12.34	8.20

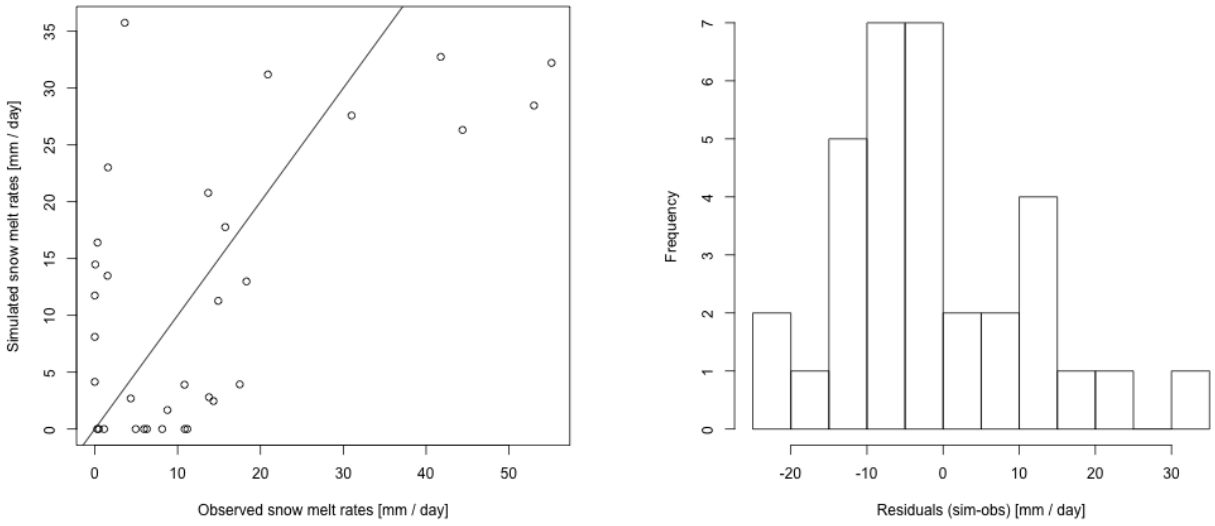

(a) (b)

Figure 70: *a) Observed vs. simulated melt rates, b) Histogram of residuals (sim-obs) of melt rates melt. Snow melt season of 2011, with observed T_{ss} as additional input data. 24 hour resolution.*

Temperature and day number were not significant in explaining the residual error when RH was included in the simulations (Fig. 71).

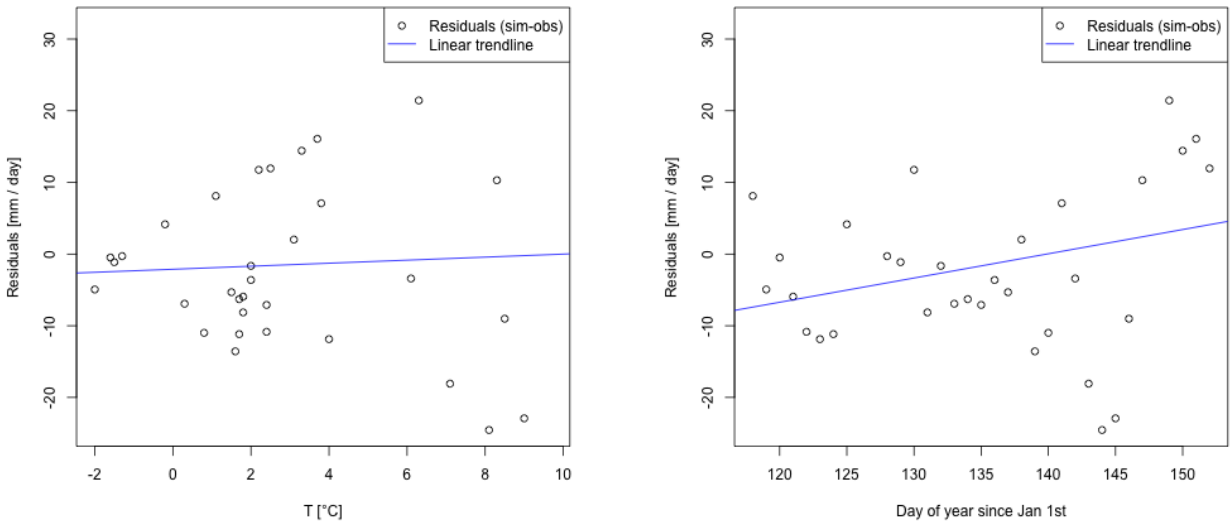

(a) (b)

Figure 71: *a) Temperature vs. residuals, p-value 0.76. b) Day number vs. residuals, p-value 0.11. Observed T_{ss} as additional input data, 24 hour resolution.*

6.4.6 $S\downarrow$, L, wind, T_{ss}

This section contains the model simulation results on 24 hour resolution with additional input data $S\downarrow$, L, wind, T_{ss} for the period October 2010-May 2011. The relative humidity data on 24 hour resolution could not be included due to missing data.

From a visual perspective the additional input data did not improve the results (SimAll in Fig. 72).

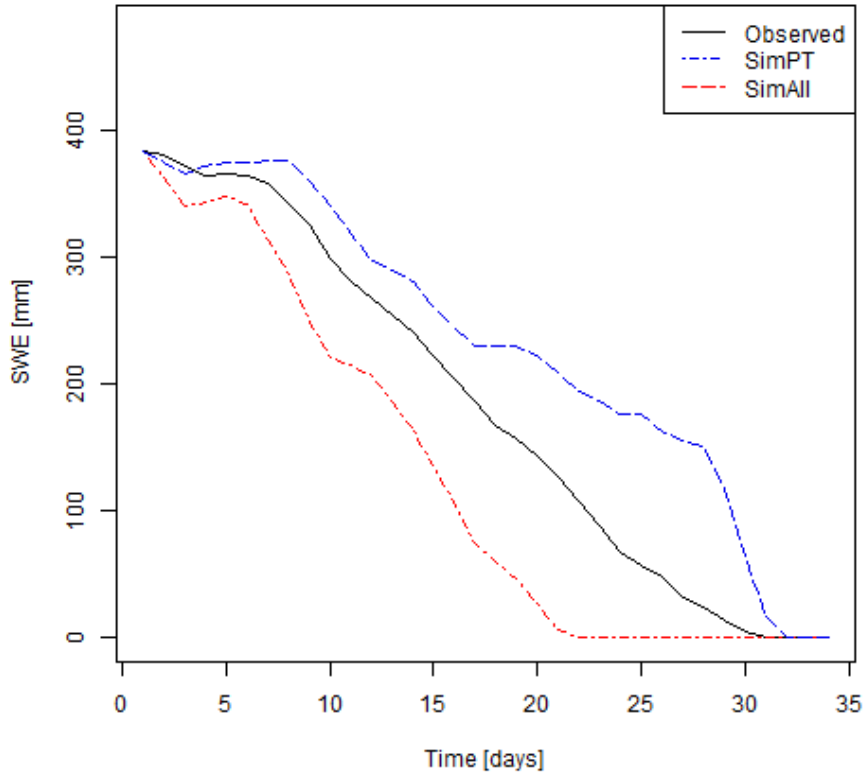

Figure 72: *Snow melt season of 2011, 3 hour resolution. SimPT: precipitation and temperature, SimAll: precipitation, temperature, $S\downarrow$, L_a and L_t, wind and T_{ss}.*

According to Table 34 the objective model evaluation criteria, the snow melt rates were improved in terms of NS ans RMSE when observed $S\downarrow$, L_a and L_t, wind and T_{ss} were included as input data, meaning that large errors and the variability of the residuals were reduced. The systematic error (ME) was increased.

Table 34: *Model evaluation of snow melt rates. melt season of 2012, 24 hour resolutions. Events were both simulated and observed SWE > 0 mm and simulation and/or observation indicate melt are evaluated.*

	SimAll	SimPT
No. of. residuals	20	30
NS	-1.56	-3.70
ME	6.64	0.06
RMSE	10.53	14.00

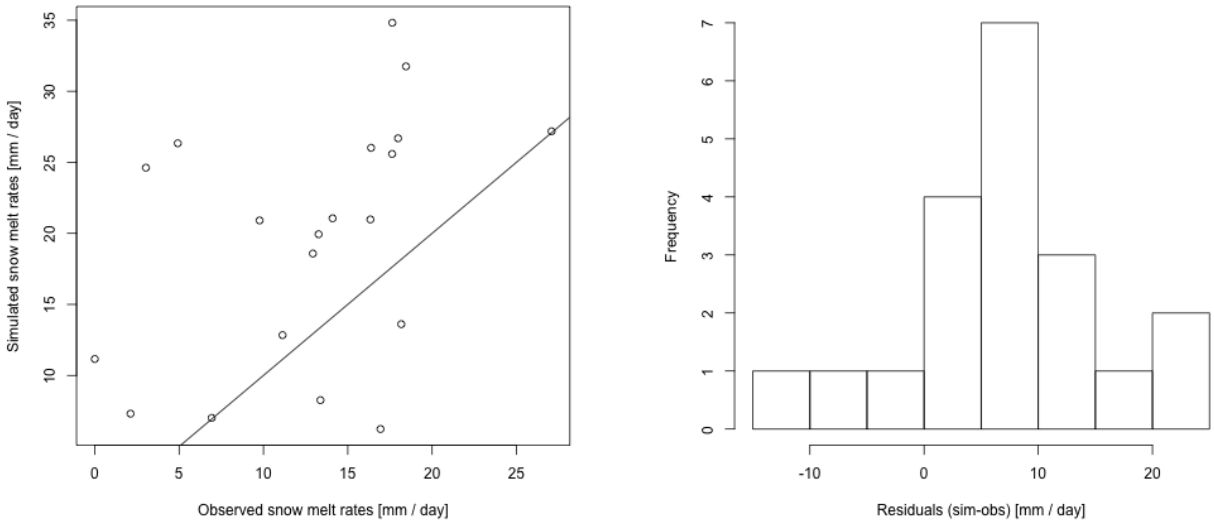

(a) (b)

Figure 73: *a) Observed vs. simulated melt rates, b) Histogram of residuals (sim-obs) of melt rates melt. Snow melt season of 2011, with observed relative humidity as additional input data. 24 hour resolution.*

Nor temperature or day number was found significant in explaining the residual error when observed $S\downarrow$, L_a and L_t, wind and T_{ss} were included in the simulations (Fig. 74).

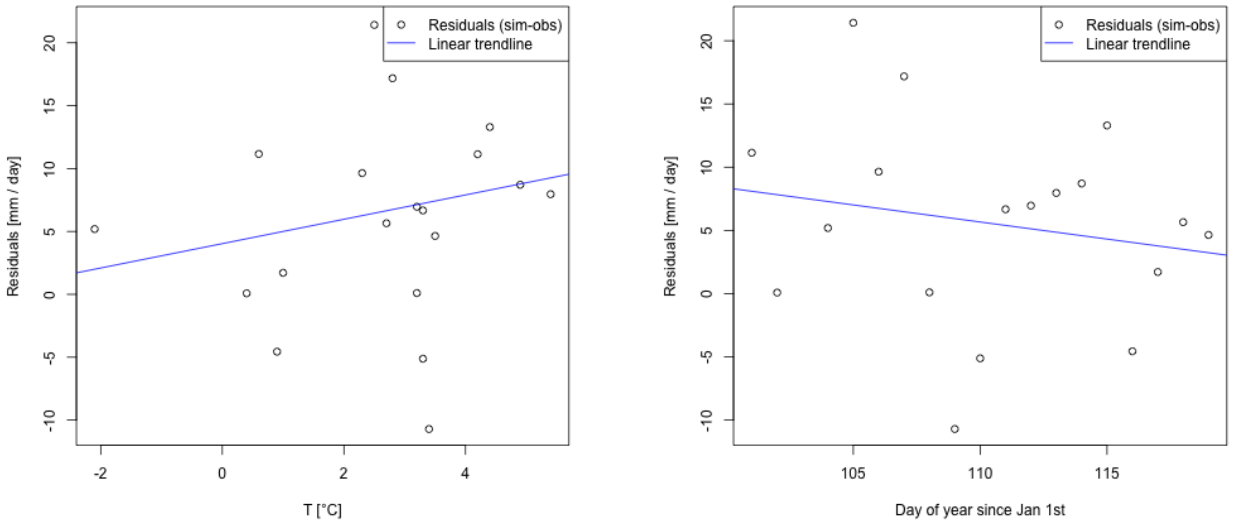

(a) (b)

Figure 74: *a) Temperature vs. residuals, p-value 0.38. b) Day number vs. residuals, p-value 0.45. Observed relative humidity as additional input data, 24 hour resolution.*

6.4.7 Summary: introducing additional data - 24 hour resolution

By simulating with observed solar radiation, $S\downarrow$, more energy was available for melt and the snow melted more rapidly during the ablation season compared to simulations with parametrized $S\downarrow$. In terms of the objective model evaluation criteria there was not a clear improvement or degradation of the snow melt rates.

Introducing observed atmospheric and terrestrial long-wave radiation data had little visual effect, but improved NS and RMSE.

The turbulent fluxes were altered by introducing observed wind, snow surface temperature and relative humidity data. Observed wind did not have a clear effect on the melt rates: in 2011 and 2012 the turbulent fluxes were increased, whereas for the 2012 and 2014 ablation seasons they remained almost unchanged. The net impression is that observed wind did not have a notable effect on the snow melt rates.

Snow surface temperature decreased the sensible and latent heat fluxes thus decreasing melt rates. The objective model evaluation criteria were not improved, except for a small improvement in NS.

Relative humidity data decreased the latent heat flux and the energy available for melt was reduced. Moreover, evaporation was facilitated from the snow to the air for both positive and negative air temperatures.

When observed $S\downarrow$, L_a and L_t, wind and T_{ss} were included as input data for the snow season of 2010-2011, the snow melt rates were improved in terms of NS and RMSE compared to simulation with only precipitation and temperature. The observed relative humidity data did not cover this period. However, if we compare the simulated SWE in which relative humidity and the SWE that has observed $S\downarrow$, L_a and L_t, wind

and T_{ss} as additional input data, combined they might give an acceptable result as they work in opposite directions.

Overall, from a visual perspective observed $S \downarrow$ had the largest effect in increasing melt and relative humidity in decreasing melt.

7 Discussion

In this chapter the results of the simulations presented in chapter 6 are discussed. The aims are to assess the model performance, which parametrizations ought to be improved and possibly how it can be done referring to previous studies. First the issue of how the data quality of the observed data affects the simulation results is addressed (section 7.1). Then the overall model performance with observed precipitation and temperature as only input data is discussed in terms of seNorge_eb's precision in predicting snow melt rates as well as the distribution of the energy fluxes (section 7.2). The successive sections (7.3-7.4) discuss how the parametrizations of the radiation fluxes perform in comparison with observed data and how the deviations may be improved. A separate section (7.5) is devoted to the issue of how to determine the cloud cover fraction as that is an important element of the parametrizations of the components of the net radiation. Section 7.6 addresses what effect the inclusion of wind, snow surface temperature and relative humidity have on the turbulent fluxes. Section 7.7 deals with the air temperature, T_a, that which in most cases was found significant in explaining the residual term of the snow melt rates (i.e. simulated minus observed snow melt rates).

7.1 Data quality and model performance

This section addresses how uncertainty of the observed data, beyond what is being informed about by the manufacturer of the measuring equipment, affects the results. The uncertainty of the data used for input and/or evaluation will in turn affect the results. This section is limited to precipitation, radiation elements and snow water equivalent.

Precipitation
That wind affects the precipitation measurements, and that there is a systematic undercatch in the data from rain gauges based on weight or quantity is a well known phenomenon (Wolff et al. 2013). This is particularly so for precipitation in the form of snow. Local precipitation and temperature measurements are common input data in hydrological models in which precipitation is accumulated. Undercatch of snow in the data will thus propagate throughout the snow season and in turn lead to incorrect forecasts of the melt-period, amount of melt water, flood risk and of reservoir levels (Wolff et al. 2013).

The most noticeable uncertainty among the input data is related to the precipitation data. As mentioned in section 4.2.2 precipitation in the form of snow was multiplied by a correction factor that compensated for the undercatch of snow. The correction factor was tuned for each season. If undercatch of snow had not been corrected the simulated cold content would have been too low as it is a function of the height of the snow (Eq. 44) and the number of events to compare would have been smaller. The analysis of the snow melt rates was concentrated on the ablation season and the simulated SWE was set equal to the observed SWE at the start of the meltdown. If we assume that there were no new snow falls of significance during the ablation period, the issue of undercatch of snow would not have much effect on the results. However, if there had not been a problem related to the precipitation data, the period analysed could have been extended to include the entire snow season.

Wolff et al. (2013) carried out a study on undercatch of snow in Norway. Based on observations from Haukeliseter they developed a formula aimed at correcting undercatch of snow caused by wind. The formula is valid for automatically precipitation gauges with wind shields, and includes the measured variables precipitation, temperature and wind speed. It would be interesting to include the formula suggested by Wolff et al. (2013) in the accumulation routine of seNorge_eb. A drawback is of course that it requires a measured variable in addition to precipitation and temperature.

Radiation elements

Incoming solar radiation

In the study area solar radiation is being recorded by two pyranometers of the same type that are, according to Møen (pers comm. 24.04.2015), expected to record the same solar radiation values. The pyranometer that provides data used for evaluation and input throughout this thesis is attached to the mast close to the snow weight 2.7 m above the ground. The pyranometer that is not used in this thesis [1] is situated 4.3 m above the ground, attached to a mast on the roof of the equipment cabin a few meters from the NVE station (Møen pers comm. 24.04.2015; Stranden and Grønsten 2011). Fig. 75 shows the residuals of recorded solar radiation values from the two pyranometers (i.e. values from sensor at 2.7 m height minus values from sensor at 4.3 m height) during the snow melt season of spring 2011. Data from the sensor at 4.3 m height are only available at 24 hour resolution, hence the comparison could not be done on 3 hour intervals. Fig. 75 shows that observations of incoming solar radiation within a limited area can deviate between location and sensor. In this case it is not possible to tell whether the deviations are caused by the location or sensor. Fig. 75 does, however, show that there is a disagreement between the observations between the two pyranometers deployed in the field. It is impossible to tell which pyranometer that records the correct values. Except for no. 11 and 12, the measurements from the two sensors do not deviate more than $\pm$ 10 %, which is the daily accuracy stated by the manufacturer. The deviations have little impact on the snow melt. Event no. 11 and 12 are for both sensors low in value (no. 11: 0.39 $W\ m^{-2}$ and 31.7 $W\ m^{-2}$, no 12: 0 $W\ m^{-2}$ 26.03 $W\ m^{-2}$ for the sensor at 4.3 m height and 2.7 m height respectively) and are the lowest in the whole period, 09.04-01.05.2011. seNorge_eb predicts a higher value (Fig. 53), but since both pyranometers record a small incoming solar radiation it it likely that the observations are true, even though it is not certain which observed value is correct.

[1] Hydra II parameter number 73.11.06.01 Global radiation (also listed in Appendix A). Daily mean values from 09.04-01.05.2011 were retrieved to generate the plot in Fig. 75

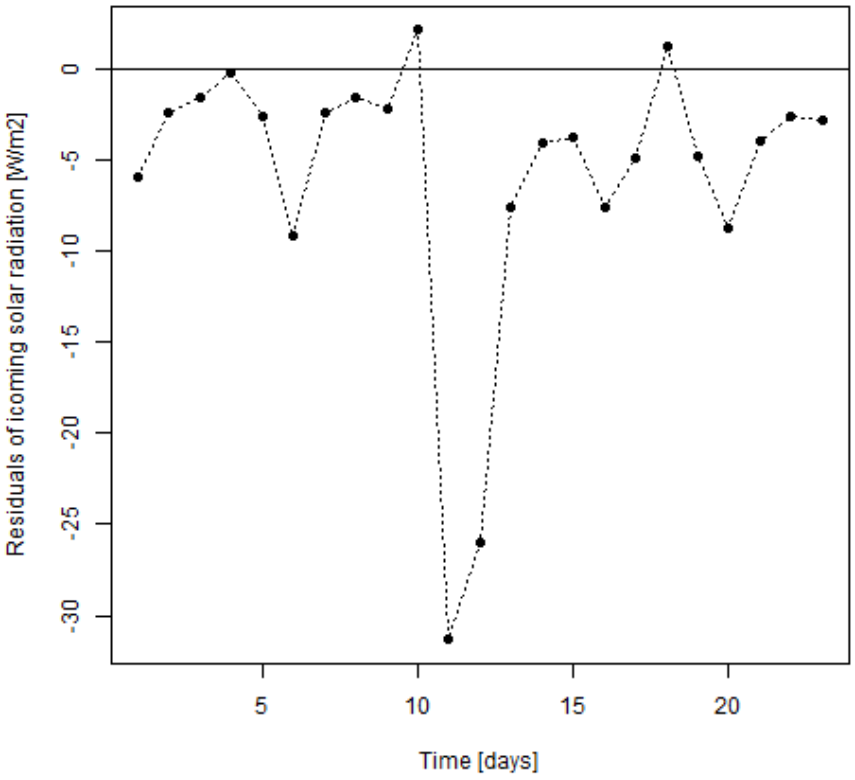

Figure 75: *Residuals of incoming solar radiation from the two pyranometers: data from sensor at 2.7 m height minus sensor at 4.3 m height. Melt season 2011, 9 April - 1 May, 24 hour resolution.*

Long-wave radiation
Regarding the atmospheric long-wave radiation we can assume that the uncertainty is in the range of the incoming solar radiation as it is measured by a pyrgeometer situated at the same sensor (CNR4 Net Radiometer) as the pyranometer. Observed terrestrial radiation took on a larger range of values than the simulated terrestrial radiation during the snow melt period. According to the theory, the snow surface temperature, T_{ss}, should be constant at 0 ℃ during the ablation period and thus a constant terrestrial radiation at about 316 $W\ m^{-2}$ is expected. The variation in the observed terrestrial radiation data might relate to uncertainty of the pyrgeometer, or it might be a result of unevenly distributed snow below the sensor; If the snow season is at its very end there might be some snow on the snow weight and bare ground below the pyrgeometer-sensor.

Snow water equivalent
The snow weight Møen2525 was chosen as reference SWE based on its performance compared to the other 7 SWE measurements at NVEs station (i.e. gamma sensor and various snow pillows). NVE-reports about evaluation of the snow measurements at Filefjell have shown that there are deviations between the SWE data from the different instruments, and that in 2009-2013 Møen2525 recorded the largest, the second or third largest SWE (Stranden and Grønsten 2011, Fjeldheim and Barfod 2013,

Ree and Stranden 2014). During winter season 2012, for 28 February to 1 March, the SWE recorded by Møen2525 deviated from the other SWE observations (Fjeldheim and Barfod 2013). In this period the other SWE data showed a decrease, whereas data from Møen2525 showed an increase, creating a deviation between the different measurements that propagated throughout the rest of the snow season. In this case the SWE used as reference after this incident might be too high.

Visual inspection of SWE on 3 hour resolution shows that there are fluctuations in the observed SWE. This is most readily seen in the 2011-melt season (ch. 6). According to Møen and Stranden (pers comm. 24.04.2015) this phenomena is believed to results from physical changes within the snow pack and compressions from the sides as the snow that is being measured by the snow weight is a part of a larger snow pack. However, these fluctuations are negligible compare to the overall uncertainty of the measurements (Møen and Stranden pers comm. 24.04.2015).

Upon evaluating seNorge_eb's performance against Møen2525 it is important to keep in mind that the observed SWE is subject to several sources of uncertainty.

7.2 Overall model performance

The discussion in this section refers to the results of model simulations on 3 hour and 24 hour resolution presented in sections 6.1 and 6.2 where precipitation and temperature data are the only observed input data.

According to the objective model evaluation criteria outlined in section 4.2.3 (i.e. NS, ME and RMSE evaluated for snow melt rates on events where both simulated and observed SWE were larger than 0 mm and melt was recorded either by observations or simulations) the simulations with 24 hour resolution data had the best performance in terms of NS and ME for all the melt seasons combined. However, the data for comparison were scarcer than for 3 hour resolution (98 vs. 587 samples in total for all snow melt seasons of 2011-2014). By looking at the seasons individually, the 3 hour resolution had for all seasons a lower RMSE, thus fewer larger error, but this is expected for narrowed time intervals. The 24 hour resolution had a NS closest to 1 for the 2012-2014-seasons, and a smaller ME for the 2012 and 2014 seasons. In terms of visual inspection of observed and simulated SWE during the main ablation seasons the 3 hour resolution gave the best result. For the 24 hour resolution version the simulated SWE was higher than the observed SWE due to underestimation of incoming solar radiation (discussed in section 7.3).

In sum, the snow melt rates were fairly well predicted by seNorge_eb even though investigations of individual energy fluxes and parameters revealed substantial disagreement compared with observed values.

Walter et al. (2005) performed a similar study on snow melt using an energy balance model where the fluxes were parametrized and the only input data were temperature and precipitation in addition to some predefined constants. In accordance with the results in this thesis Walter et al. also concluded that the snow melt predictions were good despite considerable inconsistencies of individual parameters and energy fluxes.

Kuusisto (1986) carried out a study on melting snow cover on two different sites in Finland as well as comparing 20 other studies on snow melt modelling worldwide that

used an energy balance approach. Kuusisto concluded that the energy fluxes that compose the energy balance vary in space with the specific location. In spite of the spatial variability of the study sites Kuusisto managed to outline some general characteristics associated with a melting snow cover. The major components are the net radiation and turbulent fluxes. Ground heat and heat input by precipitation can be regarded as negligible. During the melt period both evaporation and condensation may occur.

Kuusisto's findings are consistent with the simulations results in this thesis using only precipitation and temperature as input data, except for evaporation. seNorge_eb predicted evaporation during the ablation period only for events where the air temperature was less than the snow surface temperature (addressed in section 7.6.3).

7.3 Solar radiation

Outgoing solar radiation, $S\uparrow$, could not be evaluated due tothe poor data quality of the observed data. For the same reason it was not possible to evaluate the snow albedo (i.e. ration of outgoing to incoming solar radiation). However, a result from a study by Malik et al. (2014), where different types of snow albedo parametrizations were investigated, should be mentioned. Data from eight sites under prairie, alpine and tundra snow conditions in the USA, France and on the Tibetan Plateau were included in the study. Among the albedo parametrizations that they investigated is one by Dickinson et al. (1993), the same that is incorporated in seNorge_eb. According to the findings by Malik et al. Dickinson's albedo parametrization was not able to accurately capture the characteristics the albedo's development and the albedo was overestimated with the result of an extended presence of the snow-packs for all the sites. As such, in order to evaluate the albedo and verify the findings by Malik et al. (2014) it is recommended to run seNorge_eb for another site where both incoming and outgoing solar radiation data of good quality are available.

The parametrization of incoming solar radiation, $S\downarrow$, slightly overestimate compared with observations on 3 hour resolution (5.6 $W\ m^{-2}$). On 24 hour resolution the simulated values were clearly underestimated compared to observed values. Separating between cloudy and clear events (i.e. assumed full cloud cover and almost, 0.1, clear conditions) uncovered that there were large differences between these events.

The explanation for the deviation in $S\downarrow$ on 24 hour resolution is believed to result from how the algorithm of $S\downarrow$ is set up for the 24 hour version, and particularly related to the averaging of the transmissivity. Thus the algorithm for simulated $S\downarrow$ should be revised. Fig.76 shows the daily average potential clear-sky solar radiation, S_c, for Filefjell vs. day number as set up in seNorge_eb compared to an alternative algorithm suggested by Hock (1999). The latter was set up in MATLAB by Schuler (pers comm. 27.03.2015) using height and latitude:

$$S_c = S_0(\frac{R_m}{R})\Upsilon_a^{\frac{P}{P_0 cos\omega}} cos\theta \tag{57}$$

where S_0 is the solar constant, R is the sun-Earth distance (m referring to the mean), Υ_a is the atmospheric clear-sky transmissivity, P is atmospheric pressure (0 referring to the mean at sea level), ω is the local zenith angle and θ refers to the angle between the solar beam and the slope normal.

The parametrization of S_c with Eq. 57 seem to give more realistic values given that we know that the seNorge_eb's parametrization underestimates $S\downarrow$ even on clear events. A step in the improvement of seNorge_eb will be to implement Eq. 57 on daily resolution.

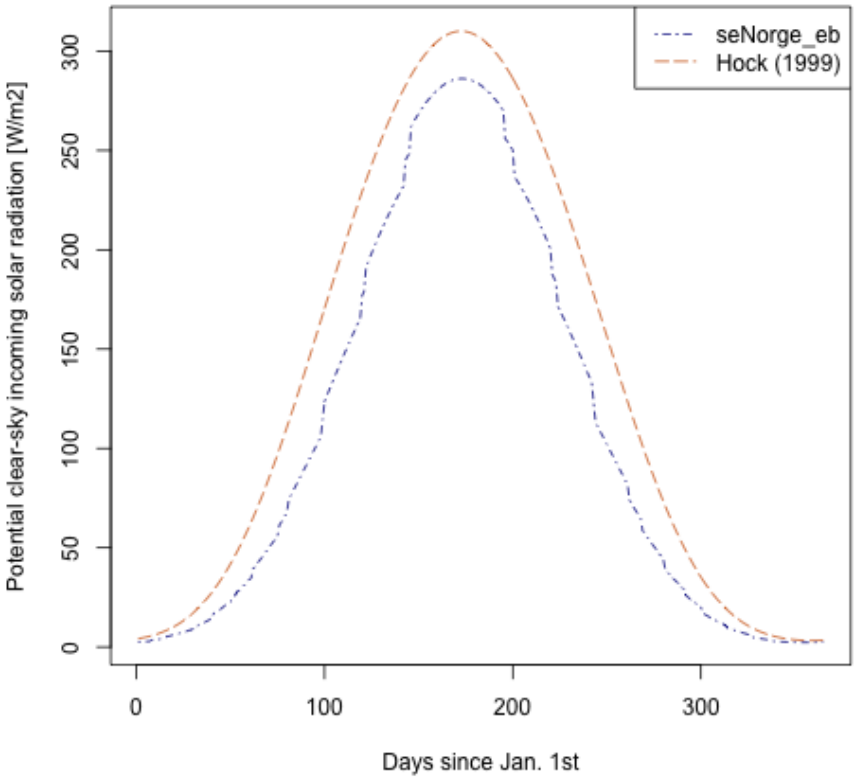

Figure 76: *seNorge_eb's parametrization of potential clear-sky solar radiation, S_c, for Filefjell compared an alternative parametrization taken from Hock (1999) (Eq. 57), 24 hour resolution. Maximum values of S_c by seNorge_eb and Hock (1999) are 286.2 $W\ m^{-2}$ and 310.1 $W\ m^{-2}$ respectively.*

7.4 Long-wave radiation

The parametrizations of the atmospheric long-wave radiation, L_a, was not able to reproduce the observed L_a from October 2010 to May 2011, neither on 3 or 24 hour resolution. ME for all events was -37.40 $W\ m^{-2}$ and -7.30 $W\ m^{-2}$ for 3 and 24 hour resolution respectively. Separating between cloudy and clear days revealed that L_a was highly underestimated on clear events (around -50 $W\ m^{-2}$ for both resolutions). The terrestrial long-wave radiation, L_t, was on events with snow only slightly underestimated on 3 hour resolution (-0.85 $W\ m^{-2}$) and somewhat overestimated on 24 hour resolution (5.52 $W\ m^{-2}$). Thus for the calculation of the net radiation (i.e. L_a minus L_t) the underestimation of L_a has the greatest impact and is most urgent to correct.

Walter et al. (2005) used the same parametrization of L_a on daily resolution at four sites across the US and set the cloud cover to be 1 on days with more than 0.5 mm observed

precipitation and otherwise 0. Without separating between cloudy and clear days Walter et al. (2005) found that the parametrization of L_a consistently underestimated compared to observed data from Danville, VT, one of the investigated sites. In fact L_a accounted for the worst absolute estimate of the parametrized fluxes.

The parametrization of L_a depends on the atmospheric emissivity, e_a, which in turn is composited by the clear sky atmospheric emissivity, ε_{cs}, and the cloud cover, Cl (see Eq. 35).

The high underestimation of L_a on clear days is related to ε_{cs}. If we consider the simulated and observed L_a on clear event on 3 hour resolution it it likely that some of the deviation is caused by the parametrization of ε_{cs}. 3 hour resolution precipitation data are accumulated precipitation from the current and previous two hours. Thus a clear event means that there was no observed precipitation for the last three hours. These events are assigned a cloud factor or 0.1, near to cloud free conditions. Thus we should expect a better fit for these events. Obviously there can be a full cloud cover without any precipitation hence the problem lies in the choice of Cl.

Juszak and Pellicciotti (2012) compared different parametrizations of incoming long-wave radiation over melting glaciers and investigated 13 clear-sky parametrizations. They concluded that it is important to recalibrate the parametrizations, as they were all empirical, for the particular location they are applied to due to differences in structure the atmosphere from site to site. In the same study Juszak and Pellicciotti quantified the effect parametrizations of L_a had on energy balance snow melt modelling, and concluded that recalibration of model parameters is needed. Sedlar and Hock (2009) performed a study in which they tested different long-wave radiation parametrizations under different sky conditions at Storglaciären in Sweden. The clear-sky parametrizations consisted of either near-surface vapour pressure and temperature or temperature alone. The latter parametrizations performed the worst.

The findings of Juszak and Pellicciotti (2012) and Sedlar and Hock (2009) are not promising regarding the clear-sky parametrization set up in seNorge_eb, an empirical relation derived by Swinbank (1963). The expression for ε_{cs} consists of only temperature as observed variable. Moreover, the expression suggested by Swinbank was derived using data from low-level stations in Australia and the Indian Ocean in 1961-62, 16-17 °South. Filefjell is, however, located at nearly 1000 masl., 61 °North. As such, a recalibration of the clear-sky atmospheric long-wave radiation is recommended, preferably by including air vapour pressure data if available.

7.5 Cloud cover

The comparison of observed $S\downarrow$ and L_a simulated values revealed that the source of error could, to a large extent, be explained by the cloud cover fraction. Increased cloud cover tend to reduce $S\downarrow$ and increase ε_{cs} (King et al. 2008). On events with observed rain the cloud cover was assumed 1 (i.e. full cloud cover) and 0.1 for events with no observed precipitation (thus assuming close to clear conditions). On rainy events a cloud cover factor of 1 was found to be an exaggerated assumption, and 0.1 on clear days an underestimation. For the latter this was particularly so for L_a, however, as noted above (section 7.4) the clear sky emissivity is also likely to be a source of error.

The cloud cover fractions observed during the field campaign during spring 2014 ranged from 0/8 to 8/8, with 4/8 (i.e. partly cloudy) as the highest frequency with 4 out of

9 registrations. This confirms the impression that seNorge_eb is using a too rough method upon determining the cloud cover.

Finding a more suitable way to determine the cloud cover fraction is highly recommended as it will improve the accuracy of the parametrized net radiation, the component most important for snow melt.

Sedlar and Hock (2009) and Juszak and Pellicciotti (2012) derived the cloud cover fraction from observed $S\downarrow$. Such an approach might be worth testing for seNorge_eb, however the drawback is that the parametrization of $S\downarrow$ and L_a become dependent on a further observed variable. This dependency will impose a constrain on the model's applicability in sites without measurements beyond meteorological.

7.6 Turbulent fluxes

Observations related to the turbulent fluxes (i.e. snow surface temperature, relative humidity and wind) had, in terms of visual inspection, varying effect on the melt rates. Snow surface temperature, T_{ss}, derived from L_t had a reducing effect on 24 hour resolution and did not alter much on 3 hour resolution. Relative humidity (RH) had a clear reducing effect on the melt rates on both resolutions, whereas wind had a small to no increasing effect on the melt rates, depending on the season. In the following sections (7.6.1-7.6.3) each of these three observed variables are discussed separately.

7.6.1 Snow surface temperature

The data series that was used as observed T_{ss} was derived from observed L_t. This data series was the only additional data that managed to improve the simulated snow melt rates, in terms of the objective efficiency criteria, on 3 hour resolution, but only in terms of NS on 24 hour resolution. In spite some improvements, there are some drawbacks related to uncertainty of the observed T_{ss}.

Observed T_{ss} is subject to uncertainties relating to the accuracy of the measurements of L_t and the conversion to T_{ss}. The uncertainty is considerable during the ablation season, where T_{ss} is expected to be constant at 0 ℃. This was, however, not the case for the observed values of T_{ss} (observed L_t was not constant during the snow melt season, thus observed T_{ss} was not fixed at 0 ℃). Even though T_{ss} was capped at 0 ℃ it is reason to question the quality of this data series. As such, it is not recommended to include T_{ss} derived from observed L_t in seNorge_eb unless the validity of the data series is further investigated and, preferably, compared to other ways of estimate T_{ss}.

On events where seNorge_eb predicts the cold content to be negative, T_{ss} is estimated as twice the snow pack temperature, which in turn is a weighted average of the air temperature from the previous 5 days or 24 hour for the 24 and 3 hour resolution model version respectively. Thus an investigation of T_{ss} ought to include an evaluation of the method of estimating the snow pack temperature.

7.6.2 Wind

Observed wind data caused the snow to melt more rapidly on 3 hour resolution. On 24 hour resolution there was a small or no change in terms of visual inspection. This result

is expected as the turbulent fluxes are considered more important on fine resolutions. A recommendation is thus to include observed wind on at least 3 hour resolution. The constant wind speed of 1.75 $m\ s^{-1}$ in seNorge_eb is loosely calibrated using data from snow pillows (Skaugen pers comm. 26.05.2015). If observed wind is not readily available a constant wind speed that is regarded as closer to the mean wind speed of the area could be used. Walter et al. (2005) used an energy balance on daily resolution and got good results by setting the wind speed equal to the geometric mean wind speed.

7.6.3 Relative humidity

In the parametrization of the latent heat flux (LE) the vapour pressure of the air and the snow surface (e_a and e_s) are assumed to be equal to their saturated vapour pressures. When melt takes place the snow surface temperature is 0 ℃ and the snow surface humidity can be assumed equal to the saturated humidity (Harding 1986). Harding (1986) applied the energy balance to investigate snow melt on a daily basis at Finse, Norway, for the ablation period of May 1983. Concerning the evaporation rates (i.e. negative values of LE) he concluded that for air temperatures above 0 ℃ the evaporation rates were small with daily variations in signs. When RH was included in the vapour pressure gradient of the latent heat flux so that the vapour pressure of the air was changed from being the saturated air vapour pressure to being the actual vapour pressure, the results were in accordance with Harding's findings. Both for 3 hour and 24 hour resolution the LE with RH included fluctuated between the positive and negative side of the zero-line. More importantly, introducing RH allowed LE to be negative also for positive air temperatures, meaning that evaporation occurred.

Because RH ensures a more realistic profile of the LE, it is recommended that the air vapour pressure in the parametrization of the LE is changed from the saturated air pressure to the actual vapour pressure. If observed RH data are not readily available parametrizations of RH through other available observed data is worth testing. Walter et al. (2005) restricted the input data to temperature and approximated the vapour density (that was used instead of the vapour pressure) of the air to be the saturation vapour density at the minimum daily air temperature since the two are strongly correlated. This approach should however be used with caution since the evaporative heat exchange in the study of Walter et al. was generally over-predicted.

7.7 Air temperature and error

For both 3 hour and 24 hour resolution the air temperature, T_a, was found significant in explaining an increase in the error between simulated and observed snow melt rates with precipitation and temperature as input data. This suggests that there is a temperature dependent term in seNorge_eb that is overestimated.

The same result was found when the additional data were included as input data, except when observed RH was included on 24 hour resolution. When all additional data were simultaneously included as input data temperature was found significant in explaining the error on 3 hour resolution but not on 24 hour resolution. In the simulations with additional data the turbulent fluxes were still estimated in terms of parametrizations and observed wind or/and snow surface temperature. Since these fluxes are generally more important on finer resolution than daily the result suggests that the temperature

dependent term in these fluxes plays a more important role on 3 hour than 24 hour resolution.

Omhura (2000) argues that the strong relationship between T_a and snow melt rates makes the temperature-index method sufficient in most cases because the long-wave, the solar radiation and the sensible heat fluxes are correlated with the air temperature. This argument together with the indication that there is a temperature dependent term in seNorge_eb propose that attention should be given to terms that include T_a upon improving seNorge_eb's precision in predicting snow melt rates. T_{ss} is derived from T_a and is included in several terms in seNorge_eb, and an error related to a temperature dependent term might result from how T_{ss} is derived. The calculation of T_{ss} should therefore be investigated.

7.8 General recommendations

Based on the analysis of seNorge_eb there are some general recommendations that may improve the model. Improvement of the method of estimating the cloud cover, as well as the parametrization of incoming atmospheric long-wave radiation are for both the 3 and 24 hour model version regarded as most crucial. For the simulations with daily values, the algorithm for incoming solar radiation should be revised.

Regarding additional data, it is recommended that relative humidity is both on 3 and 24 hour resolution, as well as wind and snow surface temperature on 3 hour resolution.

In addition to the elements investigated is this thesis, the roughness height may be worth a closer look. Brun (2008) concluded that the value of this parameter is important in energy-balance snow melt simulations.

8 Conclusion

The energy balance model seNorge_eb, with precipitation and temperature as input data, was evaluated in terms of its precision in predicting snow melt rates. Simulated snow melt rates were compared to observed values from NVEs research station at Filefjell. Further, individual radiation components and variables were compared to observed radiation and meteorological data from Filefjell. Parametrizations and variables in seNorge_eb were, one at the time, replaced with observed data, with the aim of deciding the minimum input data requirement for seNorge_eb.

seNorge_eb performed well in predicting melt rates, both on 3 hour resolution and 24 hour resolution, with the best results on 24 hour resolution in terms of the objective model efficiency criteria. Investigations of the model's individual components revealed, however, deviations in the estimates of individual energy fluxes and variables. Cloud cover and atmospheric long-wave radiation were found to represent the largest part of the discrepancies. Snow surface temperature was also identified as a source of error. By including observed relative humidity, the values of the latent heat flux became more realistic. Relative humidity on both 3 and 24 hour resolution are recommended as additional input data, as well as snow surface temperature and wind on 3 hour resolution.

With the discovered discrepancies some improvements ought to be performed before seNorge_eb is implemented in the snow routine of a hydrological model. The time frame of this thesis limited the author to identify deviations and recommend improvements. Further studies are suggested below.

Further studies
If the model is to function as a complete snow routine that comprises both the accumulation and melt of snow, the problem of undercatch of snow in the precipitation data has to be addressed. A formula suggested by Wolff et al. (2013) may be worth testing.

A meaningful estimation of the fractional cloud cover is important in order to obtain a more reliable estimate of the net radiation, the main energy source of snow melt. Several studies have used an approximation based on incoming solar radiation.

The parametrization of the atmospheric long-wave radiation ought to be improved. According to the literature (e.g. Juszak and Pellicciotti 2012) calibration of the clear-sky emissivity should be performed at each location. Hopefully is it possible to derive an expression that is valid for the whole of Norway, hence seNorge_eb can be applied nationwide.

The snow pack temperature could not be evaluated in this thesis due to lack of data. The snow pack temperature affects the cold content and, the snow surface temperature, and in turn the start of the melt season (since the snow pack has to reach 0 °C before melt can take place). It is recommended to find a method of evaluating the snow pack temperature.

A Appendix: Data from Hydra II

Table 35 contains an overview of the parameter number, station owner and archive of the data retrieved from NVEs database Hydra II. All data series were used for evaluation and/or input, except for global radiation (73.11.06.01) that was used in the discussion of the accuracy of the observations.

Table 35: *Data obtained from NVEs database Hydra II (abbreviations explained below).*

	Parameter number	**Station owner/archive**
Meteorological data		
Precipitation [mm]	3000.54710.0.0.31	MET/EKLIMA-VT-C
Temperature [°C]	3000.54710.0.17.41	MET/EKLIMA-VT-C
Wind [$m\ s^{-1}$]	3000.54710.0.16.1	MET/EKLIMA-VT-C
Relative humidity [%]	3000.54710.02.1	NVE/NVE/HYKVAL-VT-C
Radiation data		
Long-wave incoming (L_a) [$W\ m^{-2}$]	73.11.0.9.1	NVE/HYTRAN-VT-UC
Long-wave outgoing (L_t) [$W\ m^{-2}$]	73.11.0.9.2	NVE/HYTRAN-VT-UC
Short-wave incoming ($S\downarrow$) [$W\ m^{-2}$]	73.11.0.8.1	NVE/HYTRAN-VT-UC
Global radiation ($S\downarrow$) [$W\ m^{-2}$]	73.11.06.01	NVE/HYTRAN-VT-UC
Snow validation data		
Snow water equivalent [m]	73.11.0.2003.7	NVE/COMPLETE-VT-UC

Abbreviations in Table 35:
MET Meteorological Institute
NVE Norwegian Water Resources and Energy Directorate
EKLIMA Data from MET
HYTRAN Temporary uncontrolled database
HYKVAL Controlled data
COMPLETE The best data available selecting from all archives
VT Variable time resolution
UC Uncontrolled
C Controlled

References

Anderson, E. A. (1976). A Point Energy and Mass Balance Model of a Snow Cover. NOAA Technical Report NWS 19, U.S. Department of Commerce, National Oceanic and Atmospheric Administration, National Weather Service, 172 pp.

Bjørstad, H. H. [Photograph of snow melt]. *yr.no*, www.yr.no/artikkel/sendt-ut-flomvarsel-for-sor-norge-1.8151476 (accessed May 5, 2015).

Brun, E. (2008). *"Sensitivity of energy and mass fluxes at the snow-atmosphere interface to internal and interface parameters." In Snow and Climate, eds. Armstrong, R.L. and Brun, E., 136-145.* Cambridge University Press.

Corps of Engineers (1956). *Summary report of the snow investigations, snow hydrology.* Portland OR: US Army Engineer Division, 437 pp.

DeWalle, D. and A. Rango (2008). *"Snowpack energy exchange: basic theory." In Principles of Snow Hydrology, 146-181.* Cambridge University Press.

Dickinson, R., A. Henderson-Sellers, and P. Kennedy (1993). Biosphere-Atmosphere Transfer Scheme (BATS) Version le as Coupled to the NCAR Community Climate Model. NCR tecnical note NCAR/TN-387+STR, National Center for Atmospheric Research, 72 pp.

Dingman, S. L. (2002). *Physical Hydrology* (2nd ed.). New Jersey: Prentice-Hall, 646 pp.

Dozier, J. (1987). Recent research in snow hydrology. *Reviews of Geophysics 25*(2), 153–161.

Fjeldheim, H. L. and E. Barfod (2013). Filefjell forskningsstasjon: Evaluering av måledata for snø, sesongen 2011/2012. NVE report 51, Norwegian Water Resources and Energy Directorate (NVE), 73 pp.

Furmyr, S. (1975). Resultater og erfaringer av nedbørundersøkelser i Filefjell representative område 1967-1974. , Den norske komite for Den internasjonale hydrologiske dekade.

Furmyr, S. and A. Tollan (1975). Resultater og erfaringer av snøundersøkelser i Filefjell representative område 1967-1974. , Den norske komite for Den internasjonale hydrologiske dekade.

Han, D. (2011). *Flood Risk Assessment and Management.* Bentham Science Publishers, 237 pp.

Harding, R. (1986). Exchanges of energy and mass associated with a melting snowpack. *Modelling Snowmelt-Induced Processes (Proceedings of the Budapest Symposium, July 1986. IAHS Publ.no.* (155), 3–15.

Hock, R. (1999). A distributed temperature-index ice- and snowmelt model including potential direct solar radiation. *Journal of Glaciology 45*(149), 101–111.

Hock, R. (2005). Glacier melt: a review of processes and their modelling. *Progress in Physical Geography 29*(3), 362–391.

Hock, R. (2014). Energy balance of snow and ice. Geophysical Institute University of Alaska Fairbanks, 11 pp.

Juszak, I. and F. Pellicciotti (2013). A comparison of parametrizations of incoming longwave radiation over melting glaciers: Model robustness and seasonal variability. *Journal of Geophysical Research: Atmospheres 118*, 3066–3084.

King, J., J. Pomeroy, D. Gray, C. Fierz, P. Föhn, R. Harding, R. Jordan, E. Martin, and C. Plüss (2008). *"Snow-atmosphere energy and mass balance", in Snow and Climate, eds. Armstrong, R.L. and Brun, E. (Cambridge University Press, 2008), 70-124.* Cambridge University Press.

König-Langlo, G. and E. Augstein (1994). Parametrization of the downward long-wave radiation at the earth's surface in polar regions. *Meteorologische Zeitschrift* (3), 343–47.

Krause, P., D. P. Boyle, and F. Bäse (2005). Comparison of different efficiency criteria for hydrological model assesment. *Advances in Geosciences* (5), 89–97.

Kuusisto, E. (1986). The energy balance of a melting snow cover in different environments. In *Modelling Snowmelt-Induced Processes.* Budapest Symposium: IAHS, no. 155, 37-45.

Kuzmin, P. (1961). *Melting of snow cover.* Israel Program of Scientific Translation, 290 pp.

Liston, G. (1995). Local advection of momentum, heat and moisture during melt of psatchy snow cover. *Journal of applied meteorology 34*, 1705–1715.

Male, D. and R. Granger (1981). Snow surface energy exchange. *Water Resources Research 17*(3), 609–627.

Malik, M. J., R. van der Velde, Z. Vekerdy, and Z. Su (2014). Improving modeled snow albedo estimates during the spring melt season. *Journal of Geophysical Research: Atmospheres 119*, 7311–7331.

Møen, K. M. NVE, employee. Personal communication 24.04.2015.

Norge i bilder. www.norgeibilder.no (accessed April 4, 2015).

Omhura, A. (2001). Physical basis for the temperature-based melt-index method. *Journal of applied meteorology 40*, 753–761.

Ree, B. L. and H. B. Stranden (2014). Filefjell forskningsstasjon: Evaluering av måledata for snø, sesongen 2012/2013. NVE report 73, Norwegian Water Resources and Energy Directorate (NVE), 79 pp.

Schuler, T. V. University of Oslo, associate professor. Personal communication via email. 27.03.2015.

Sedlar, J. and R. Hock (2009). Testing longwave radiation parametrizations under clear and overcast skies at Storglaciären, Sweden. *The Cryosphere* (3), 75–84.

Skaugen, T. NVE, research scientist. Personal communication 26.05.2015.

Skaugen, T. and T. Saloranta (2015). Simplified energy-balance snowmelt modelling. NVE report 31, Norwegian Water Resources and Energy Directorate (NVE), 27 pp.

Store norske leksikon (2009). Skydekke. https://snl.no/skydekke (accesses April 26, 2015).

Stranden, H. B. NVE, employee. Personal communication 24.04.2015.

Stranden, H. B. and H. A. Grønsten (2011). Filefjell forskningsstasjon: Evaluering av måledata for snø, sesongene 2009/2010 og 2010/2011. NVE report 23, Norwegian Water Resources and Energy Directorate (NVE), 65 pp.

Swinbank, W. C. (1963). Long-wave radiation from clear skies. *Quarterly Journal of the Royal Meteorological Society 89*, 339–348.

Tarboton, D. G. and C. H. Luce (1996, December). Utah Energy Balance Snow Accumulation and Melt Model (UEB): Computer model technical description and users guide. Technical report, Utah Water Research Laboratory: Utah State University and USDA Forest Service: Intermountain Research Station, 61 pp.

Unsworth, M. H. and J. L. Monteith (1975). Long-wave radiation at the ground: I. angular distribution of incoming radiation. *Quarterly Journal of the Royal Meteorological Society 101*, 13–24.

Walter, M., E. Brooks, D. McCool, L. King, M. Molnau, and J. Boll (2005). Process-based snowmelt modeling: does it requires more input data than temperature-index modeling? *Journal of hydrology 300*, 65–75.

Wolff, M., K. Isaksen, K. Ødemark, A. Petersen-Øverleir, T. Reitan, and R. Brækkan (2013). Vindkorreksjon av nedbør: et Energi Norge prosjekt. MET report 22, Meteorologisk institutt, 80 pp.